BILINGUAL PUBLISHING GROUP

Journal of Atmospheric Science Research

Volume 6 • Issue 4 • October 2023 ISSN 2630-5119(Online)

Volume 6 Issue 4 • October 2023 • ISSN 2630-5119 (Online)

Journal of Atmospheric Science Research

BILINGUAL PUBLISHING GROUP

BILINGUAL PUBLISHING GROUP

Volume 6 | Issue 4 | October 2023 | Page1-85

Journal of Atmospheric Science Research

Contents

Articles

BILINGUAL PUBLISHING GROUP

Journal of Atmospheric Science Research

https://journals.bilpubgroup.com/index.php/jasr

ARTICLE

Snowfall Shift and Precipitation Variability over Sikkim Himalaya Attributed to Elevation-Dependent Warming

Pramod Kumar [*], ***Khushboo Sharma***

Department of Geology, Sikkim University, Tadong, Gangtok, Sikkim, 737102, India

ABSTRACT

Sikkim Himalaya hosts critical water resources such as glacial, rain, and snow-fed springs and lakes. Climate change is adversely affecting these resources in various ways, and elevation-dependent warming is prominent among them. This study is a discussion of the elevation-dependent warming (EDW), snowfall shift, and precipitation variability over Sikkim Himalaya using a high-resolution ERA5-land dataset. Furthermore, the findings show that the Sikkim Himalaya region is experiencing a warming trend from south to north. The majority of the Sikkim Himalayan region shows a declining trend in snowfall. A positive advancement in snowfall trend (at a rate of 1 mm per decade) has been noticed above 4500 meters. The S/P ratio indicates a shift in snowfall patterns, moving from lower elevations to much higher regions. This suggests that snowfall has also transitioned from Lachung and Lachen (3600 m) to higher elevated areas. Moreover, the seasonal shifting of snowfall in the recent decade is seen from January-March (JFM) to February-April (FMA). Subsequently, the preceding 21 years are being marked by a significant spatiotemporal change in temperature, precipitation, and snowfall. The potent negative correlation coefficient between temperature and snowfall (–0.9), temperature and S/P ratio (–0.5) suggested the changing nature of snowfall from solid to liquid, which further resulted in increased lower elevation precipitation. The entire Sikkim region is transitioning from a cold-dry to a warm-wet weather pattern. In the climate change scenario, a drop in the S/P ratio with altitude will continue to explain the rise in temperature over mountainous regions.

***Keywords*:** Sikkim Himalaya; EDW; Snowfall; Seasonal shift; Precipitation variability; S/P ratio; ERA5-land

*CORRESPONDING AUTHOR:

Pramod Kumar, Department of Geology, Sikkim University, Tadong, Gangtok, Sikkim, 737102, India; Email: promnagar1@gmail.com

ARTICLE INFO

Received: 25 July 25 2023 | Revised: 17 September 2023 | Accepted: 25 September 2023 | Published Online: 28 September 2023

DOI: https://doi.org/10.30564/jasr.v6i4.5854

CITATION

Kumar, P., Sharma, K., 2023. Snowfall Shift and Precipitation Variability over Sikkim Himalaya Attributed to Elevation-Dependent Warming. Journal of Atmospheric Science Research. 6(4): 1-25. DOI: https://doi.org/10.30564/jasr.v6i4.5854

1. Introduction

In recent years, the scientific community and society have begun devoting significant attention to global warming and climate change. Though scientific organizations all over the world have extensively conveyed global climate change studies, the repercussions of these effects on regional climate need more attention and to be addressed. Regional landform processes, as well as land-use profiles, influence the costs of climate change. The Himalayan region has complex landform inadequacy. These landforms are changing in recent times as developmental and anthropogenic activities are rising, which is triggering erratic climate change consequences over the Himalayan region. The warming of the Himalayan region is inadequately reported in several researches [1-4]. Scientists observed that the highest temperature increase occurred across the northern slope of the central Himalayas during the cold season. However, winter season precipitation also has a significant influence on glacier simulation [5-7]. Furthermore, the majority of research focuses on the western and central Himalayas [5,6,8-14]. There is a knowledge gap about the eastern Himalaya's climate change impact behaviour and pattern. Therefore, this study focuses on the snowfall and precipitation variability and changes over the Sikkim Himalayan region. The mountain region's snowfall pattern has been altered as the global average temperature is rising [15]. During the seasonal accumulation period, a variety of climatological factors that affect snowfall distribution and accumulation (such as wind-gust, precipitable water, circulation systems, frontal behaviour, surface temperature, adiabatic lapse rate, as well as atmospheric boundary layer stability) have an impact on snowfall, either directly or indirectly [16]. The North Atlantic Oscillation (NAO), El Nio Southern Oscillation (ENSO), Jet Stream, Indian Ocean Dipole (IOD) and other monsoons teleconnection climatic factors also influence precipitation distribution and amount over the Himalayan region [5,17-19]. By utilizing Weather Research Forecast simulation, Norris et al. (2015) addressed extreme snowfall events over the entire Himalayan region [14,20-29]. The amount of snowfall and resulting snow accumulation are recommended as key indicators of climatic change [11,30-34].

The temperature and precipitation have a very peculiar and complex relationship. The changing temperature is affecting various meteorological variables, which are directly or indirectly linked with the cryosphere, and biosphere. Snowfall is one of the major sources of water over Sikkim. Snow and rain-fed springs are the major sources of Sikkim's potable water [26,35]. Agrawal et al. (2014) found that declining air quality is causing regional climate changes in Sikkim [36]. This is evidenced by an increase in temperature at higher altitudes, less snowfall/precipitation, decreased water availability, and rapid loss of glacierized landscape [37]. Airborne aerosols, such as pollutants, can act as cloud condensation nuclei (CCN), which can change snowflake formation and snowfall patterns [38]. Poor air quality, often linked to greenhouse gas emissions, can cause black carbon and dust particles to settle on snow and glaciers, reducing their reflectivity [39-41]. This causes them to absorb more heat and melt faster, intensifying the impact of poor air quality [10]. As glaciers retreat due to climate change, they expose more terrain, which can release additional dust and debris into the atmosphere, worsening air quality and further accelerating glacial melting and retreat [42,43]. Air quality indirectly affects snowfall and glaciers by influencing aerosols, black carbon, dust deposition, precipitation patterns, and the broader climate system [40,41]. These factors collectively lead to observable changes in snowfall and glacier dynamics in regions with poor air quality and ongoing climate change. The impact of climate change on air quality is also a concern, as it can contribute to air pollution and further exacerbate the effects of poor air quality on snowfall and glaciers. This study of Sikkim Himalaya highlights the importance of understanding the region's climate, which is still underrated due to limited research.

The elevation-dependent warming (EDW) in the Himalayan region has a different signature than any other region. EDW is affecting precipitation and

snowfall, which are the key sources of water [44,45]. The warming in the Eastern Himalayan region is inducing more convective precipitation during the summer season and suppressing orographic rain. The researchers [46] synthesized several studies' results on climate change in Sikkim, which suggested the various impacts of climate change on Sikkim's Himalayan indigenous population [47-51]. Viste and Sorteberg (2015) suggested that the uppermost western Brahmaputra basins have the greatest relative variability in snowfall [28]. The majority of this basin will experience temperatures above freezing, particularly in the summer season, under the highest forcing scenario. The yearly average snowfall is expected to decrease by 65-75% [28]. The rise in temperature reduces the portion of precipitation that occurs as snowfall, greatly reduces the period of snowpack during the winter season, causes thawing to occur during the spring, and enhances the intensity of melting [52]. On the basis of reanalysis data, the unequal distribution of snowfall has mostly been investigated statistically. Moreover, the data from observations (including the gridded data from the analysis of in-situ observation by IMD) somehow doesn't adequately describe the actual regional climate feature and neither provides spatiotemporally relevant information of snowfall over the study region, particularly in higher elevations at which stations are ill-equipped, due to the limitation of weather stations owing to geographic variation and the multifaceted topography in Sikkim Himalaya [26,53-56]. The accurate assessment of the shift in snowfall with respect to precipitation in a warming climate is very intricate. Summer snowfall has reduced while winter snowfall has increased over the Tibetan Plateau [57]. Berghuijs et al. (2014) addressed how increasing temperatures promote conversion from snowfall to rain [58]. According to scientists [59], changes in the snowfall/precipitation (S/P) ratio throughout time were established to be accurate markers of changing climate. Warming has reduced snowfall in the cold season, causing snowmelt to occur earlier [60,61]. However, the significant decline in snowpack and snowfall is not uniform. Sikkim's high altitudes receive a large majority of its yearly precipitation in the form of snowfall during the winter and spring seasons with a major contribution from monsoon and summer seasons rainfall. However, the habitat of the region primarily depends on water accessibility from snowmelt [36,56]. Significant variations in the S/P ratio may be essential for understanding other hydrometeorological patterns because there may be an impact on the timing of spring drainage, the freezing point of streams, and delayed winter snow accumulation [62]. Dubey et al. (2022) suggest that the warm and wet days have risen from 1951 to 2018 [53]. Therefore, it would be sensible to adequately monitor the S/P ratio and snowfall in order to manage regional climate crises and natural resources.

Concerning the Sikkim Himalaya, the present research attempts to succeed in the following particular objectives. (1) To carry out a long-term investigation of the snowfall and precipitation using high-resolution datasets available. (2) To accurately describe the seasonal shift and regional variability in precipitation, the S/P ratio, and snowfall over Sikkim with challenging topography as well as elevation gradient. (3) To investigate the use of the findings to understand whether regional climatic change is affecting snowfall over Sikkim Himalaya.

2. Study area

Figure 1 shows the land use cover (LUC) for the year 2021 from sentinel-2 classifications focusing on built-up, glaciated regions, water bodies, vegetation cover, cropland, and fallow land. The study region has a very typical landscape, and for a better understanding of atmospheric processes, the LUC has been applied in the context of natural and anthropogenic influences on temperature, snowfall, and total precipitation variability over Sikkim. LUC of the southern part of Sikkim reveals a high sprawl of built-up regions, which is a strong sign of anthropogenic activity over the region. Gangtok Municipal Corporation (GMC) region has an enormous built-up area compared to the rest of Sikkim. This indicates that the surface radiation and 2-meter temperature

change are greater in the build-up region than in the forest cover area [56].

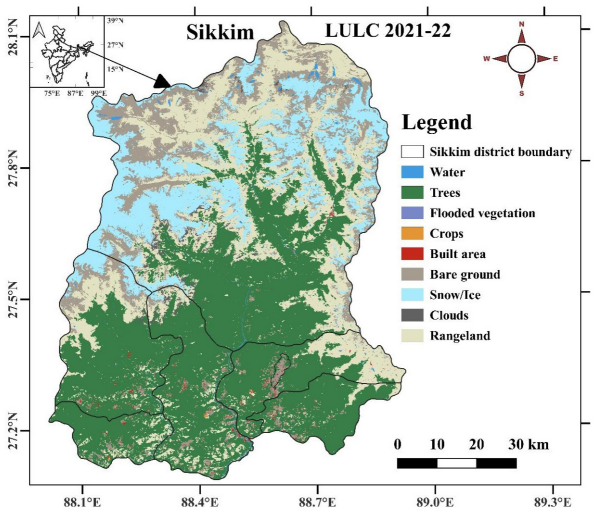

Figure 1. The study region and its land cover for the year 2021 using Sentinel-2 LULC classification. Here, a small boundary represents Gangtok Municipal Corporation (GMC).

3. Dataset and methodology

The present study used various basic as well as advanced statistical techniques to analyze the temperature, precipitation, snowfall changes, and seasonal shifts in four decades (1980-2021) for the Sikkim Himalaya (**Figure 1**). The climatology, anomaly, significant change, linear trend, and Theil-Sen estimator trend analysis [59,63,64] for snowfall and total precipitation ratio [(S/P) ratio] have been computed. The seasonal shifts of temperature, snowfall, and total precipitation are examined. The seasons have been classified as abjointed twelve seasons (DJF: December, January, February; JFM: January, February, March; FMA: February, March, April; MAM: March, April, May; AMJ: April, May, June; MJJ: May, June, July; JJA: June, July, August; JAS: July, August, September; ASO: August, September, October; SON: September, October, November; OND: October, November, December; NDJ: November, December, January) to understand the shift of snowfall, temperature and precipitation temporal regimes. The steps of the seasonality computation are discussed in Supplementary Method SM6 and **Figures S1-S5b**.

The anomaly is also analysed to quantify the abnormal change in the time series (from 1980 to 2021) from the long-term average of the time series as Equation (1):

$$\text{Anomaly } (A) = (X - \overline{X}) \quad (1)$$

where X is the time series of the yearly dataset, and $\overline{X} = \frac{\sum_{i=1}^{n=42} X}{n}$, i is the initial, n last number of the time series.

Percentage precipitation change is calculated to see the wetness, and dryness [65] as Equation (2):

$$Precipitation\ Change(\%) = \Delta P\% = \left(\frac{A}{\overline{X}}\right) * 100 \quad (2)$$

where A, and $\overline{X}$ are the anomaly, and long-term average, respectively as Equation (1).

Theil-Sen estimator trend analysis is calculated [64] as Equation (3):

$$trend = \frac{\partial S}{\partial P} = \frac{(\partial S * P - S * \partial P)}{P^2} \ or \ \frac{\partial S}{\partial P} = \frac{\overline{S}}{\overline{P}}[(\partial lnS) - (\partial lnP)] \quad (3)$$

where $\overline{S}$, $\overline{P}$ are long-term averages over the study region. And, (lnS), (lnP) are logarithms of snowfall and total precipitation. However, (∂lnS) and (∂lnP) are the linear trend of logarithmic terms for the study period (1980-2021). The details of the methodology can be seen in the supplementary method section SM6.

The t-test [66] has been applied for the significant difference and trend values as Equation (4).

$$t\ test = \frac{(\overline{Y_1} - \overline{Y_2})}{\sqrt[2]{\left(\frac{\sigma_1^2}{n_1} + \frac{\sigma_2^2}{n_2}\right)}} \quad (4)$$

where $(\overline{Y_1})$, $(\overline{Y_2})$, σ_1, σ_2, and $n_1 = n_2 = 21$ are mean of first time series slice (from 1980 to 2000) of the variables, the mean of the second time series slice (from 2001 to 2021), standard deviation for the first time slice, standard deviation for the second time slice, total number years for the first time slice 1980 to 2000 (21 years), and total number of years for the second time slice 2001 to 2021 (21 years), respectively. This is used to find the p-values and significant investigation with a p-value table [67].

The present study used the high-resolution reanalysis open-source dataset ERA5-land (**Table 1**). Reanalysis is a process that combines model data with observations from around the world to create a glob-

ally complete and consistent dataset [68]. ERA5 is the fifth generation of atmospheric reanalysis produced by the European Centre for Medium-Range Weather Forecasts (ECMWF) and is the latest climate reanalysis [68,69]. It provides hourly data on many atmospheric, land-surface, and sea-state parameters, along with estimates of uncertainty. ERA5-Land is a reanalysis dataset that provides a consistent view of the evolution of land variables over several decades at an enhanced resolution [70,71]. The products of the reanalysis are available to the public through the Climate Data Store. ERA5 has several benefits, including the ability to provide spatiotemporally consistent data, which is useful for climate studies [72,73]. It also allows for the study of long-term trends in temperature and precipitation, which can help understand the physical atmospheric system and assess the influence of any climatic change on the biophysical and socio-economic setup of a region [68-71,74]. Station data from the India Meteorological Department (IMD) have been used for the primary result analysis. However, as the result was absurd in the case of snowfall, we visited the nearby locations for cross-checking of IMD stations and found that there was a lack of maintenance. Only five of the IMD-installed automatic weather stations (AWS) are working. Additionally, IMD observation standards measure quality issues in time series data as well and facilities measurement uncertainty during traditional meteorological observation is significant, especially in the winter season over northern Sikkim. At higher elevations, errors due to lack of maintenance of precipitation gauge measurements may range from 10 to 100%. The above factors invoked the present research work to choose the ERA5-land reanalysis dataset for Sikkim (see **Table 1**). Some of the studies are reported in detail about the ERA5 dataset and Its performance for the Himalayan region [20,43,56,72,75,76].

Sentinel-2 bands 3 (green, 10 m), 4 (red, 10 m), 8 (near-infrared, 10 m), 11 (SWIR, 20 m), and 12 (SWIR, 20 m) are utilized for land cover classification. Band 2 is beneficial for distinguishing soil and plants, charting forest types, and detecting man-made objects. It is absorbed by the atmosphere, illuminates things in shadows more effectively than longer wavelengths, and penetrates clear water better than other colours. Chlorophyll absorbs it, resulting in darker plants. Band 8 is helpful for identifying water vapour, while band 9 is good for distinguishing plants. Cirrus band 10 is excluded since it has no surface information [77,78]. LULC Classes are discussed in detail in the supplementary section SM7.

4. Results

According to **Figure 2a**, the climatology (i.e., long-term annual average) of temperature over southern Sikkim is much higher than the rest of Sikkim. The temperature ranges from 15 °C to –6 °C from south to north, resulting in a wide gradient. **Figures 2a and 2b** show the long-term annual average pattern of the temperature and snowfall. And peak of the snowfall can be seen at the isothermal line of 0 °C and –3 °C, from **Figures 2a and 2b**. The snowfall over the north-central (27.7°N) is found to be the highest, whereas to the south (27.3°N) there is

Table 1. Details of the data sets used for the study.

Variables	Temporal resolution	Horizontal resolution	Source	Reference
Temperature (2m air mean) Snowfall Total precipitation	1980-2021 (daily)	0.1^{O} x 0.1^{O} Or (9 km.)	ERA5-Land (ECMWF)	Muñoz-Sabater et al., 2021
LULC	December 2021-2022	Band-2 (blue), Band-3 (green), Band-4 (red), Band-8 (near-infrared), 10 m resolution.	Esri Inc. Sentinel-2 (https://www.arcgis.com/home/item.html?id=fc92d38533d440078f17678ebc20e8e2)	Karra et al., 2021

almost no snowfall (**Figure 2b**). However, the total precipitation follows an almost similar pattern to that of temperature. In **Figure 2c**, the climatology of total precipitation shows that most of the Sikkim region receives precipitation > 110 mm per day. However, the northernmost part of Sikkim is receiving 30 to 50 mm/day (**Figure 2c**). **Figure 2d** depicts the decadal temperature trend in Sikkim, ranging from –0.05 °C to 0.4 °C, with a peak (0.4 °C/decade) over central and the lowest (–0.05 °C/decade) over southwest Sikkim. The snowfall trend shows negative values over most of the regions with the lowest (–4 mm/decade) over central Sikkim. In **Figure 2e**, a positive trend value of snowfall has been observed over the northernmost part of Sikkim with a peak value of 2 mm/decade. The strong decreasing trend of snowfall over the central part of Sikkim has a resemblance with a strong warming trend in the same region (**Figures 2d and 2e**). In **Figure 2f**, the decadal trend of total precipitation has a positive value over the entire Sikkim, ranging from 2 to > 5 mm/decade with the highest measure over the central part of Sikkim (i.e., > 5 mm/decade). **Figures 2g, 2h, and 2i** are anomalies with respect to the 1980-2021 long-term mean for temperature, snowfall, and total precipitation at 27.6°N along with longitudinal cross-section. The temperature anomaly suggests that the nonstop abnormal warming has been stirring since 2002 and in the year 2021 attained a 1.5 °C above average value. The snowfall anomaly shows unusually intense and frequently occurring positive values against the long-term average before 2015. However, since 2015, there has been an anomalous negative shift of snowfall relative to the long-term average over 88.2°E-88.8°E (**Figure 2h**). Nevertheless, the total precipitation anomaly indicates anomalous high precipitation from 2009 to 2021 and intense low precipitation from 2000 to 2001. **Figures 2g, 2h, and 2i** reveal the snowfall reduction from 2000 to 2021. The anomalous temperature rise causes massive precipitation, signifying that the snowfall has been altered to liquid precipitation as a result of the anomalous warming.

4.1 Elevation dependent warming (EDW)

The elevation-dependent variations in temperature, snowfall, and total precipitation have been depicted in **Figure 3**. The climatology of temperature along with elevation ranges from –8 °C to 20 °C. The elevation zones above 3500 m elevation show negative annual long-term average temperature and below 3500 m elevation values are positive (**Figure 3a**). The annual long-term average of snowfall ranges from 1 to 140 mm/day for all the grids from lower to higher elevations. At the elevation of 1500 m, three grids show snowfall ranging from 5 mm to 55 mm/day, with no snowfall received below 1400 m (**Figure 3b**). The majority of elevation zones up to 3500 m elevation are clustered to minimal snowfall. However, above 4500 m elevation, the majority of the elevation zones are scattered from 10 mm to 140 mm/day (**Figure 3b**). In **Figure 3c**, the decadal temperature trend is observed between –0.1 °C to 0.5 °C/decade over all the grids from lower to higher elevation. Only three elevation points indicate a negative temperature trend from 1400 m to 2000 m elevation. The majority of elevation zones > 4500 m elevation are clustered around 0.2 °C to 0.3 °C/decade warming rate (**Figure 3c**). In **Figure 3d**, above 4000 m elevation, snowfall shows an increasing trend and is clustered near 1 mm/decade. On the other hand, below 4000 m all elevation zones show a decreasing trend and are scattered from –1 mm to –2.5 mm/decade (**Figure 3d**). Hence, the warming is increasing, and corresponding to this, the snowfall is decreasing along the elevation. **Figure 3e** shows the total precipitation climatology along the elevation. This ranges from 30 mm to 255 mm/day. The total amount of precipitation that elevation zones receive decreases with elevation. Most of the elevation zones are clustered together to a total precipitation rate of 50 mm/day above 4500 meters (**Figure 3e**). The trend of the total precipitation shows an increase, which is highest at lower elevations and minimum at higher elevations (ranging from 1 mm to 14 mm/decade rate). Above 4000 m elevation, there is a clear margin which suggests the total precipitation is clustered above this height (**Figure 3f**). At elevations

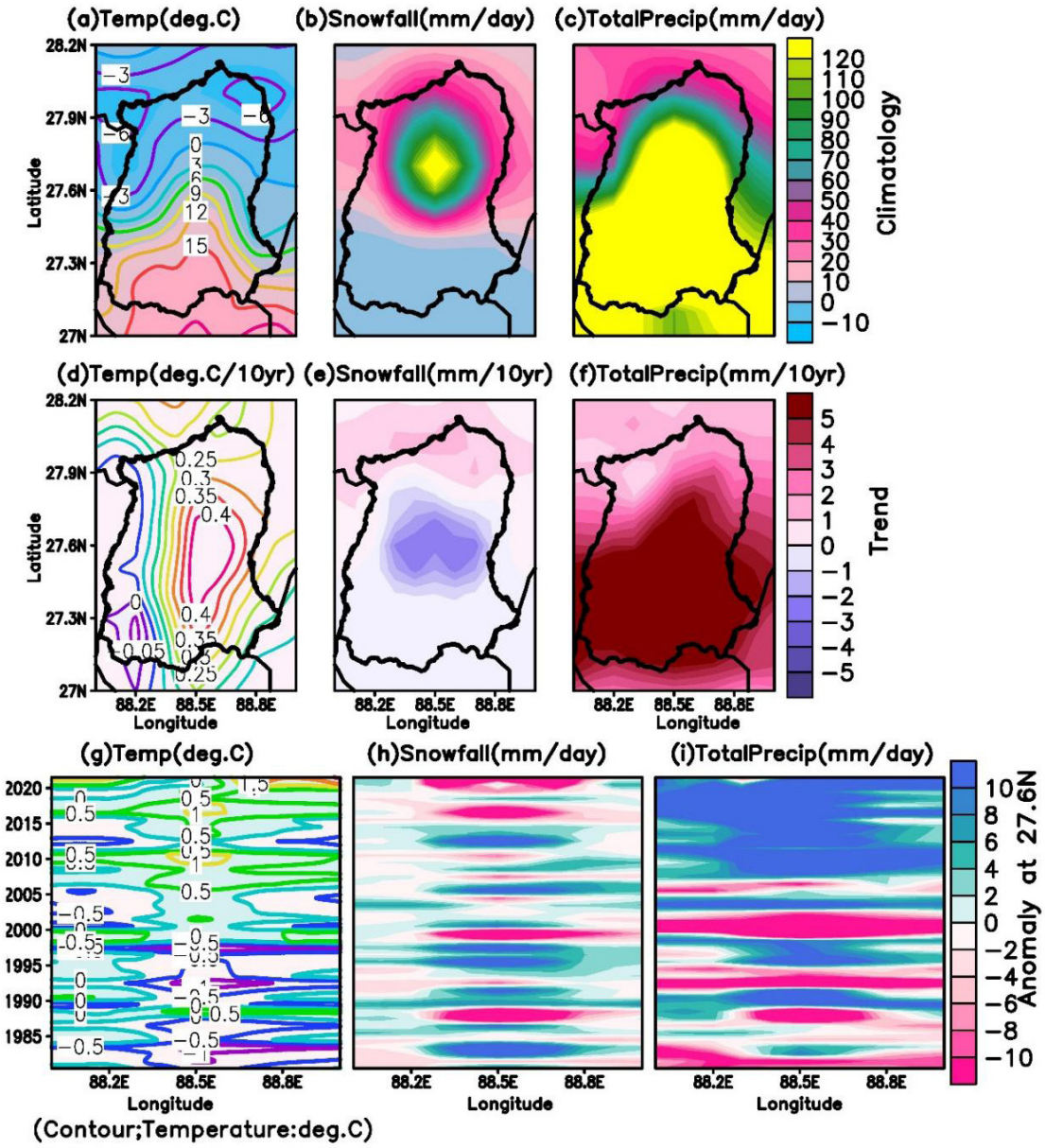

Figure 2. The climatology (long-term annual average), linear trend (decadal), and anomalies at 27.6°N latitude along with longitudinal cross-section are shown as climatology: (a) for temperature, (b) for snowfall, and (c) for total precipitation; linear trend: (d) for temperature, (e) for snowfall, and (f) for total precipitation; respectively, for anomalies: (g) temperature, (h) snowfall, and (i) total precipitation.

below 1500 m, the highest variability in precipitation trend is observed. There are three elevation zones between 1500 m to 1400 m that receive total precipitation with the highest rate of 12 to 15 mm per decade. However, the snowfall shows a negative inclination at the same elevation zones, and the warmer temperature trend explains that accordingly more liquid precipitation has been raising the total precipitation trend. This can be understood by the S/P ratio along with elevation.

4.2 S/P ratio analysis

To see the spatiotemporal variability of snowfall, the S/P ratio has been described in **Figure 4**. **Figure 4a** shows the spatial distribution of the long-term average of snowfall to total precipitation ratio (S/P ratio). The S/P ratio suggests a higher chance of

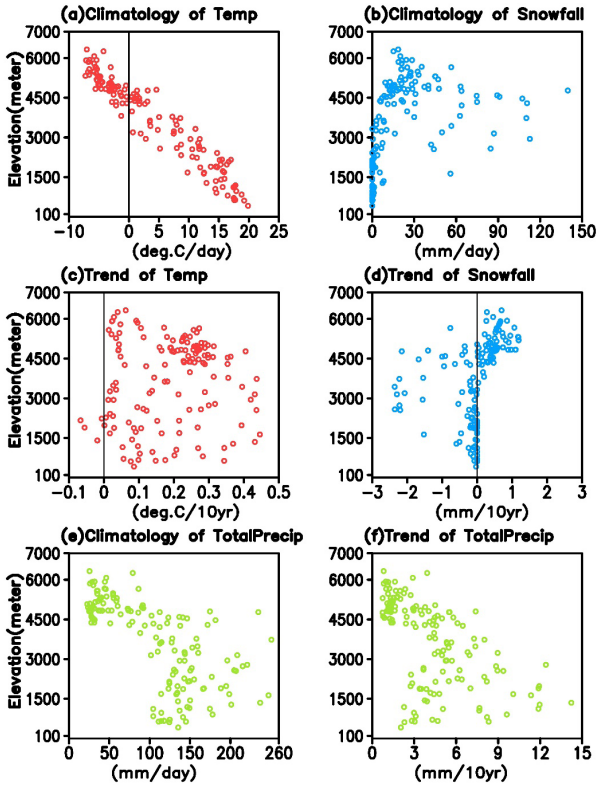

Figure 3. Elevation-dependent variation in temperature, snowfall, and total precipitation. The long-term annual average (climatology) (a) for temperature, (b) for snowfall, and (e) for total precipitation. The linear trend (decadal) is shown in (c) for temperature, (d) for snowfall, and (f) for total precipitation along with elevation over Sikkim.

snowfall when the percentage of the S/P ratio is higher. The region beyond the 27.6°N shows more snowfall region in Sikkim, with maxima over the northernmost part of Sikkim. Theil-Sen estimator is utilized to calculate linear trends [84] for these variables over 42 years. The decadal trend of the S/P ratio suggests a negative trend over the entire Sikkim (except the northernmost of Sikkim) (**Figure 4b**). The S/P ratio decadal trend values are most negative over central Sikkim (i.e., –2% per decade), which suggests drastic snowfall reduction over this region in 42 years of the study period (**Figure 4b**). For temporal variability of the S/P ratio, the anomaly has been assessed to explain the annual deviation from the long-term average over Sikkim. Prior to 2000, the majority of the years had anomalously positive values of the S/P ratio (**Figure 4c**). Afterwards, the S/P ratio is found to be more anomalously negative. The S/P ratio has shifted towards abnormal negative years in recent times. The elevation-dependent S/P ratio decadal trend shows that the majority of the elevation zones have negative trend values ranging from –3.5 to –0.01. Some of the grids are showing positive trend values from 0.01 to 0.5% per decade for elevation > 4000 m, while the rest of the grids are scattered in a negative trend, suggestive of the snowfall reduction in the majority of the grids. The trend of the S/P ratio also explains the seasonal shifting during the study period over Sikkim (**Table 2** and **Figure S4**).

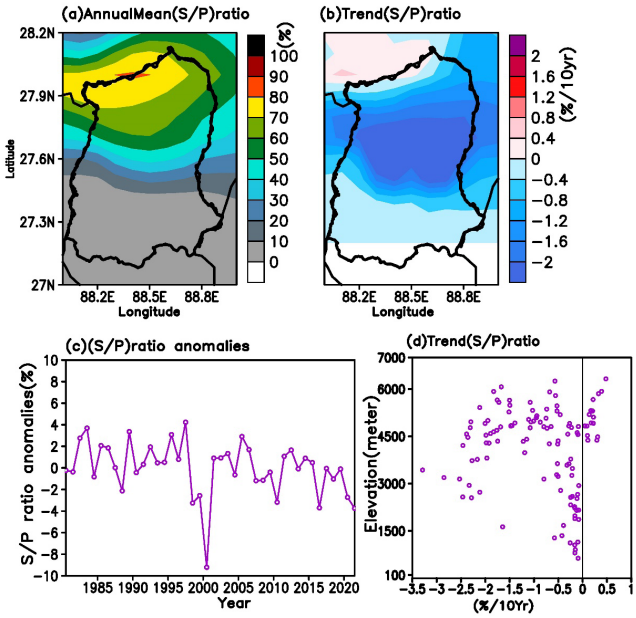

Figure 4. S/P ratio and its features for snowfall change over the region are shown in (a) for annual long-term average, (b) linear trend, (c) anomalies, and (d) decadal trend along with elevation over Sikkim.

4.3 Seasonal shift

In **Figure 5a**, the seasonal variation of long-term averaged temperature, snowfall, total precipitation, and S/P ratio show the peaks and troughs with respective seasons. The temperature is the lowest in NDJ followed by JFM. However, the warmest seasons are observed to be JJA, and JAS followed by MJJ, ASO, AMJ, and SON. Total precipitation has a similar pattern, with a significant fall particularly compared to temperature. The peak of snowfall

has been observed in JFM and NDJ followed by DJF, FMA, MAM, and OND. A similar paradigm is observed in the case of S/P ratio. **Figures 5b, 5c, 5d, and 5e** are the annual averaged seasonal variation of temperature, snowfall, total precipitation, and S/P ratio. **Figure 5b** shows temperature incident escalation especially in OND, NDJ, and DJF from 1980 to 2021. The extension of high temperature is found to be expanding from seasons AMJ, MJJ, JJA, JAS, ASO to MAM, AMJ, MJJ, JJA, JAS, ASO, and SON in 42 years. A significant surging trend of temperature has been observed in seasons DJF, JFM, JAS, SON, OND, and NDJ (**Table 2** and **Figure S1**). **Figure 5c** shows that the magnitude of snowfall has declined throughout the peak seasons NDJ, DJF, JFM, and FMA. In addition to this, seasons MAM, AMJ, and MJJ have evidenced a significant rise in snowfall in recent decades (**Table 2** and **Figure S2**). In **Figure 5d**, total precipitation shows the seasonal widening to ASO after the year 2007. A significantly increasing trend of total precipitation is detected in seasons DJF, FMA, MAM, AMJ, MJJ, JJA, JAS, and ASO (**Table 2** and **Figure S3**) which is attributed to the warming as temperature patterns have a similarity. In **Figure 5e**, S/P ratio shows the seasonal shift in snowfall from JFM to FMA after the year 2001. The values of snowfall have dropped, and this occurs frequently during NDJ season. A significant decreasing trend in the S/P ratio has been observed in the seasons DJF, JFM, and NDJ over the entire Sikkim (**Table 2** and **Figure S4**).

4.4 Climate change attribution

Temperature and S/P ratio have a linear relation with a negative slope, which helps to understand the seasonal temperature change affecting snowfall. Thereafter, the S/P ratio decreases with temperature rise for seasons as well as annually (see supplementary **Figures S5a and S5b**). The significant change in temperature and precipitation observed after the year 2000 encourages the further study of deferential change in the two time periods (i.e., 1980-2000 and 2001-2021). Temperature is a controlling factor of snowfall and total precipitation. The significant change has been compared from the past 21 years (1980-2000) to the recent 21 years (2001-2021). Temperature change has been noted to be significantly positive over most of the region. The highest magnitude of temperature change (1 °C) has been found in the central part of Sikkim (**Figure 6a**). West Sikkim has undergone cooling in the recent two decades (–0.2 °C). The snowfall has been reduced significantly (–4 mm/day) from the central to southern part of Sikkim (**Figure 6b**). The northernmost part of Sikkim has shown a significant

Table 2. Seasonal variation trend of temperature, snowfall, total precipitation and S/P ratio. The stars (***) indicate 95% significant confidence, the upward arrow (▲) indicates an increasing trend, and the downward arrow (▼) indicates a decreasing trend.

Variables / Seasons	Temperature	Snowfall	Total precipitation	S/P ratio
DJF	▲***	▲	▲***	▼***
JFM	▲***	▼	▲	▼***
FMA	▲	▲	▲***	▼
MAM	▲	▲***	▲***	▼
AMJ	▲	▲***	▲***	▲
MJJ	▲	▲***	▲***	▲
JJA	▲	▲	▲***	▼
JAS	▲***	▼	▲***	▼
ASO	▲	▲	▲***	▼
SON	▲***	▼	▲	▼
OND	▲***	▼	▲	▼
NDJ	▲***	▼	▼	▼***

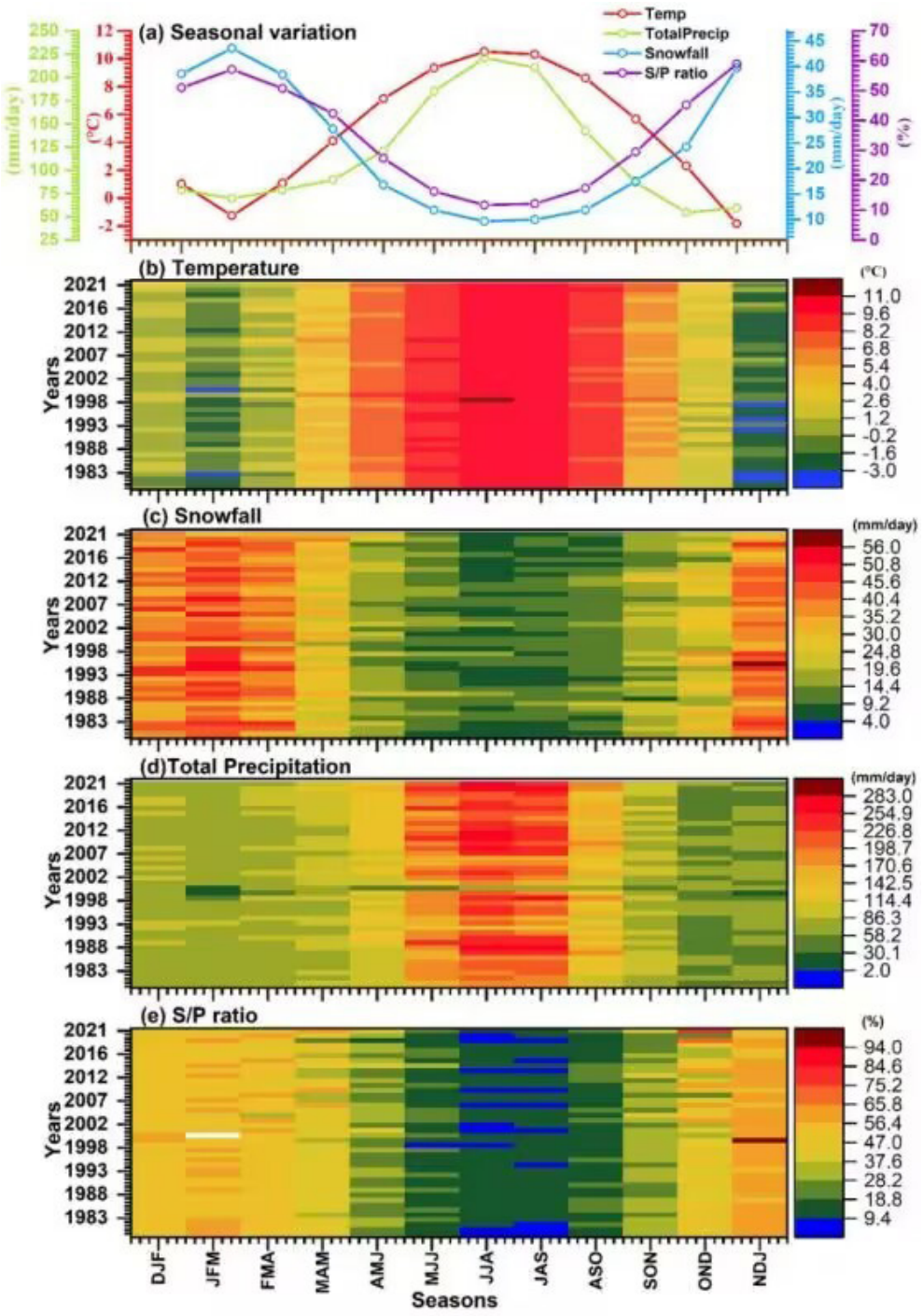

Figure 5. Seasonal variation in temperature, snowfall, total precipitation, and S/P ratio over Sikkim, (a) for long-term average, but (b), (c), (d), and (e) for time series for the study period 1980-2021 over Sikkim. Figures (b), (c), (d), and (e) show each year's seasonal variation for the corresponding variables such as temperature, snowfall, total precipitation and the S/P ratio. This heatmap clearly shows the pragmatic shifting in the snowfall season from 1980 to 2021.

positive change in snowfall in recent decades (3 mm/day). Total precipitation has been elevated significantly over the entire Sikkim with a peak at central Sikkim (30 mm/day). These changes in the snowfall may be attributed to significant warming over the entire Sikkim (and at the same place rise in total precipitation reveals the rise in warming and liquid form of precipitation).

The correlation among temperature vs. snowfall, total precipitation, and the S/P ratio explains the

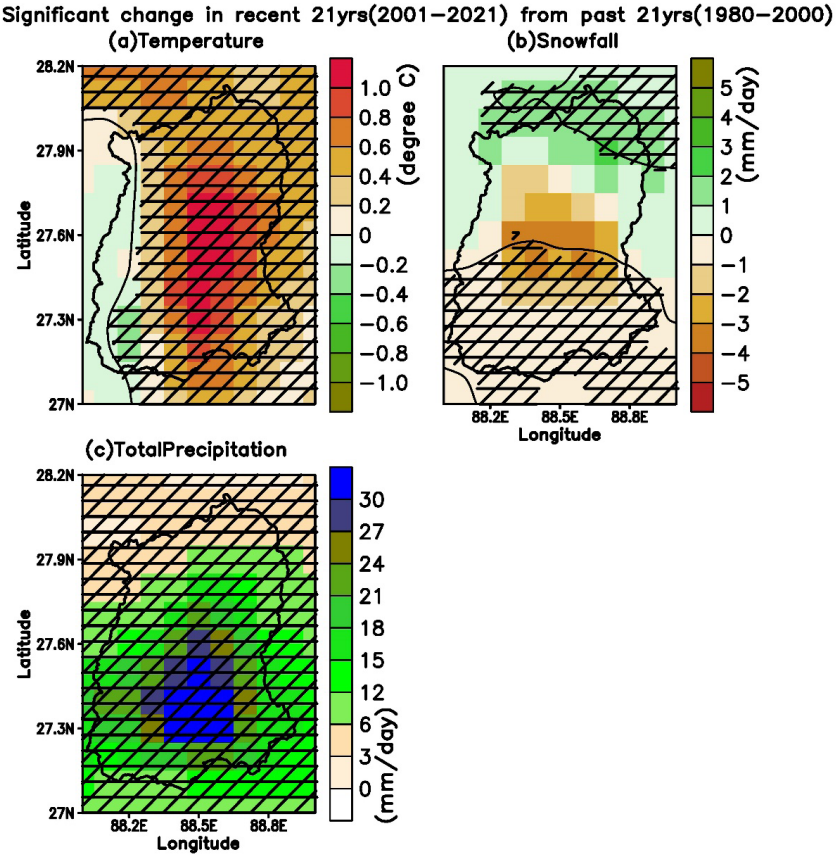

Figure 6. The changes from the past 21 years (1980-2000) to the recent 21 years (2001-2021) are at a 95% significant level over the Sikkim. The shading shows the change in magnitude for corresponding variables, and hatching shows the significance at 95% confidence.

dependency of snowfall on the temperature. As the temperature rises, the snowfall is reduced along with a corresponding total precipitation rise; as higher temperature favours convective rain and liquid precipitation as well. **Figure 7a** shows a strong negative correlation between temperature and snowfall over the entire Sikkim. However, **Figure 7b** suggests a good positive correlation between temperature and total precipitation. **Figure 7c** discusses the correlation between temperature and S/P ratio. The spatial distribution of correlation explains the regional features playing an important role in controlling temperature, snowfall, and total precipitation dependency. **Figure 7d** shows the temporal variation of correlation among the variables. The temperature vs. total precipitation correlation coefficient varies from 0.6 to 0.8 (except in 2000). Similarly, temperature vs. snowfall has a strong negative correlation coefficient varying from –0.82 to –0.88 (except 2000) followed by an S/P ratio. **Figure 8** suggests the dryness and wetness conditions of the region. **Figure 8a** shows the majority of the grids indicating the cold-dry, a few warm-dry, a few cold-wet, and one warm-wet weather system during the first decade (1980-1990) of the study period. However, in **Figure 8b** i.e., during the second decade (1991-2000), the majority of grids are pointing towards cold-dry and warm-dry weather systems. In addition to this, the third and fourth decades are prioritizing warm-wet, and cold-wet weather systems (**Figures 8c and 8d**). Decades 1 and 3 have less precipitation change variance (–4 to 1%). However, decades 2 and 4 have more precipitation change variance (–17 to 17%), respectively (**Figure 8**).

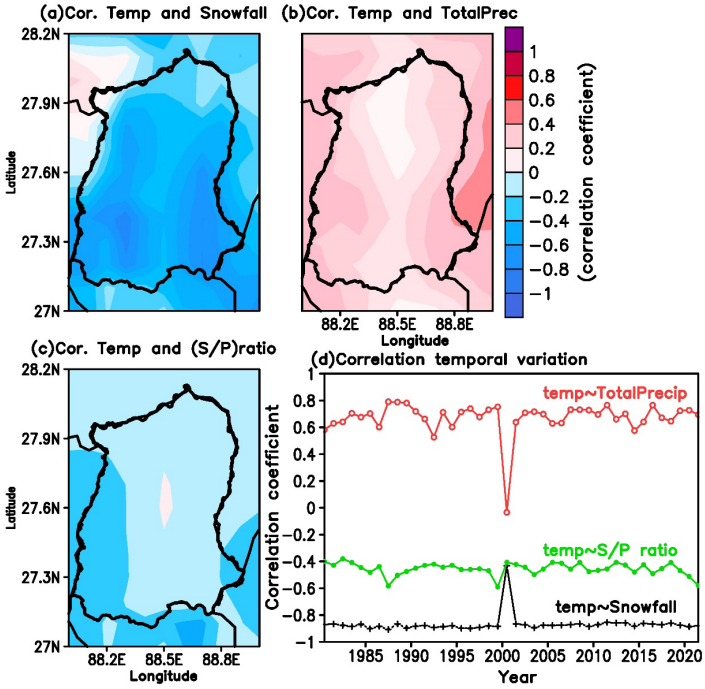

Figure 7. The spatiotemporal variation in correlation for temperature versus snowfall, total precipitation, and S/P ratio. The spatial variation in correlation (i.e., correlation over time) is shown for (a) temperature vs. snowfall, (b) Temperature vs. total precipitation, and (c) temperature vs. S/P ratio. The temporal variation in correlation (i.e., correlation in grid space) is shown for (d) temperature vs. snowfall, total precipitation, and S/P ratio over Sikkim.

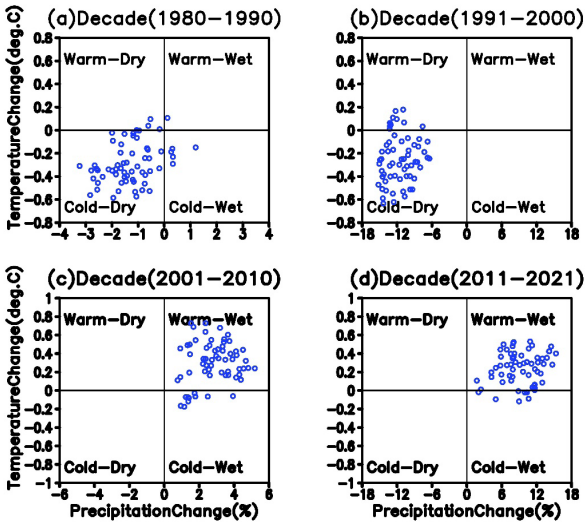

Figure 8. Decadal temperature-precipitation changes, dryness, and wetness extent for the Sikkim Himalaya. Figure shows four weather patterns warm-dry, warm-wet, cold-dry, and cold-wet.

5. Discussion

In recent decades, the land use of Sikkim has changed considerably [79]. The settlement is replacing the green vegetation regions as well making more anthropogenic contributions to the regional warming and emissions that are adversely impacting the microclimatic region [56]. This study tries to establish the fact that warming is the major accountable behind the changing snowfall pattern over the Sikkim Himalayan region. The rate of warming over the Himalayan Mountains is increasing rapidly, making them more vulnerable to disasters [3,40,80,81]. The snowfall is closely connected with warming; as

the temperature rises, the snowfall reduces [16,82-85]. In addition to this, total precipitation is positively connected with warming; as temperature rises, total precipitation intensifies following the Clausius-Clapeyron relationship [86]. The anomalous warming over Sikkim has resulted in anomalously high total precipitation every year [53]. The warming trend over higher elevations is much faster than at lower elevations. However, the lower elevation is suffering a significant decline in snowfall due to significant anomalous warming [5]. The enormous variability in snowfall and total precipitation below 1500 m elevation highlights the lower elevation warming significance and precipitation extreme. Total precipitation is increasing along the elevation and following the temperature trend over the entire Sikkim, which is also addressed by some studies [46,87]. Subsequently, EDW is greatly affecting the precipitation as well as snowfall over the entire Sikkim Himalaya. Some elevation zones over 1300 to 2000 m have a negative warming trend that is possibly the west Sikkim region which includes dense forest region and less human disturbances. However, an insignificant cooling change has been found in western Sikkim as well.

The S/P ratio suggests a decline in snowfall over 1500 m elevation and above. A strong declining trend in the S/P ratio over central Sikkim caused by warming indicates an increase in liquid precipitation, which eventually stimulates an increase in total precipitation with an anomalous low annual S/P ratio. The temperature and S/P ratio relationship justifies the variation of snowfall with warming. The fraction of precipitation in the region that occurs in the form of snow, as reported by Sharma and Goyal (2020), is declining as a result of the region's rising temperature [87]. Some of the research articles also suggest the subsequent trends in Sikkim Himalayas due to climate change [35,46,87,88]. The decadal trend of the S/P ratio suggests a negative trend over the entire Sikkim (except the northernmost of Sikkim) [46]. The S/P ratio decadal trend values are most negative over central Sikkim, which suggests drastic snowfall reduction over this region in 42 years of the study period [46]. The S/P ratio has shifted towards abnormal negative years in recent times [35,46,87,88]. These trends indicate that climate change and rapid warming are affecting snowfall patterns in the Sikkim Himalayas, which can have significant impacts on the region's ecology, economy, and society.

Seasonal shift of the snowfall has been found over the central part of Sikkim. It is seen that the snowfall has been shifting from NDJ, and DJF to JFM, and FMA respectively. In fact, the seasons MAM, AMJ, and MJJ have seen a significant upsurge in snowfall in the last decade [82,84,85,89]. Climate change is directly influencing snowfall, as the global average temperature rises at a faster rate [90]. In recent decades, higher warming has significantly declined the winter season (NDJ, and DJF) snowfall (–4 mm/day) from the central to southern parts of Sikkim. In the analyzed results spanning from 1980 to 2021, a significant rise in temperatures was observed during the OND, NDJ, and DJF seasons, with this warming trend extending to encompass additional seasons. Conversely, snowfall has decreased notably during peak seasons (NDJ, DJF, JFM, FMA) but has shown a significant increase in MAM, AMJ, and MJJ. Moreover, total precipitation has exhibited a seasonal expansion, particularly post-2007, with a noticeable increase in various seasons, including DJF, FMA, MAM, AMJ, MJJ, JJA, JAS, and ASO. These patterns align with the effects of climate change and warming on seasonal weather [91-93]. Le et al. (2023) also support climate-driven changes in the amounts of precipitation and their seasonal variability [91]. The seasonal shift is going to make it more difficult for farming and crop production. As Wang et al. (2021) also suggested that summer and winter have become longer and hotter, while spring and autumn have become shorter and warmer [93].

Snowfall drop is justified by a strong inverse relationship between temperature and snowfall. The two-tailed Student's t-test is employed to assess significant differences. Climatic change and differences are only presented if they are statistically significant at the 95% significance level (**Figure 6** and **Table 2**). This emphasizes the significant seasonal change

as well as the alteration in the spatial distribution of snowfall. Temperature versus total precipitation for four decades indicates that most of the elevation zones are tending from cold-dry towards warm-wet weather systems of the Sikkim Himalaya. Dubey et al. (2022) have also reported that Sikkim has witnessed warm and wet days from 1951 to 2018 [53]. The result examined the correlation between temperature, total precipitation, and snowfall using correlation coefficients [94]. The correlation coefficient between temperature and total precipitation varied from 0.6 to 0.8, while the correlation coefficient between temperature and snowfall was strongly negative, ranging from –0.82 to –0.88. This suggests the major cause of the snowfall change and precipitation variability [52,94]. The changing pattern of the precipitation and snowfall along with the temperature rise influences the weather system of the mountainous region [90]. Thereafter, the dryness and wetness conditions of the study region are observed to be altered, which showed that the majority of elevation zones indicated cold-dry during the first and second decades (1980-1990, 1991-2000) and warm-wet weather systems during the third and fourth decade (2001-2010, 2011-2021) of the study period.

Henceforth, Climate change and EDW are affecting vegetation, and shifting it to higher elevations due to temperature and precipitation changes. These shifts affect the ecosystems and biodiversity of the mountainous region [95]. Thereafter, interactions with hydrological factors like evapotranspiration and soil moisture anomalies also influence regional precipitation patterns [95]. However, some researchers have suggested that EDW and climate change are affecting vegetation and other hydrometeorological parameters over the Himalayan region at a faster rate, and collectively altering snowfall patterns in the Sikkim Himalayas. Furthermore, recent studies have highlighted those human activities, such as deforestation and urbanization, emissions, contribute to the intricacy of regional climate dynamics [18,52,94,95].

6. Conclusions

The temperature is rising across the entire region, with maxima over the central part of Sikkim. As temperature and snowfall have an inverse relation, the snowfall has been dropping throughout the entire region, with a negative peak over the central part of Sikkim Himalaya. Across Sikkim's zonal cross-section, anomalous warming since 2000, abnormally low snowfall since 2015, and contrastively heavy precipitation since 2007 have been observed. The snowfall seasons are shifting from NDJ, and DJF to JFM, and FMA [96]. Snowfall is declining along elevations up to 4500 m with huge variance. Snowfall is slowly rising above 5000 m elevation with minimal variance. The precipitation is rising over the entire Sikkim from lower elevation (with greater variability) to higher elevation (with least variability). The rise in temperature, which boosted rainfall while cutting down snowfall, was precisely explained by a drop in the S/P ratio with altitude. Temperature, snowfall, and precipitation have changed significantly from the previous two decades (1980 to 2000) to the most recent two decades (2001 to 2021). The weather system of the entire Sikkim is also shifting from cold-dry to warm-wet weather. Essentially, the Sikkim Himalaya is undergoing significant snowfall shifts and precipitation variability caused by EDW in recent decades. The findings of this study will be helpful for policymakers and the scientific community in better comprehending the long-term implications of climate change.

People's perceptions

People believe that such non-climatic issues (like land degradation, land use, urbanization, and air pollution) make it particularly challenging for them to mitigate the hazards created by climatic changes, and act as obstacles for them to escape from it. The present study concludes that programs must be designed in a way that addresses the region's multidimensional problems since achieving this will improve the community's innate ability to adapt to both present and future climate-related risks.

The majority of people think and consider that the weather system over the entire Sikkim is changing, which is the root cause for snowfall pattern change

as per the survey response of 51 people of the entire Sikkim region.

Authors Contribution

Pramod Kumar: Formulated the concept, plotted the figures, drafted the original work, and wrote the manuscript.

Khushboo Sharma: Created seasonal analysis figures, and conducted the local people's perception survey and manuscript editing.

Conflict of Interests

The authors declare that there is no conflict of interest.

Funding

No Funding has been provided for this study.

Acknowledgement

The authors appreciated the DST Centre of Excellence (DST's CoE) Department of Geology, Sikkim University, for providing the working space. The authors acknowledged all DST-CoE staff members for their moral support. We also acknowledged open-source data sets and tools used for the present study such as ERA5-land, CDO, R, QGIS, and GrADS. We acknowledge Dr. Saumya G. Kutty and Dr. Thupstan Angchuk for proofreading and their insights. We appreciate Dr. Rakesh Kumar Ranjan for mentoring. We express our gratitude to the anonymous reviewers and the editor for their contributions and support.

References

[1] Adhikari, B.R., Gautam, S., Paudel, B., 2022. Landslide, land cover, and land use changes and its impacts in Nepal. Impact of climate change, land use and land cover, and socio-economic dynamics on landslides. Springer: Berlin. pp.149-164.
DOI: https://doi.org/10.1007/978-981-16-7314-6_6

[2] Aggarwal, S., Rai, S.C., Thakur, P.K., et al., 2017. Inventory and recently increasing GLOF susceptibility of glacial lakes in Sikkim, Eastern Himalaya. Geomorphology. 295, 39-54.
DOI: https://doi.org/10.1016/j.geomorph.2017.06.014

[3] Dimri, A.P., Allen, S., Huggel, C., et al., 2021. Climate change, cryosphere and impacts in the Indian Himalayan Region. Current Science. 120, (5).
DOI: https://doi.org/10.18520/cs/v120/i5/774-790

[4] Messerli, B., Grosjean, M., Hofer, T., et al., 2000. From nature-dominated to human-dominated environmental changes. Quaternary Science Reviews. 19(1-5), 459-479.
DOI: https://doi.org/10.1016/S0277-3791(99)00075-X

[5] Banerjee, A., Chen, R., Meadows, M.E., et al., 2021. Tracking 21st century climate dynamics of the Third Pole: An analysis of topo-climate impacts on snow cover in the central Himalaya using Google Earth Engine. International Journal of Applied Earth Observation and Geoinformation. 103, 102490.
DOI: https://doi.org/10.1016/j.jag.2021.102490

[6] Dawadi, B., Sharma, S., Reynard, E., et al., 2023. Climatology, variability, and trend of the winter precipitation over Nepal. Earth Systems and Environment. 7, 381-391.
DOI: https://doi.org/10.1007/s41748-023-00338-0

[7] Liu, X., Chen, B., 2000. Climatic warming in the Tibetan Plateau during recent decades. International Journal of Climatology: A Journal of the Royal Meteorological Society. 20(14), 1729-1742.
DOI: https://doi.org/10.1002/1097-0088(20001130)20:14<1729::AID-JOC556>3.0.CO;2-Y

[8] Dimri, A.P., Mohanty, U.C., 1999. Snowfall statistics of some SASE field stations in J&K. Defence Science Journal. 49(5), 437.

[9] Kapnick, S.B., Delworth, T.L., Ashfaq, M., et al., 2014. Snowfall less sensitive to warming in Karakoram than in Himalayas due to a unique seasonal cycle. Nature Geoscience. 7(11), 834-840.
DOI: https://doi.org/10.1038/ngeo2269

[10] Kumar, R., Barth, M.C., Pfister, G.G., et al.,

2018. How will air quality change in South Asia by 2050?. Journal of Geophysical Research: Atmospheres. 123(3), 1840-1864.
DOI: https://doi.org/10.1002/2017JD027357

[11] Mir, R.A., Jain, S.K., Saraf, A.K., et al., 2015. Decline in snowfall in response to temperature in Satluj basin, western Himalaya. Journal of Earth System Science. 124, 365-382.
DOI: https://doi.org/10.1007/s12040-015-0539-z

[12] Mishra, A.K., Rafiq, M., 2017. Analyzing snowfall variability over two locations in Kashmir, India in the context of warming climate. Dynamics of Atmospheres and Oceans. 79, 1-9.
DOI: https://doi.org/10.1016/j.dynatmoce.2017.05.002

[13] Negi, V.S., Maikhuri, R.K., Pharswan, D., et al., 2017. Climate change impact in the Western Himalaya: people's perception and adaptive strategies. Journal of Mountain Science. 14(2), 403-416.
DOI: https://doi.org/10.1007/s11629-015-3814-1

[14] Shekhar, M.S., Chand, H., Kumar, S., et al., 2010. Climate-change studies in the western Himalaya. Annals of Glaciology. 51(54), 105-112.
DOI: https://doi.org/10.3189/172756410791386508

[15] Stewart, I.T., 2009. Changes in snowpack and snowmelt runoff for key mountain regions. Hydrological Processes: An International Journal. 23(1), 78-94.
DOI: https://doi.org/10.1002/hyp.7128

[16] Kumar, P., Saharwardi, M.S., Banerjee, A., et al., 2019. Snowfall variability dictates glacier mass balance variability in Himalaya-Karakoram. Scientific Reports. 9(1), 18192.
DOI: https://doi.org/10.1038/s41598-019-54553-9

[17] Goswami, B.N., Chakraborty, D., Rajesh, P.V., et al., 2022. Predictability of South-Asian monsoon rainfall beyond the legacy of Tropical Ocean Global Atmosphere program (TOGA). npj Climate and Atmospheric Science. 5(1), 58.
DOI: https://doi.org/10.1038/s41612-022-00281-3

[18] Mal, S., Dimri, A.P., Jeelani, G., et al., 2021. Determining the quasi monsoon front in the Indian Himalayas. Quaternary International. 599, 4-14.
DOI: https://doi.org/10.1016/j.quaint.2021.02.010

[19] Yadav, R.K., Ramu, D.A., Dimri, A.P., 2013. On the relationship between ENSO patterns and winter precipitation over North and Central India. Global and Planetary Change. 107, 50-58.
DOI: https://doi.org/10.1016/j.gloplacha.2013.04.006

[20] Krishnan, R., Sabin, T.P., Madhura, R.K., et al., 2019. Non-monsoonal precipitation response over the Western Himalayas to climate change. Climate Dynamics. 52, 4091-4109.
DOI: https://doi.org/10.1007/s00382-018-4357-2

[21] Li, M., Ma, Y., Hu, Z., et al., 2009. Snow distribution over the Namco lake area of the Tibetan Plateau. Hydrology and Earth System Sciences. 13(11), 2023-2030.
DOI: https://doi.org/10.5194/hess-13-2023-2009

[22] Liu, L., Ma, Y., Yao, N., et al., 2021. Diagnostic analysis of a regional heavy snowfall event over the Tibetan Plateau using NCEP reanalysis data and WRF. Climate Dynamics. 56, 2451-2467.
DOI: https://doi.org/10.1007/s00382-020-05598-4

[23] Norris, J., Carvalho, L.M., Jones, C., et al., 2015. WRF simulations of two extreme snowfall events associated with contrasting extratropical cyclones over the western and central Himalaya. Journal of Geophysical Research: Atmospheres. 120(8), 3114-3138.
DOI: https://doi.org/10.1002/2014JD022592

[24] Rafiq, M., Meraj, G., Kesarkar, A.P., et al., 2022. Hazard mitigation and climate change in the Himalayas—policy and decision making. Disaster management in the complex Himalayan terrains: Natural hazard management, methodologies and policy implications. Springer International Publishing: Cham. pp. 169-182.
DOI: https://doi.org/10.1007/978-3-030-89308-8_12

[25] Sabin, T.P., Krishnan, R., Vellore, R., et al., 2020. Climate change over the Himalayas. Assessment of climate change over the Indian region. Springer: Berlin. pp. 207-222.

[26] Sharma, G., Namchu, C., Nyima, K., et al., 2020. Water management systems of two towns in the Eastern Himalaya: Case studies of Singtam in Sikkim and Kalimpong in West Bengal

states of India. Water Policy. 22(S1), 107-129.
DOI: https://doi.org/10.2166/wp.2019.229

[27] Thadani, R., 2023. Snow damage in a Himalayan forest maintains the dominance of evergreen oaks. Biotropica.
DOI: https://doi.org/10.1111/btp.13236

[28] Wang, J., Guan, Y., Wu, L., et al., 2021. Changing lengths of the four seasons by global warming. Geophysical Research Letters. 48(6), e2020GL091753.
DOI: https://doi.org/10.1029/2020GL091753

[29] Zhu, J., Weng, X., Guo, B., et al., 2023. Investigating extreme snowfall changes in China based on an ensemble of high-resolution regional climate models. Sustainability. 15(5), 3878.
DOI: https://doi.org/10.3390/su15053878

[30] Blanford, H.F., 1884. II. On the connexion of the Himalaya snowfall with dry winds and seasons of drought in India. Proceedings of the Royal Society of London. 37(232-234), 3-22.
DOI: https://doi.org/10.1098/rspl.1884.0003

[31] Gusain, H.S., Mishra, V.D., Bhutiyani, M.R., 2014. Winter temperature and snowfall trends in the cryospheric region of north-west Himalaya. Mausam. 65(3), 425-432.
DOI: https://doi.org/10.54302/mausam.v65i3.1053

[32] Serreze, M.C., Clark, M.P., Armstrong, R.L., et al., 1999. Characteristics of the western United States snowpack from snowpack telemetry (SNOTEL) data. Water Resources Research. 35(7), 2145-2160.
DOI: https://doi.org/10.1029/1999WR900090

[33] Goodison, B.E., Walker, A.E., 1993. Use of snow cover derived from satellite passive microwave data as an indicator of climate change. Annals of Glaciology. 17, 137-142.
DOI: https://doi.org/10.3189/S0260305500012738

[34] Derksen, C., Wulder, M., LeDrew, E., et al., 1998. Associations between spatially autocorrelated patterns of SSM/I-derived prairie snow cover and atmospheric circulation. Hydrological Processes. 12(15), 2307-2316.
DOI: https://doi.org/10.1002/(SICI)1099-1085(199812)12:15<2307::AID-HYP798>3.0.CO;2-0

[35] Sharma, R.K., Shrestha, D.G., 2016. Climate perceptions of local communities validated through scientific signals in Sikkim Himalaya, India. Environmental Monitoring and Assessment. 188, 1-11.
DOI: https://doi.org/10.1007/s10661-016-5582-y

[36] Agrawal, A., Sharma, A.R., Tayal, S., 2014. Assessment of regional climatic changes in the Eastern Himalayan region: A study using multi-satellite remote sensing data sets. Environmental Monitoring and Assessment. 186, 6521-6536.
DOI: https://doi.org/10.1007/s10661-014-3871-x

[37] Kumar, P., Sharma, M.C., Saini, R., et al., 2020. Climatic variability at Gangtok and Tadong weather observatories in Sikkim, India, during 1961-2017. Scientific Reports. 10(1), 15177.
DOI: https://doi.org/10.1038/s41598-020-71163-y

[38] Doherty, R.M., Heal, M.R., O'Connor, F.M., 2017. Climate change impacts on human health over Europe through its effect on air quality. Environmental Health. 16(1), 33-44.
DOI: https://doi.org/10.1186/s12940-017-0325-2

[39] Climate Change Decreases the Quality of the Air We Breathe [Internet]. Centers for Disease Control and Prevention. Available from: https://www.cdc.gov/climateandhealth/pubs/air-quality-final_508.pdf

[40] Kumari, S., Middey, A., 2023. A comprehensive appraisal on the effect of aerosol on mountain glaciers: Special reference to Sikkim Himalayan region of India. Sādhanā. 48(2), 50.
DOI: https://doi.org/10.1007/s12046-023-02097-0

[41] Platt, R.V., Ogra, M., Kisak, N., et al., 2021. Climate change perceptions, data, and adaptation in the Garhwal Himalayas of India. Climate and Development. 13(2), 95-106.
DOI: https://doi.org/10.1080/17565529.2020.1724069

[42] Dahal, K.R., Dahal, P., Adhikari, R.K., et al., 2022. Climate change impacts and adaptation in a hill farming system of the Himalayan Region: Climatic trends, farmers' perceptions and practices. Climate. 11(1), 11.

DOI: https://doi.org/10.3390/cli11010011

[43] Krishnan, R., Shrestha, A.B., Ren, G., et al., 2019. Unravelling climate change in the Hindu Kush Himalaya: Rapid warming in the mountains and increasing extremes. The Hindu Kush Himalaya assessment: Mountains, climate change, sustainability and people. Springer: Berlin. pp. 57-97.
DOI: https://doi.org/10.1007/978-3-319-92288-1_3

[44] Rangwala, I., Miller, J.R., 2012. Climate change in mountains: A review of elevation-dependent warming and its possible causes. Climatic Change. 114, 527-547.
DOI: https://doi.org/10.1007/s10584-012-0419-3

[45] Trujillo, E., Molotch, N.P., Goulden, M.L., et al., 2012. Elevation-dependent influence of snow accumulation on forest greening. Nature Geoscience. 5(10), 705-709.
DOI: https://doi.org/10.1038/ngeo1571

[46] Bawa, K.S. and Ingty, T., 2012. Climate Change in Sikkim: A Synthesis [Internet]. Available from: http://www.sikkimforest.gov.in/climate-change-in-sikkim/23-Chapter-CLIMATE%20CHANGE%20IN%20SIKKIM%20A%20SYNTHESIS.pdf

[47] Basnett, S., Kulkarni, A.V., Tambe, S., 2012. Monitoring of Seasonal Snow Cover in Sikkim Himalaya Using Remote Sensing Techniques [Internet]. Available from: https://www.researchgate.net/profile/A-Kulkarni-4/publication/281451598_MONITORING_OF_SEASONAL_SNOW_COVER_IN_SIKKIM_HIMALAYA_USING_REMOTE_SENSING_TECHNIQUES/links/55e8601008ae3e1218423141/MONITORING-OF-SEASONAL-SNOW-COVER-IN-SIKKIM-HIMALAYA-USING-REMOTE-SENSING-TECHNIQUES.pdf

[48] Luitel, K.K., Shrestha, D.G., Sharma, N.P., et al., 2012. Impact of Climate Change on East-Rathong Glacier In Rangit Basin, West Sikkim [Internet]. Available from: http://www.sikkimforest.gov.in/climate-change-in-sikkim/4-Chapter-Impact%20of%20climate%20change%20on%20east%20-%20Rathong%20Glacier.pdf

[49] Rahman, H., Karuppaiyan, R., Senapati, P.C., et al., 2012. An Analysis of Past Three Decade Weather Phenomenon in the Mid-hills of Sikkim and Strategies for Mitigating Possible Impact of Climate Change on Agriculture [Internet]. Available from: http://sikkimforest.gov.in/climate-change-in-sikkim/2-chapter-An%20analysis%20of%20past%20three%20decade%20weather.pdf

[50] Seetharam, K., 2012. Climate Change Synthetic Scenario over Gangtok [Internet]. Available from: http://sikkimforest.gov.in/climate-change-in-sikkim/1-chapter-Climate%20Change%20Synthetic%20Scenario%20over%20Gangtok.pdf

[51] Shrestha, U.B., Gautam, S., Bawa, K.S., 2012. Widespread climate change in the Himalayas and associated changes in local ecosystems. PloS One. 7(5), e36741.
DOI: https://doi.org/10.1371/journal.pone.0036741

[52] Li, H., Choy, S., Zaminpardaz, S., et al., 2023. Investigating the inter-relationships among multiple atmospheric variables and their responses to precipitation. Atmosphere. 14(3), 571.
DOI: https://doi.org/10.3390/atmos14030571

[53] Dubey, S.K., Ranjan, R.K., Misra, A.K., et al., 2022. Variability of precipitation extremes and drought intensity over the Sikkim State, India, during 1950-2018. Theoretical and Applied Climatology. 148, 1-14.
DOI: https://doi.org/10.1007/s00704-022-03931-x

[54] Rai, S.C., Mukherjee, N.R., 2021. Spatio-temporal change delineation and forecasting of snow/ice-covered areas of Sikkim Himalaya using multispectral and thermal band combinations of Landsat imagery. Environmental Challenges. 4, 100163.
DOI: https://doi.org/10.1016/j.envc.2021.100163

[55] Rai, S.C., 2023. Spatio-temporal change delineation and forecasting of snow/ice-covered areas. Food and livelihood securities in changing climate of the Himalaya. Springer International Publishing: Cham. pp. 61-77.
DOI: https://doi.org/10.1007/978-3-031-22817-9_4

[56] Sharma, K., Kumar, P., Sharma, J., et al., 2023. Characterization of Polycyclic Aromatic Hydrocarbons (PAHs) associated with fine aerosols in ambient atmosphere of high-altitude urban environment in Sikkim Himalaya. Science of the Total Environment. 870, 161987.
DOI: https://doi.org/10.1016/j.scitotenv.2023.161987

[57] Deng, H., Pepin, N.C., Chen, Y., 2017. Changes of snowfall under warming in the Tibetan Plateau. Journal of Geophysical Research: Atmospheres. 122(14), 7323-7341.
DOI: https://doi.org/10.1002/2017JD026524

[58] Berghuijs, W.R., Woods, R.A., Hrachowitz, M., 2014. A precipitation shift from snow towards rain leads to a decrease in streamflow. Nature Climate Change. 4(7), 583-586.
DOI: https://doi.org/10.1038/nclimate2246

[59] Dong, W., Ming, Y., 2022. Seasonality and variability of snowfall to total precipitation ratio over high mountain Asia simulated by the GFDL high-resolution AM4. Journal of Climate. 35(17), 5573-5589.
DOI: https://doi.org/10.1175/JCLI-D-22-0026.1

[60] Somorowska, U., 2023. Warming air temperature impacts snowfall patterns and increases cold-season baseflow in the Liwiec River Basin (Poland) of the Central European Lowland. Resources. 12(2), 18.
DOI: https://doi.org/10.3390/resources12020018

[61] Knowles, N., Dettinger, M.D., Cayan, D.R., 2006. Trends in snowfall versus rainfall in the western United States. Journal of Climate. 19(18), 4545-4559.
DOI: https://doi.org/10.1175/JCLI3850.1

[62] Huntington, T.G., Hodgkins, G.A., Keim, B.D., et al., 2004. Changes in the proportion of precipitation occurring as snow in New England (1949-2000). Journal of Climate. 17(13), 2626-2636.
DOI: https://doi.org/10.1175/1520-0442(2004)017<2626:CITPOP>2.0.CO;2

[63] Sen, P.K., 1968. Estimates of the regression coefficient based on Kendall's tau. Journal of the American Statistical Association. 63(324), 1379-1389.

[64] Theil, H., 1950. A rank-invariant method of linear and polynomial regression analysis. Indagationes Mathematicae. 12(85), 173.

[65] Yang, S.E., Wu, B.F. (editors), 2010. Calculation of monthly precipitation anomaly percentage using web-serviced remote sensing data. 2010 2nd International Conference on Advanced Computer Control; 2010 Mar 27-29; Shenyang, China. New York: IEEE. p. 621-625.
DOI: https://doi.org/10.1109/ICACC.2010.5486796

[66] Kim, T.K., 2015. T test as a parametric statistic. Korean Journal of Anesthesiology. 68(6), 540-546.
DOI: https://doi.org/10.4097/kjae.2015.68.6.540

[67] Piegorsch, W.W., 2002. Tables of P-values for t-and chi-square reference distributions [Internet]. Available from: http://math.arizona.edu/~piegorsch/571A/TR194.pdf

[68] Hersbach, H., Bell, B., Berrisford, P., et al., 2020. The ERA5 global reanalysis. Quarterly Journal of the Royal Meteorological Society. 146(730), 1999-2049.
DOI: https://doi.org/10.1002/qj.3803

[69] Hersbach, H., 2016. The ERA5 Atmospheric Reanalysis [Internet]. Available from: https://ui.adsabs.harvard.edu/abs/2016AGUFMNG33D..01H/abstract

[70] Bell, B., Hersbach, H., Simmons, A., et al., 2021. The ERA5 global reanalysis: Preliminary extension to 1950. Quarterly Journal of the Royal Meteorological Society. 147(741), 4186-4227.
DOI: https://doi.org/10.1002/qj.4174

[71] Muñoz-Sabater, J., Dutra, E., Agustí-Panareda, A., et al., 2021. ERA5-Land: A state-of-the-art global reanalysis dataset for land applications. Earth System Science Data. 13(9), 4349-4383.
DOI: https://doi.org/10.5194/essd-13-4349-2021

[72] Chen, Y., Sharma, S., Zhou, X., et al., 2021. Spatial performance of multiple reanalysis precipitation datasets on the southern slope of central Himalaya. Atmospheric Research. 250, 105365.
DOI: https://doi.org/10.1016/j.atmosres.2020.105365

[73] Kishore, P., Jyothi, S., Basha, G., et al., 2016. Precipitation climatology over India: Validation with observations and reanalysis datasets and spatial trends. Climate Dynamics. 46, 541-556. DOI: https://doi.org/10.1007/s00382-015-2597-y

[74] Hersbach, H., Bell, B., Berrisford, P., et al., 2020. The ERA5 Global Reanalysis: Achieving a Detailed Record of the Climate and Weather for the Past 70 Years [Internet]. Available from: https://presentations.copernicus.org/EGU2020/EGU2020-10375_presentation.pdf

[75] Khadka, A., Wagnon, P., Brun, F., et al., 2022. Evaluation of ERA5-Land and HARv2 reanalysis data at high elevation in the upper Dudh Koshi basin (Everest region, Nepal). Journal of Applied Meteorology and Climatology. 61(8), 931-954. DOI: https://doi.org/10.1175/JAMC-D-21-0091.1

[76] Nayak, M.A., Azam, M.F., Lyngwa, R.V., 2021. ERA5-based database of atmospheric rivers over Himalayas. Earth System Science Data Discussions. (preprint). 1-35. DOI: https://doi.org/10.5194/essd-2020-397

[77] Karra, K., Kontgis, C., Statman-Weil, Z., et al. (editors), 2021. Global land use/land cover with Sentinel 2 and deep learning. 2021 IEEE International Geoscience and Remote Sensing Symposium IGARSS; 2021 Jul 11-16; Brussels, Belgium. New York: IEEE. p. 4704-4707. DOI: https://doi.org/10.1109/IGARSS47720.2021.9553499

[78] Nguyen, H.T.T., Doan, T.M., Tomppo, E., et al., 2020. Land Use/land cover mapping using multitemporal Sentinel-2 imagery and four classification methods—A case study from Dak Nong, Vietnam. Remote Sensing. 12(9), 1367. DOI: https://doi.org/10.3390/rs12091367

[79] Paul, K., Sharma, D., Mukherjee, R., et al., 2016. Demographic characteristics and changing land use pattern in Gangtok, Sikkim (1971-2011). International Journal of Geomatics and Geosciences. 6(4), 1769-1781.

[80] Kattel, G.R., 2022. Climate warming in the Himalayas threatens biodiversity, ecosystem functioning and ecosystem services in the 21st century: is there a better solution?. Biodiversity and Conservation. 31(8-9), 2017-2044. DOI: https://doi.org/10.1007/s10531-022-02417-6

[81] Pfeifer, L., Otto, I.M., 2023. Changing seasonal temperature offers a window of opportunity for stricter climate policy. Environmental Science & Policy. 140, 35-45. DOI: https://doi.org/10.1016/j.envsci.2022.11.010

[82] Chen, H., Sun, J., Lin, W., 2020. Anthropogenic influence would increase intense snowfall events over parts of the Northern Hemisphere in the future. Environmental Research Letters. 15(11), 114022. DOI: https://doi.org/10.1088/1748-9326/abbc93

[83] Davis, R.E., Lowit, M.B., Knappenberger, P.C., et al., 1999. A climatology of snowfall-temperature relationships in Canada. Journal of Geophysical Research: Atmospheres. 104(D10), 11985-11994. DOI: https://doi.org/10.1029/1999JD900104

[84] Kawase, H., Yamazaki, T., Sugimoto, S., et al., 2020. Changes in extremely heavy and light snow-cover winters due to global warming over high mountainous areas in central Japan. Progress in Earth and Planetary Science. 7(1), 1-17. DOI: https://doi.org/10.1186/s40645-020-0322-x

[85] Quante, L., Willner, S.N., Middelanis, R., et al., 2021. Regions of intensification of extreme snowfall under future warming. Scientific Reports. 11(1), 16621. DOI: https://doi.org/10.1038/s41598-021-95979-4

[86] Dimri, A.P., Kumar, P., Maharana, P., 2021. On the global contrasting temperature-precipitation phase mechanisms in the last century. Journal of Climate Change. 7(3), 9-21. DOI: https://doi.org/10.3233/JCC210015

[87] Sharma, A., Goyal, M.K., 2020. Assessment of the changes in precipitation and temperature in Teesta River basin in Indian Himalayan Region under climate change. Atmospheric Research. 231, 104670. DOI: https://doi.org/10.1016/j.atmosres.2019.104670

[88] Desinayak, N., Prasad, A.K., El-Askary, H.,

et al., 2022. Snow cover variability and trend over the Hindu Kush Himalayan region using MODIS and SRTM data. Annales Geophysicae. 40(1), 67-82.
DOI: https://doi.org/10.5194/angeo-2021-29

[89] Marshall, A.M., Link, T.E., Robinson, A.P., et al., 2020. Higher snowfall intensity is associated with reduced impacts of warming upon winter snow ablation. Geophysical Research Letters. 47(4), e2019GL086409.
DOI: https://doi.org/10.1029/2019GL086409

[90] O'Gorman, P.A., 2014. Contrasting responses of mean and extreme snowfall to climate change. Nature. 512(7515), 416-418.
DOI: https://doi.org/10.1038/nature13625

[91] Le, P.V., Randerson, J.T., Willett, R., et al., 2023. Climate-driven changes in the predictability of seasonal precipitation. Nature Communications. 14(1), 3822.
DOI: https://doi.org/10.1038/s41467-023-39463-9

[92] Pfeifer, L., Otto, I.M., 2023. Changing seasonal temperature offers a window of opportunity for stricter climate policy. Environmental Science & Policy. 140, 35-45.
DOI: https://doi.org/10.1016/j.envsci.2022.11.010

[93] Wang, J., Guan, Y., Wu, L., et al., 2021. Changing lengths of the four seasons by global warming. Geophysical Research Letters. 48(6), e2020GL091753.
DOI: https://doi.org/10.1029/2020GL091753

[94] Zhang, C., Mou, N., Niu, J., et al., 2021. Spatio-temporal variation characteristics of snow depth and snow cover days over the Tibetan Plateau. Water. 13(3), 307.
DOI: https://doi.org/10.3390/w13030307

[95] Banerjee, A., Kang, S., Meadows, M.E., et al., 2023. Quantifying climate variability and regional anthropogenic influence on vegetation dynamics in northwest India. Environmental Research. 234, 116541.
DOI: https://doi.org/10.1016/j.envres.2023.116541

[96] Karimi, S., Nawaz, M.A., Naseem, S., et al., 2021. The response of culturally important plants to experimental warming and clipping in Pakistan Himalayas. Plos One. 16(5), e0237893.
DOI: https://doi.org/10.1371/journal.pone.0237893

Appendix

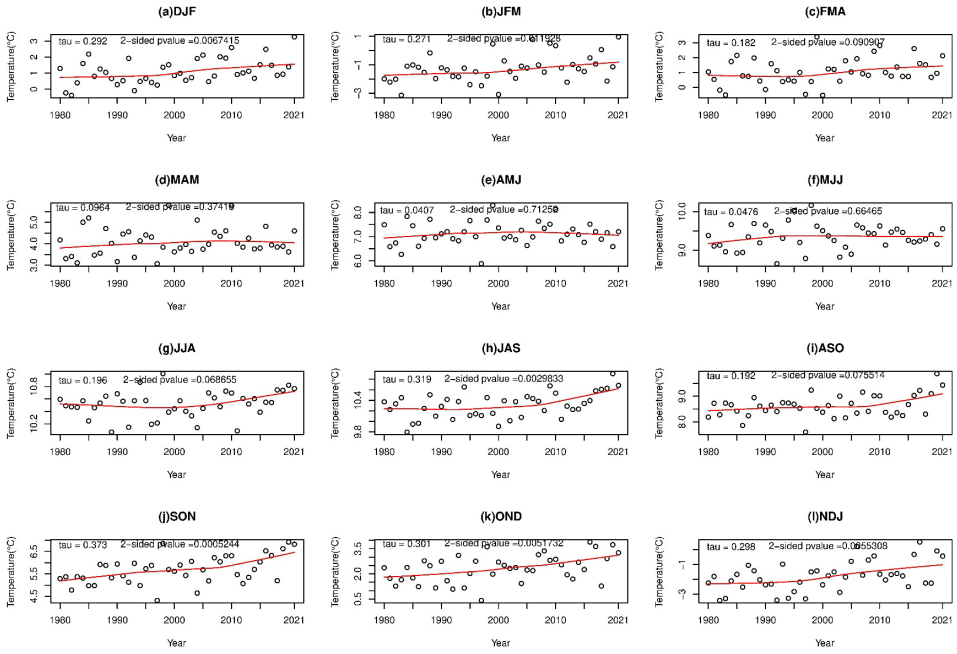

Figure S1. Mann-Kendall trend of temperature with significant t-test analysis; if the p-value is less than 0.05 the trend is significant, p-value greater than 0.05 shows the insignificant trend. The tau value suggests that the trend is negative or positive based on the sign of the tau values [(a) DJF, (b) JFM, (h) JAS, (i) ASO, (j) SON, (k) OND, and (l) NDJ are significant, remaining are insignificant].

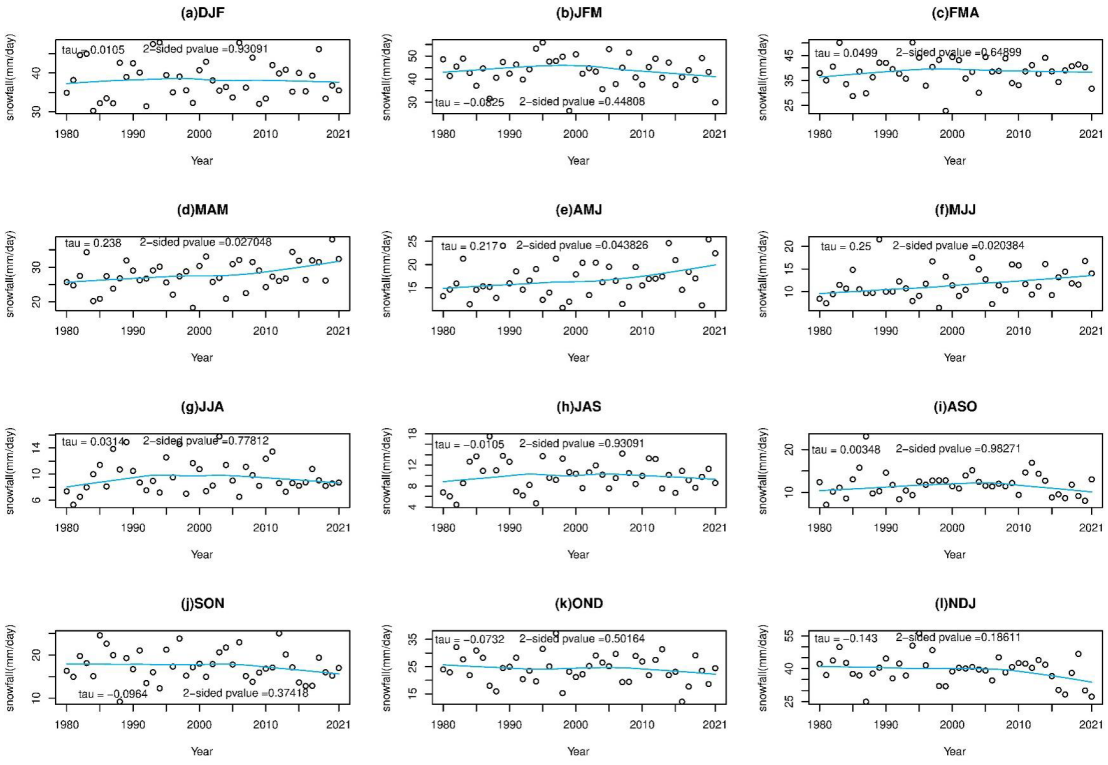

Figure S2. The Mann-Kendall trend of snowfall with significant t-test analysis; if the p-value is less than 0.05 the trend is significant. The tau value suggests that the trend is negative or positive based on the sign of the tau values [(d) MAM, (e) AMJ, and (f) MJJ are significant, remaining are insignificant].

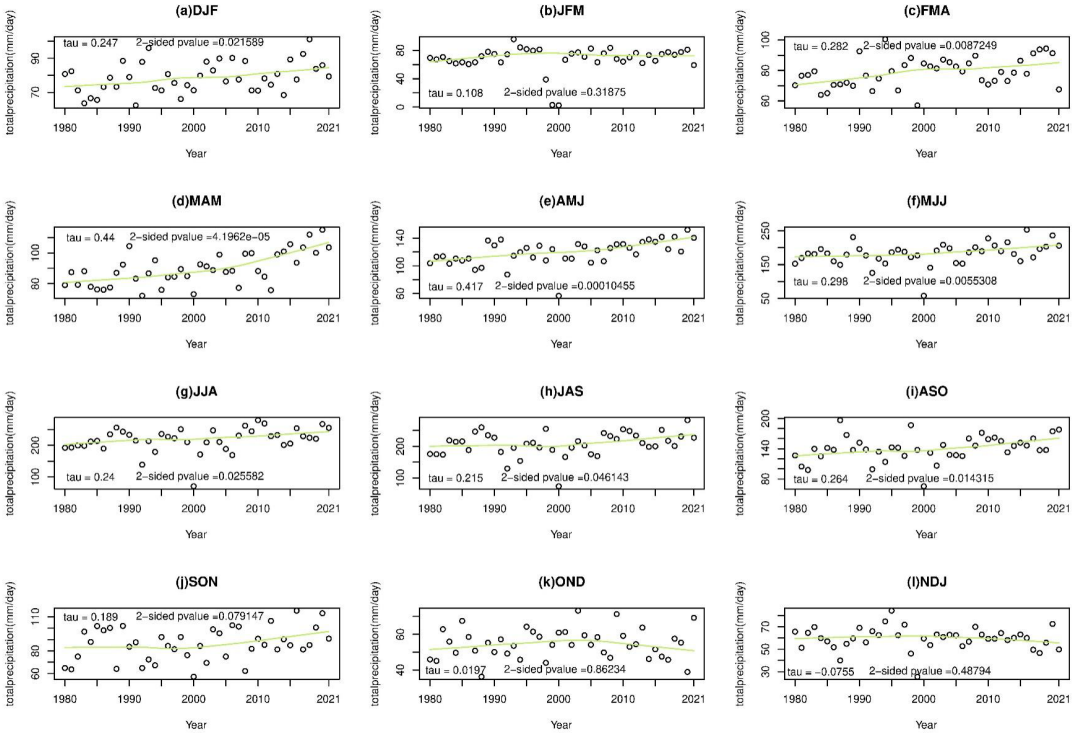

Figure S3. The Mann-Kendall trend of total precipitation with significant t-test analysis; if the p-value is less than 0.05 the trend is significant. The tau value suggests that the trend is negative or positive based on the sign of the tau values [(a) DJF, (c) FMA, (d) MAM, (e) AMJ, (f) MJJ, (g)JJA, (h) JAS, and (i) ASO, are significant, remaining are insignificant].

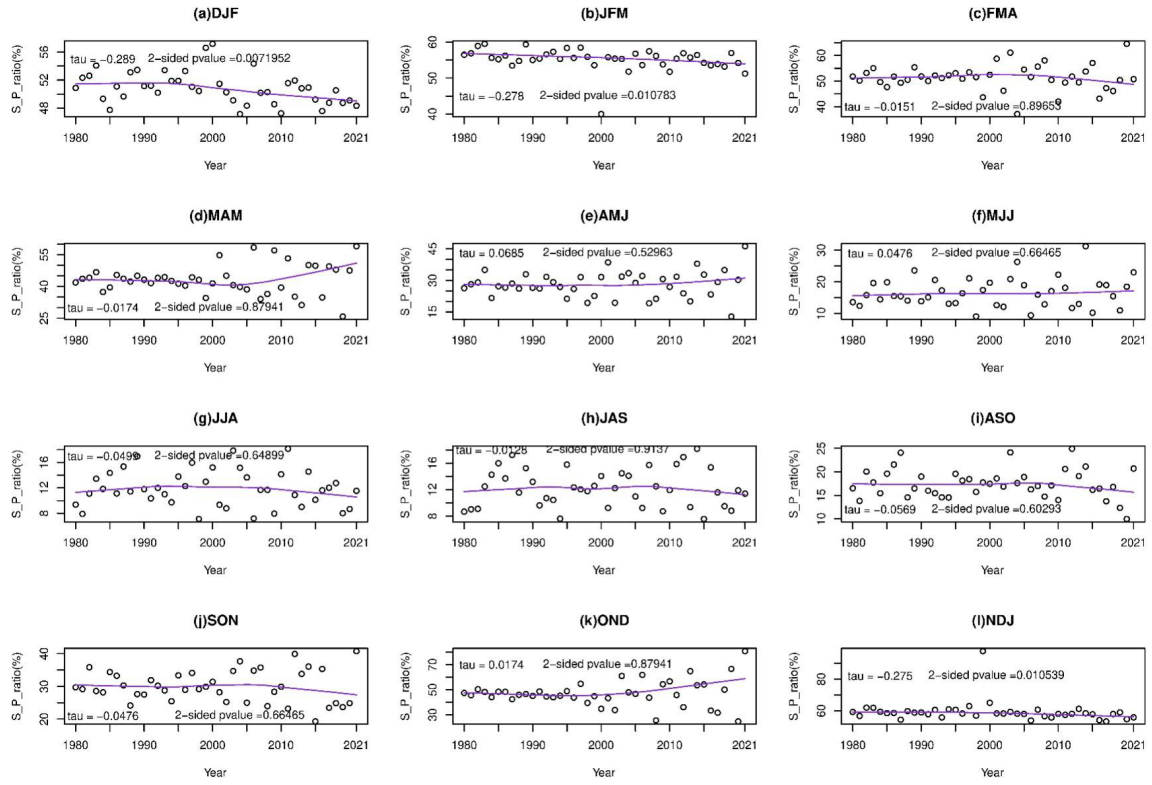

Figure S4. The Mann-Kendall trend of S/P ratio with significant t-test analysis; if the p-value is less than 0.05 the trend is significant. The tau value suggests that the trend is negative or positive based on the sign of the tau values [(a) DJF, (b) JFM, and (l) NDJ are significant, remaining are insignificant].

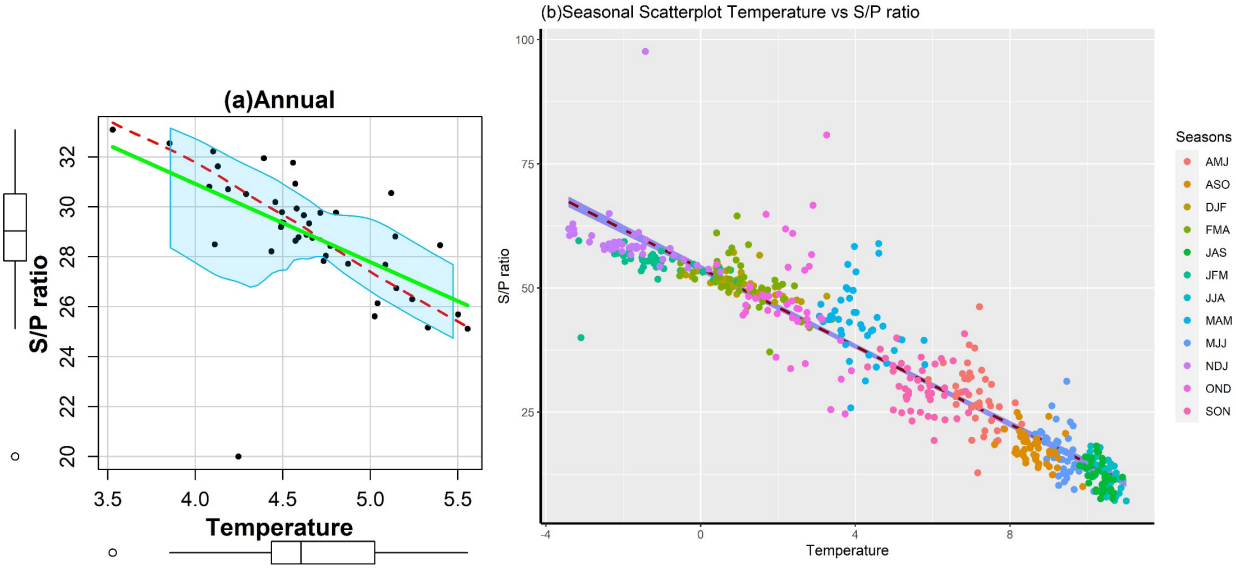

Figure S5. Scatterplot (a) annual, and (b) seasonal variations in temperature versus S/P ratio over Sikkim Himalaya for 1980 to 2021. Shading along the lines shows 95% significance confidence level.

Supplementary Method SM6

They suggested outlining the methodology for conducting the seasonal analysis and investigating the shifts in temperature, snowfall, and total precipitation. (1) Data Preparation: Organized the collected data into a suitable format for analysis, ensuring proper labelling and data integrity. Verify the accuracy and consistency of the data, checking for any missing values or outliers that may require handling. (2) Seasonal Classification: Defined the twelve seasons based on the chosen seasonal classification (DJF, JFM, FMA, MAM, AMJ, MJJ, JJA, JAS, ASO, SON, OND, NDJ) as described in the manuscript's methodology section. Group the data into these defined seasons by extracting the respective months' data for each season. (3) Seasonal Analysis: Calculate the seasonal means or sums for temperature, snowfall, and total precipitation within each defined season. Compare the seasonal values across different years to identify any temporal shifts or trends. (4) Visualization: Created visual representations such as line plots or bar graphs to depict the seasonal variations of temperature, snowfall, and total precipitation (**Figures 5, S1, S2, S3, S4, and S5b**). Overlayed the data from different years or seasons to visualize the shifts and identified notable patterns. (5) Statistical Analysis: Applied statistical methods (e.g., t-tests, regression analysis, and time series analysis) to quantitatively analyze the data and determine the significance of the observed shifts and trends.

A non-parametric method 'Theil-Sen estimator' is used for estimating the slope of a linear trend between snowfall and total precipitation. The present study opted for this method because it is easy to compute, can control outliers well, and doesn't make any conventions regarding the data's distribution. The steps have been used for the calculation of the Theil-Sen estimator trend analysis: (1) Sorted the data in ascending order based on the values of the independent variable (e.g., snowfall and total precipitation for 1981 to 2021). (2) For each pair of observations (x1, y1) and (x2, y2), compute the slope of the line connecting the two points as (y2 – y1)/(x2 – x1). (3) Stored all of the slopes computed in previous step in a list. (4). Computed the median of the list of slopes computed in previous step. Now we found the Theil-Sen estimator for the slope of the linear trend for snowfall and total precipitation. (5) Computed the intercept of the line using the median slope and the median values of the independent (snowfall) and dependent (total precipitation) variables.

Equation (3) provided in the methodology section shows the calculation of the slope of a linear trend using the long-term averages of two variables (snowfall and total precipitation), and their logarithms. The first expression of Equation (3) is the derivative of the ratio of the partial derivatives of the variables S (snowfall) and P (total precipitation) with respect to P. This expression calculates the slope of the linear trend between S and P using the partial derivatives of the variables. The second expression of Equation (3) is a simplified version of the first expression, using the long-term averages of S and P, and their logarithms. It calculates the slope of the linear trend using the average values and the partial derivatives of the logarithms of S and P over the study period (1980-2021). The terms (∂lnS) and (∂lnP) represent the linear trends of the logarithms of snowfall and total precipitation, respectively, over the study period. These terms are calculated using the Theil-Sen estimator method explained earlier, as applied to the logarithms of the variables.

Supplementary Method SM7

LULC Class

Water: Areas where water was predominantly present throughout the year; may not cover areas with sporadic or ephemeral water; contains little to no sparse vegetation, no rock outcrop nor built up features like docks; examples: rivers, ponds, lakes, oceans, flooded salt plains.

Trees: Any significant clustering of tall (~15-m or higher) dense vegetation, typically with a closed or dense canopy; examples: wooded vegetation, clusters of dense tall vegetation within savannas, plantations, swamp or mangroves (dense/tall vege-

tation with ephemeral water or canopy too thick to detect water underneath).

Flooded vegetation: Areas of any type of vegetation with obvious intermixing of water throughout a majority of the year; seasonally flooded area that is a mix of grass/shrub/trees/bare ground; examples: flooded mangroves, emergent vegetation, rice paddies and other heavily irrigated and inundated agriculture.

Crops: Humans planted/plotted cereals, grasses, and crops not at tree height; examples: corn, wheat, soy, fallow plots of structured land.

Built Area: Human made structures; major road and rail networks; large homogenous impervious surfaces including parking structures, office buildings and residential housing; examples: houses, dense villages/towns/cities, paved roads, asphalt.

Bare ground: Areas of rock or soil with very sparse to no vegetation for the entire year; large areas of sand and deserts with no to little vegetation; examples: exposed rock or soil, desert and sand dunes, dry salt flats/pans, dried lake beds, mines.

Snow/Ice: Large homogenous areas of permanent snow or ice, typically only in mountain areas or the highest latitudes; examples: glaciers, permanent snowpack, snow fields.

Clouds: No land cover information due to persistent cloud cover.

Rangeland: Open areas covered in homogenous grasses with little to no taller vegetation; wild cereals and grasses with no obvious human plotting (i.e., not a plotted field); examples: natural meadows and fields with sparse to no tree cover, open savanna with few to no trees, parks/golf courses/lawns, pastures. A mix of small clusters of plants or single plants dispersed on a landscape that shows exposed soil or rock; scrub-filled clearings within dense forests that are clearly not taller than trees; examples: moderate to sparse cover of bushes, shrubs and tufts of grass, savannas with very sparse grasses, trees or other plants.

BILINGUAL PUBLISHING GROUP

Journal of Atmospheric Science Research

https://journals.bilpubgroup.com/index.php/jasr

ARTICLE

Spatial and Temporal Variation of Particulate Matter (PM10 and PM2.5) and Its Health Effects during the Haze Event in Malaysia

Afiqah Ma'amor[1], Norazian Mohamed Noor[1,2*], Izzati Amani Mohd Jafri[1,2], Nur Alis Addiena[1,2], Ahmad Zia Ul Saufie[3], Nor Azrita Amin[4], Madalina Boboc[5], Gyorgy Deak[5]

[1] Faculty of Civil Engineering & Technology, Universiti Malaysia Perlis, Jejawi, Arau, Perlis, 02600, Malaysia

[2] Sustainable Environment Research Group (SERG), Centre of Excellence Geopolymer and Technology (CEGeoGTech), Jejawi, Arau, Perlis, 02600, Malaysia

[3] Faculty of Computer and Mathematical Sciences, Universiti Teknologi Mara (UiTM), Shah Alam, 40450, Malaysia

[4] Institute of Engineering Mathematics, Universiti Malaysia Perlis, Pauh Putra Campus, Arau, Perlis, 02600, Malaysia

[5] National Institute for Research and Development in Environmental Protection INCDPM, Splaiul Independentei 294, Bucharest, 060031, Romania

ABSTRACT

This study aims to assess and compare levels of particulate matter (PM10 and PM2.5) in urban and industrial areas in Malaysia during haze episodes, which typically occur in the south west monsoon season. The high concentrations of atmospheric particles are mainly due to pollution from neighbouring countries. Daily PM concentrations were analysed for urban and industrial areas including Alor Setar, Tasek, Shah Alam, Klang, Bandaraya Melaka, Larkin, Balok Baru, and Kuala Terengganu in 2018 and 2019. The analysis employed spatiotemporal to examine how PM levels were distributed. The data summary revealed that PM levels in all study areas were right-skewed, indicating the occurrence of high particulate events. Significant peaks in PM concentrations during haze events were consistently observed between June and October, encompassing the south west monsoon and inter-monsoon periods. The study on acute respiratory illnesses primarily focused on Selangor. Analysis revealed that Klang had the highest mean number of inpatient cases for acute exacerbation of bronchial asthma (AEBA) and acute exacerbation of chronic obstructive pulmonary disease (AECOPD) with values of 260.500 and 185.170, respectively. Similarly, for outpatient cases of AEBA and AECOPD, Klang had the highest average values of 41.67 and 14.00, respectively. Shah Alam and Sungai Buloh did not show a significant increase in cases during periods of biomass burning. The statistical analysis concluded that higher concentrations of PM were associated with increased hospital admissions, particularly from June to September, as shown in the bar diagram. Haze episodes were associated with more healthcare utilization due to haze-related respiratory illnesses, seen in higher inpatient and outpatient visits ($p < 0.05$). However, seasonal variability had minimal impact on healthcare utilization. These findings offer a comprehensive assessment of PM levels during historic haze episodes, providing valuable insights for authorities to develop policies and guidelines for effective monitoring and mitigation of the negative impacts of haze events.

Keywords: Haze; Particulate matter (PM10 and PM2.5); AEBA and AECOPD; Spatial variability

*CORRESPONDING AUTHOR:

Norazian Mohamed Noor, Faculty of Civil Engineering & Technology, Universiti Malaysia Perlis, Jejawi, Arau, Perlis, 02600, Malaysia; Sustainable Environment Research Group (SERG), Centre of Excellence Geopolymer and Technology (CEGeoGTech), Jejawi, Arau, Perlis, 02600, Malaysia; Email: norazian@unimap.edu.my

ARTICLE INFO

Received: 2 August 2023 | Revised: 3 October 2023 | Accepted: 8 October 2023 | Published Online: 16 October 2023

DOI: https://doi.org/10.30564/jasr.v6i4.5873

CITATION

Ma'amor, A., Noor, N.M., Jafri, I.A.M., et al., 2023. Spatial and Temporal Variation of Particulate Matter (PM10 and PM2.5) and Its Health Effects during the Haze Event in Malaysia. Journal of Atmospheric Science Research. 6(4): 26-47. DOI: https://doi.org/10.30564/jasr.v6i4.5873

1. Introduction

The haze event is defined as the presence of fine particles (0.1-1.0 μm in diameter) dispersed at a high concentration through a portion of the atmosphere that diminishes the horizontal visibility, giving the atmosphere a characteristic opalescent appearance [1]. In the meantime, China Meteorological Administration defined haze as a pollution phenomenon that cuts atmospheric visibility to 10 km due to complex materials that are suspended in the atmosphere, such as solid or liquid particulates, dust, smoke, and vapour [2]. Due to a toxic mixture of air pollutants, including particulate matter and toxic gases, that are impacted by weather patterns including ambient temperature, relative humidity, and wind speed, these circumstances enhance the severity of the air quality [3]. Since the 1980s until recently, Malaysia has endured this terrible phenomenon for a decade. Whenever the relative humidity is less than 80% and vision is less than 10 km, haze is observed if the surrounding air has a high concentration of particulate matter remaining in the air, which could or could not been seen with the naked eye [4].

Transboundary smoke haze from open biomass burning in Indonesia can affect Malaysia's air quality. This environmental issue is a seasonal occurrence [5]. Haze pollution, caused by the burning of forests, has been identified as a global environmental issue affecting South East Asian countries such as Malaysia, Singapore, Indonesia, Brunei Darussalam, and Southern Thailand [6]. Haze occurs in Indonesia because of recurring biomass burning, including wildfires, wetlands, and agricultural burning. The effect of uncertain monsoon rain as well as the El-Nino event are worsening the transboundary haze given the long and dry meteorological conditions, particularly throughout the south west monsoon condition [7].

Indonesia, being the largest global producer, relies heavily on palm oil production as its primary economic driver. The country supplies approximately half of the world's palm oil. This industry has witnessed a remarkable surge, escalating from 157,000 tonnes in 1964 to an astounding 43.5 million tonnes in 2020 [8]. The islands of Borneo and Sumatra are the primary contributors to Indonesia's palm oil output. Unfortunately, a prevalent practice among many landholders involves the deliberate burning of forests and peatlands to facilitate clearance, drainage, and subsequent replanting for industrial plantation purposes [9].

Regrettably, this method leads to the occurrence of haze, an atmospheric phenomenon, which can disperse to neighboring nations such as Malaysia, Singapore, and other countries in South-east Asia [10]. This dispersion is influenced by key meteorological factors including temperature (T), relative humidity (RH), wind speed (WS), and wind direction (WD). During haze episodes, there is a significant increase in the concentration of particulate matter, particularly those with an aerodynamic diameter equal to or less than 10 μm (PM10), in the surrounding air. These concentrations often exceeded the Malaysian Ambient Air Quality Standard (MAAQS) for PM10, which is set at 100 $\mu g/m^3$ for a 24-hour average [11].

Typically, the seasonal transboundary haze occurs due to the release of smoke from combustion, resulting in high concentrations of airborne particulate matter. Most of these particles have a size of less than 2.5 microns (PM2.5), allowing them to remain suspended in wind currents for extended durations. Furthermore, their small size enables them to penetrate deep into the respiratory tract of humans [12]. During seasonal haze episodes, there is a noticeable exacerbation of asthma and other respiratory-related symptoms in the short term. However, the long-term health implications of intermittent extreme episodes of seasonal haze exposure are still not well understood. While some studies have indicated a potentially elevated risk of chronic diseases like lung cancer, these findings have primarily been observed in the context of chronic exposure [13,14].

Consequently, lack of conclusive evidence regarding the potential health impacts of haze-induced morbidity in developing countries within ASEAN especially Malaysia. Therefore, further research particularly in Malaysia is necessary to facilitate more effective public health planning in the future. Taking this into account, the objective of this study

is to identify the spatiotemporal patterns of particulate matter (PM10 and PM2.5 level) and assess the potential health impacts of seasonal haze exposure resulting from biomass burning in Malaysia using statistical methods.

2. Materials and methods

2.1 Study area and dataset

In this research, the daily measurement data (2018-2019) for PM10 and PM2.5 of air monitoring stations in Peninsular Malaysia were collected from the Department of Environmental (DOE) Malaysia. This study focused on peninsular Malaysia with certain locations including Shah Alam and Klang (Selangor), Bandaraya Melaka (Melaka), Balok Baru (Kuantan), Larkin (Johor Bahru), Alor Setar (Kedah), Kuala Terengganu (Terengganu) and Tasek (Ipoh) since peninsular Malaysia are closer to Sumatera and are more densely populated [11] as well as have experienced significant haze events in the past, making them relevant study sites for understanding the historical and ongoing impacts of transboundary haze. Besides, these areas have established research infrastructure, including monitoring stations and data collection systems [15]. This infrastructure can provide a valuable foundation for conducting comprehensive studies on the effects of transboundary haze. The air quality dataset that was acquired from the Department of Environment, Malaysia was commonly subjected to standard quality control processes and quality assurance procedures [16]. The procedures that were used in the monitoring stations followed the standards outlined States Environmental Protection Agency (USEPA) [17].

Figure 1 shows the location of the study area in Peninsular Malaysia. **Table 1** provides a detailed description of the selected monitoring areas and the climatic conditions such as the average wind speed (m/s), relative humidity (%) and temperature (°C). The lowest wind speed was observed in Shah Alam and Larkin (0.89 m/s) whereas the highest temperature was recorded in Klang (28.4 °C) and Melaka (28.2 °C).

There was no exact article that mentioned the starting and end date of haze episode in 2019 but there was one newspaper article written by Sinar Harian dated 21st September 2019 mentioned that the hazy weather that hit the region of the country was expected to improve within the week due to the monsoon transition phase [18]. In addition, it was reported by the Department of Environment [19] that air quality in Malaysia is considered rather degraded, as the annual mean PM2.5 concentration was about 20 μg m^{-3} in 2019, thus exceeding the limit set by WHO.

In addition, the health data for two consecutive years (2018-2019) of monthly in-patients and out-patients diagnosed with Acute Exacerbation of Bronchial Asthma (AEBA) and Acute Exacerbation of Chronic Obstructive Pulmonary Disease (AECOPD) due to the association with particulate matter during haze events were collected from the Ministry of Health (MOH). Respiratory health data from eight hospitals in Peninsular Malaysia were used for the analysis. However, due to limited cooperation from some hospitals, the respiratory health data were only obtained from hospitals in Selangor.

2.2 Contour plot (ArcGIS and Kriging Method)

GIS is a significant tool for monitoring and analysing air quality. GIS has been used in certain significant studies for geographical and temporal characterization of emitted air pollutants [20]. A spatial interpolation method is one of the common techniques for mapping air pollution [21]. Furthermore, incorporating spatial analysis in GIS can assist researchers in expanding their understanding of the distribution of pollutants in specific locations or areas, as well as understanding the factors that influence trends and significance. The spatial map may give an initial overview of the potential health risks faced by people living in areas with high levels of air pollution [22].

Interpolation involves utilizing sample data from neighboring locations and considering spatial autocorrelation-variogram to predict the pollutant values in areas where direct measurements are not available. By leveraging GIS and interpolation techniques,

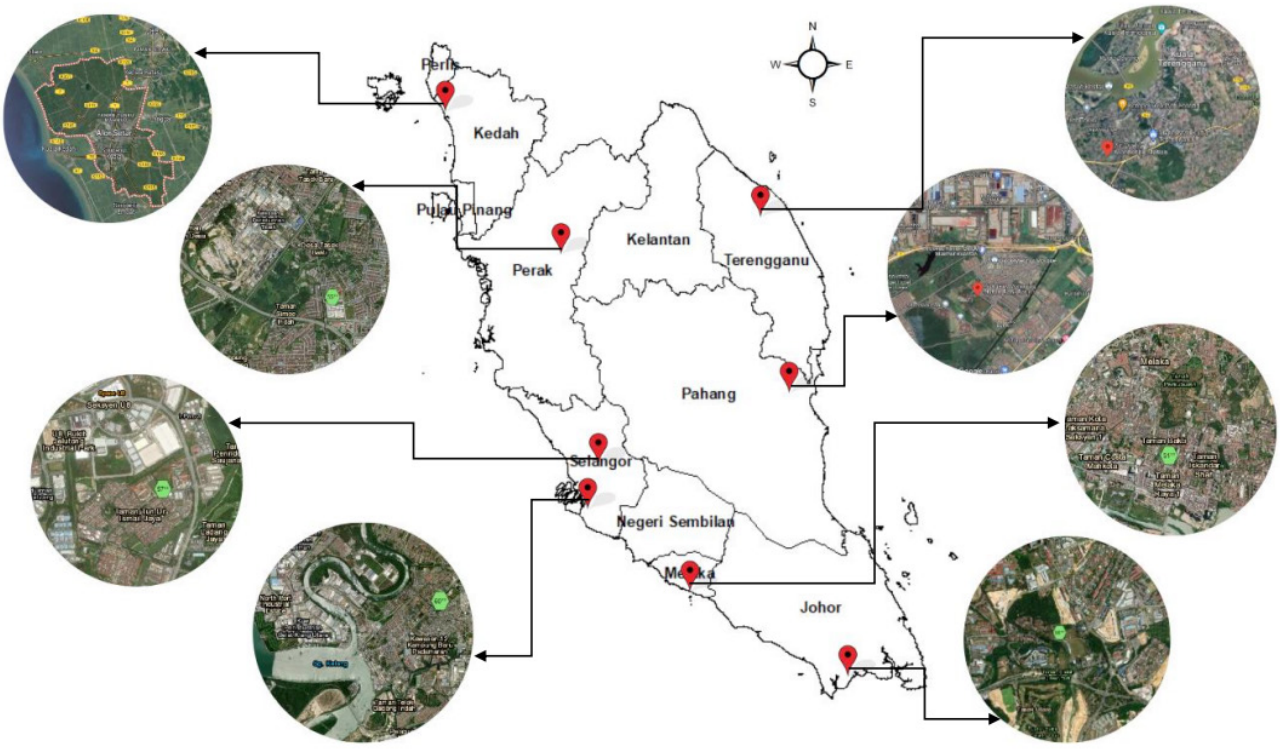

Figure 1. Air quality monitoring station in Peninsular Malaysia.

Table 1. Air quality monitoring station.

Monitoring location	Area	Coordinates	Background	Average wind speed (m/s)	Average relative humidity (%)	Average temperature (°C)
Secondary Islamic School of Kedah	Alor Setar	N 6.213148 E 100.329915	Urban	1.33	79.10	27.92
Jalan Tasek National Secondary School	Tasek	N 4.630805 E 101.117826	Industrial	1.28	74.71	27.69
TTDI Jaya Primary School	Shah Alam	N 3.104710 E 101.556179	Urban	0.86	78.24	27.49
Raja Zarina Secondary Girls School	Klang	N 3.009994 E 101.408374	Urban	1.38	78.55	28.40
Melaka Secondary High School	Bandaraya Melaka	N 2.191726 E 102.254588	Urban	1.41	78.02	28.24
IPG, Campus Temenggong Ibrahim	Larkin	N 1.492353 E 103.738014	Industrial	0.89	83.47	27.59
Balok Baru Primary School	Balok Baru	N 3.96175 E 103.38212	Industrial	1.94	82.28	26.79
Pusat Chabang Tiga Primary School	Kuala Terengganu	N 5.306791 E 103.122190	Urban	1.26	82.44	26.88

it becomes possible to gain additional insights into the distribution of PM10 and PM2.5 beyond the coverage of monitoring stations. In this study, spatial analysis was performed using Ordinary Kringing Interpolation Method (OKM) using ArcGIS software version 10.5 to analyze the continuous distribution of PM10 and PM2.5 concentration for all the stations [23]. Compared with the Inverse Distance Weighted (IDW) interpolation method, the output of the OKM has better continuity. In addition, OKM is widely applied to study the spatiotemporal distribution of air quality, and the corresponding model has the best superiority in cross validation [24].

3. Results and discussion

3.1 Temporal analysis of particulate matter concentration

Table 2 presented data on the concentration of particulate matter (PM) in the eight different locations over a two-year period. According to the Malaysian Ambient Air Quality Standard (MAAQS) interim target 2 (IT-2), the recommended limit for the 1-year average of PM10 is 45 μg/m^3. The mean PM10 values in the selected study areas for all stations were below this threshold, however, the mean values of PM10 and PM2.5 level for all stations in 2018 and 2019 exceeded their median values, suggesting that the distribution of the data were skewed or extreme concentrations of PM10 were present during those years.

Overall, the mean values observed in all stations during the two years were higher than the median values, indicating a positively skewed distribution of PM10 concentrations. This suggests a higher likelihood of PM10 measurements exceeding the permissible value of MAAQS (IT-2), which was 120 μg/m^3 for the 24-hour average. The skewness values, mostly greater than +1 in most areas, further indicate that the data was highly skewed to the right.

In 2019, the maximum PM10 concentration was recorded as the highest value compared to all study areas during the two-year period. Bandaraya Melaka and Klang had the highest concentrations, with measurements of 173.897 μg/m^3 and 163.536 μg/m^3 respectively. Alor Setar, Tasek, Shah Alam, Larkin, Balok Baru, and Kuala Terengganu recorded their highest PM10 concentrations ranging from 80.015 μg/m^3 to 156.553 μg/m^3. In general, most of the maximum values in each year of the study exceeded the MAAQS.

For PM2.5, the MAAQS sets a guideline of 25 μg/m^3 for the 1-year average. The mean PM2.5 values in the study area, which is primarily categorized as an urban industrial area, exceeded this standard. Similar to PM10, the mean values of PM2.5 concentration for all stations in 2018 and 2019 exceeded their median values, indicating the concentration was right skewed hence signifying the extreme concentrations of PM2.5 during those years. This suggests a positively skewed distribution of PM2.5 concentrations, with a higher possibility of exceeding the permissible value of MAAQS, which is 50 μg/m^3 for the 24-hour average.

The highest PM2.5 concentration in 2019 was recorded in Bandaraya Melaka and Shah Alam, with measurements of 151.105 μg/m^3 and 144.917 μg/m^3, respectively, compared to the other study areas. The standard deviation indicates that the PM2.5 measurements showed more variability, with a higher range of PM2.5 levels observed in Shah Alam. In general, the concentrations of PM10 and PM2.5 in 2019 were significantly higher compared to 2018, indicating the occurrence of an intense haze event during 2019. Despite the lower particulate matter concentration in 2018, it still exceeded the standard value set by the MAAQS.

Daily variations of particulate matter PM10 and PM2.5 were shown in **Figures 2 and 3** respectively. The black solid line indicates the Malaysian Ambient Air Quality Standard (MAAQS) for 24-hour average time which was 120 μg/m^3 for PM10 and 50 μg/m^3 for PM2.5. Seasonal patterns were clearly observed in **Figure 3** in which higher PM10 concentration values can be seen during the South west monsoon (June to September). During this period, almost all air quality monitoring stations in the Malaysian Peninsular area were affected by the transboundary

Table 2. Data summary of PM10 and PM2.5 concentration.

Stations	Statistics	2018		2019	
		PM10 (μg/m³)	PM2.5 (μg/m³)	PM10 (μg/m³)	PM2.5 (μg/m³)
Alor Setar	N (Valid)	365	365	365	365
	Mean	21.514	14.659	22.278	16.103
	Median	19.116	12.336	19.026	12.804
	Std Dev	10.756	9.264	12.710	10.989
	Variance	115.683	85.828	161.554	120.762
	Skewness	2.392	2.919	1.730	2.198
	Minimum	6.072	3.335	5.516	3.288
	Maximum	95.089	84.178	80.015	71.074
Tasek	N (Valid)	365	365	365	365
	Mean	28.757	18.752	31.142	22.843
	Median	28.627	17.862	27.199	18.889
	Std Dev	9.969	6.949	17.653	16.032
	Variance	99.377	48.293	311.639	257.040
	Skewness	0.858	1.568	3.470	3.471
	Minimum	11.266	6.702	11.113	6.606
	Maximum	78.185	60.630	149.742	133.332
Shah Alam	N (Valid)	365	365	365	365
	Mean	34.508	25.202	41.989	32.138
	Median	32.898	23.773	37.129	27.273
	Std Dev	10.367	8.148	21.607	19.708
	Variance	107.485	66.384	466.842	388.392
	Skewness	0.721	0.832	2.643	2.961
	Minimum	11.757	8.155	15.023	10.111
	Maximum	78.380	62.641	156.553	144.917
Klang	N (Valid)	365	365	365	365
	Mean	40.898	27.787	41.419	33.037
	Median	39.889	25.976	36.104	28.909
	Std Dev	15.730	11.234	22.582	18.517
	Variance	247.440	126.197	509.967	342.864
	Skewness	1.319	2.387	2.597	2.930
	Minimum	13.588	9.210	11.688	9.764
	Maximum	135.369	117.015	163.536	140.321
Bandaraya Melaka	N (Valid)	365	365	365	365
	Mean	25.595	18.692	30.624	23.491
	Median	23.542	16.847	24.797	18.782
	Std Dev	10.780	8.890	21.125	18.348
	Variance	116.200	79.027	446.273	336.656
	Skewness	1.660	2.400	2.947	3.092
	Minimum	7.571	3.200	9.147	5.223
	Maximum	98.075	94.033	173.897	151.105

Table 2 continued

Stations	Statistics	2018		2019	
		PM10 (μg/m³)	PM2.5 (μg/m³)	PM10 (μg/m³)	PM2.5 (μg/m³)
Larkin	N (Valid)	365	365	365	365
	Mean	29.248	20.479	35.604	24.660
	Median	27.554	19.629	31.812	21.492
	Std Dev	8.625	6.783	16.139	14.180
	Variance	74.386	46.011	260.472	201.063
	Skewness	0.633	0.592	2.584	2.658
	Minimum	8.184	5.285	10.339	6.750
	Maximum	56.704	42.954	135.588	112.243
Balok Baru	N (Valid)	365	365	365	365
	Mean	28.555	17.846	33.818	23.184
	Median	27.025	16.431	28.755	18.177
	Std Dev	9.934	7.754	18.587	17.400
	Variance	98.694	60.129	345.492	302.743
	Skewness	0.534	0.887	2.704	2.765
	Minimum	7.316	3.533	9.965	4.563
	Maximum	58.324	47.538	141.645	129.584
Kuala Terengganu	N (Valid)	365	365	365	365
	Mean	25.344	17.343	28.862	19.738
	Median	24.334	16.324	26.175	17.291
	Std Dev	10.169	8.138	14.072	12.840
	Variance	103.417	66.224	198.032	164.860
	Skewness	0.997	0.851	2.735	2.766
	Minimum	6.057	3.011	8.325	3.566
	Maximum	76.347	53.167	118.189	103.259

sources of biomass burning from Sumatra, Indonesia [21]. In 2018, the level of PM10 began to increase in early May and reached its peak by the end of September and October. This peak can be clearly observed before weakening in November when the arrival of delayed monsoonal rain helped extinguish fires and improve air quality in the region [22]. During the peak period, all study areas were found to have similar intensities of PM10 levels.

However, Klang recorded the highest concentration, with levels reaching almost 135.659 μg/m^3, exceeding the 120 μg/m^3 threshold set for a 24-hour duration. Conversely, the lowest concentration of PM10 during the peak was observed in Larkin, with a concentration of 56.704 μg/m^3. In early March, Melaka exhibited a higher PM10 concentration, although it did not exceed the MAAQS value. Overall, a significant peak in PM10 concentration was observed from June during the south west monsoon until the inter-monsoon period in October. Although Melaka experienced higher PM10 concentrations in early March, it remained within the acceptable MAAQS limits. In general, all monitoring stations recorded PM10 concentrations below the standard value, except for Klang.

Meanwhile, in 2019, the concentration of PM10 was significantly higher compared to 2018. It was evident that haze events occurred more frequently, starting around June and lasting until October, with the peak period observed in September and October. However, for certain locations like Shah Alam, Klang, and Melaka, the peak extended until the end of December. Among these areas, Melaka recorded the highest PM10 concentration at 173.897 μg/m^3,

followed by Klang and Shah Alam with 163.536 μg/m^3 and 156.553 μg/m^3 respectively. The distribution of pollutants during this period was likely influenced by monsoons.

The transboundary air pollution resulting from the burning of fires on Indonesia's Sumatra Island was a major contributor to the haze event. Strong winds carried the smoke across the Melaka Strait during the south west monsoon season. The peak concentration levels of PM10 were mostly detected from June to September, coinciding with the south west monsoon when low-level winds facilitated the long-range transport of pollutants [22]. These fine particles were able to be transported across borders from Sumatra and Kalimantan, moving northward to peninsular Malaysia due to the prevailing regional wind direction [25].

The daily concentrations of PM2.5 in all study areas mostly exceed the standard value of the Malaysian Ambient Air Quality Standard (MAAQS) for 24-hour which is 50 μg/m^3 (**Figure 3**). The concentration of PM2.5 was higher during the haze episode than before it. The highest PM2.5 value was 117.015 μg/m^3 in Klang in 2018 and 151.105 μg/m^3 in Melaka in 2019. Each highest result was in June to September which may be related to the South west Monsoon. During the haze episode, the smoke from Sumatra will travel to Peninsular Malaysia. In most cases, all the stations located on the west coast of Peninsular Malaysia have similar patterns of PM2.5

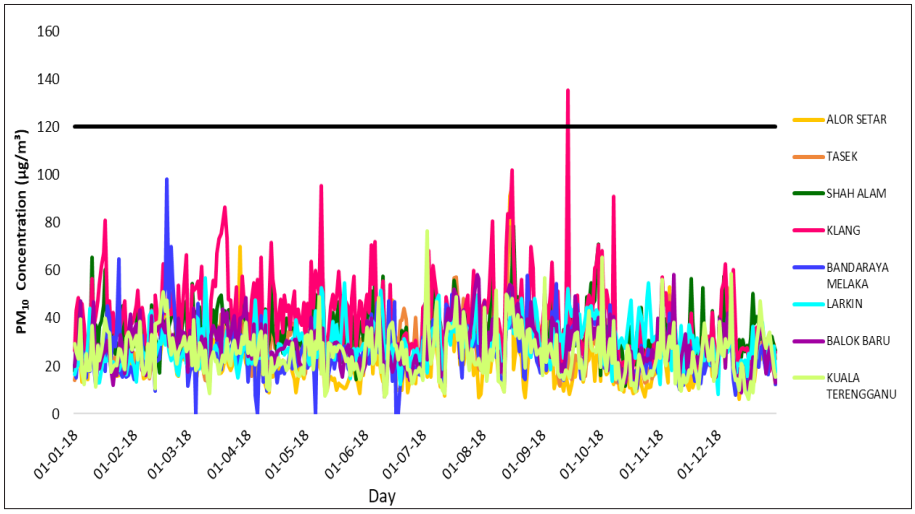

(a)

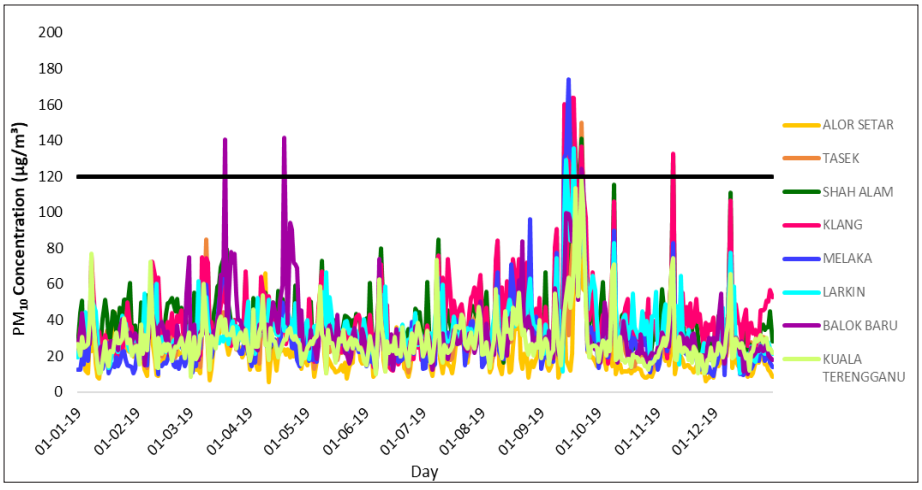

(b)

Figure 2. Daily time-series plot of PM10 concentration (a) 2018 and (b) 2019.

concentration during the haze episode based on the intensity of the smoke and wind direction.

On top of that, Balok Baru, Kuantan recorded the highest peak in late March until late May. During this period, the eastern coast of peninsular Malaysia was influenced by the northeast monsoon, which brought dry and stagnant weather conditions. These conditions can lead to the accumulation of pollutants in the air, resulting in higher PM2.5 concentrations [26]. Besides, Balok Baru, being an urban area with industrial activities and transportation, has local pollution sources that contribute to the higher PM10 levels. Industrial emissions, vehicle exhaust, and construction activities can all release particulate matter into the air, increasing the concentration of PM10.

South west monsoon largely influenced phases of the El Nino phenomenon [27]. These dry conditions coupled with the warm temperatures associated with El Nino create an extremely favorable and conducive environment for large-scale outbreaks in Sumatra and Kalimantan. PM2.5 concentrations were strongly affected by meteorological parameters such as wind direction, wind speed, temperature, and relative humidity [4]. At low wind speeds, the atmosphere tends to stabilize and spread slowly, and discharged contaminants easily accumulate, resulting in a higher concentration of particulate matter [22]. Lower wind speeds might inhibit the dispersion of pollutants in

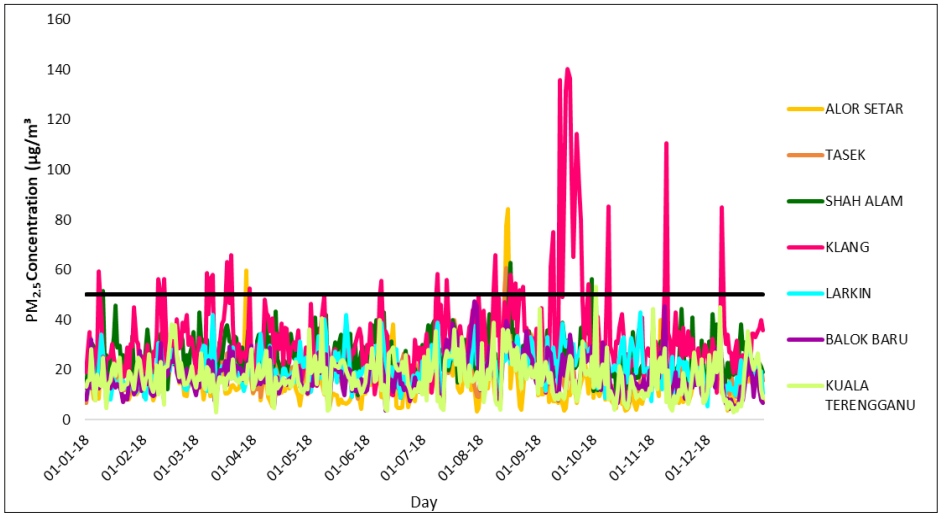

(a)

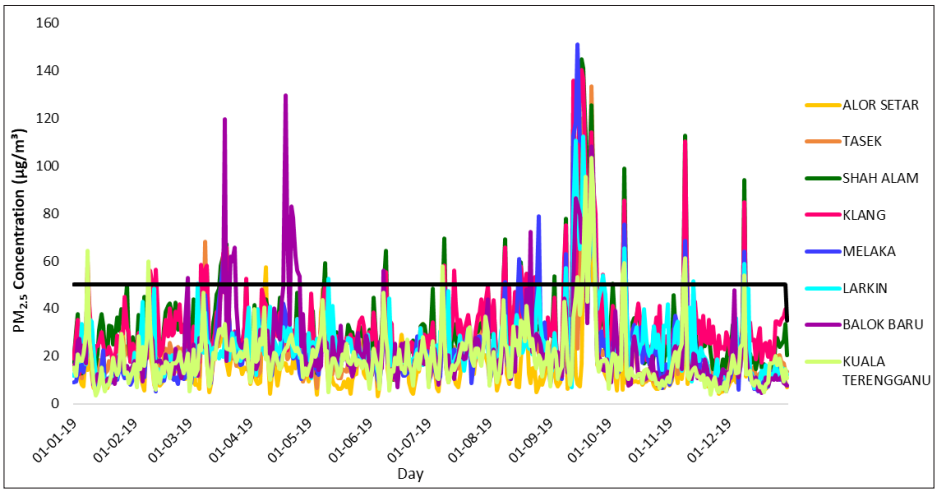

(b)

Figure 3. Daily time-series plot of PM2.5 concentration (a) 2018 and (b) 2019.

vertical and horizontal directions, while higher temperatures and humidity promote gas-to-particle conversion and generate secondary aerosols [28].

3.2 Spatial variation of particulate matter concentration

Monthly variations of PM10 and PM2.5 concentration for all study areas were analyzed by using contour plots as depicted in **Figures 4 and 5**. The spatial variation of PM10 and PM2.5 for selected study areas showed spatial variability from January to December. In general, the levels of PM10 concentration were in the range of 19 to 74 μg/m^3 while PM2.5 concentration was in the range of 13 to 61 μg/m^3 from January to December. From January to March, Klang and Shah Alam stations recorded elevated PM10 and PM2.5 concentrations of between 38 to 46 and 29 to 35 respectively and the other stations also displayed a similar but smaller distribution range while Melaka showed the highest PM10 and PM2.5 concentration in April.

However, monthly PM10 and PM2.5 concentration was observed higher from May until September which was during the south west monsoon. From previous analysis, it can be determined that seasonal variation of PM10 and PM2.5 levels seem much related to south-westerly winds which coincides with the regional biomass burning period which starts around May and lasts until September. The seasonal variations, El Nino modulation enhance the effects of haze and the pollutants concentration in the region during the south west monsoon dry season [29]. Overall, the highest monthly concentration was observed during the end of the south west monsoon especially in August and September whereas the concentration dropped in November when the north east monsoon started.

A study by Elhadi et al. [30] revealed that the south west monsoon wind from Sumatra reaches the central area of peninsular Malaysia within 48-h during south west monsoon season prevailing every year. Overall, the higher PM10 and PM2.5 observed during the south west monsoon season were influenced by local sources of emissions. In addition, low wind speeds, low temperature, low humidity, and low rainfall promote higher concentrations of PM2.5 and PM10, especially during this season [31]. On top of that, spatial variation in particulate matter levels has been observed during the wet season which is north east monsoon. A Low level of particulate matter can be seen from November until March with the range of 38 to 46 μg/m^3 for PM10 and 27 to 35 μg/m^3 for PM2.5. During the wet season, the humidity level is high and there is a higher chance of rainfall. The water vapors wash away all the suspended particles from the atmosphere, thereby reducing the particulate matter level [32,22].

3.3 Descriptive analysis of acute respiratory disease

Data summary for respiratory disease hospitalizations in three study areas, namely Hospital Shah Alam, Hospital Sungai Buloh, and Hospital Tengku Ampuan Rahimah in Klang, are presented in **Table 3** for 2018 and 2019. The statistics include mean, median, standard deviation, skewness, minimum, and maximum values. Overall, Klang had the highest number of patients admitted to the hospital for ACOPD and AEBA.

For inpatient AECOPD and AEBA cases, Hospital Tengku Ampuan Rahimah in Klang recorded the highest mean values of 185.17 and 260.50, respectively, in 2018, with standard deviations of 40.296 and 54.959. The mean values observed in all study areas and years were higher than the corresponding medians, indicating a positively skewed distribution for inpatient AECOPD and AEBA cases. Similarly, for outpatient AECOPD and AEBA cases, Hospital Tengku Ampuan Rahimah in Klang had the highest mean values of 14.00 and 41.67, with standard deviations of 12.799 and 17.385, respectively.

Furthermore, the highest maximum values for hospital admissions were 400 in 2018 and 297 in 2019, both for AEBA inpatient cases at Hospital Tengku Ampuan Rahimah in Klang. However, the specific data on hospital admissions for AECOPD and AEBA at Hospital Shah Alam and Hospital Sungai Buloh may not indicate a significant increase during periods of biomass burning from forest and

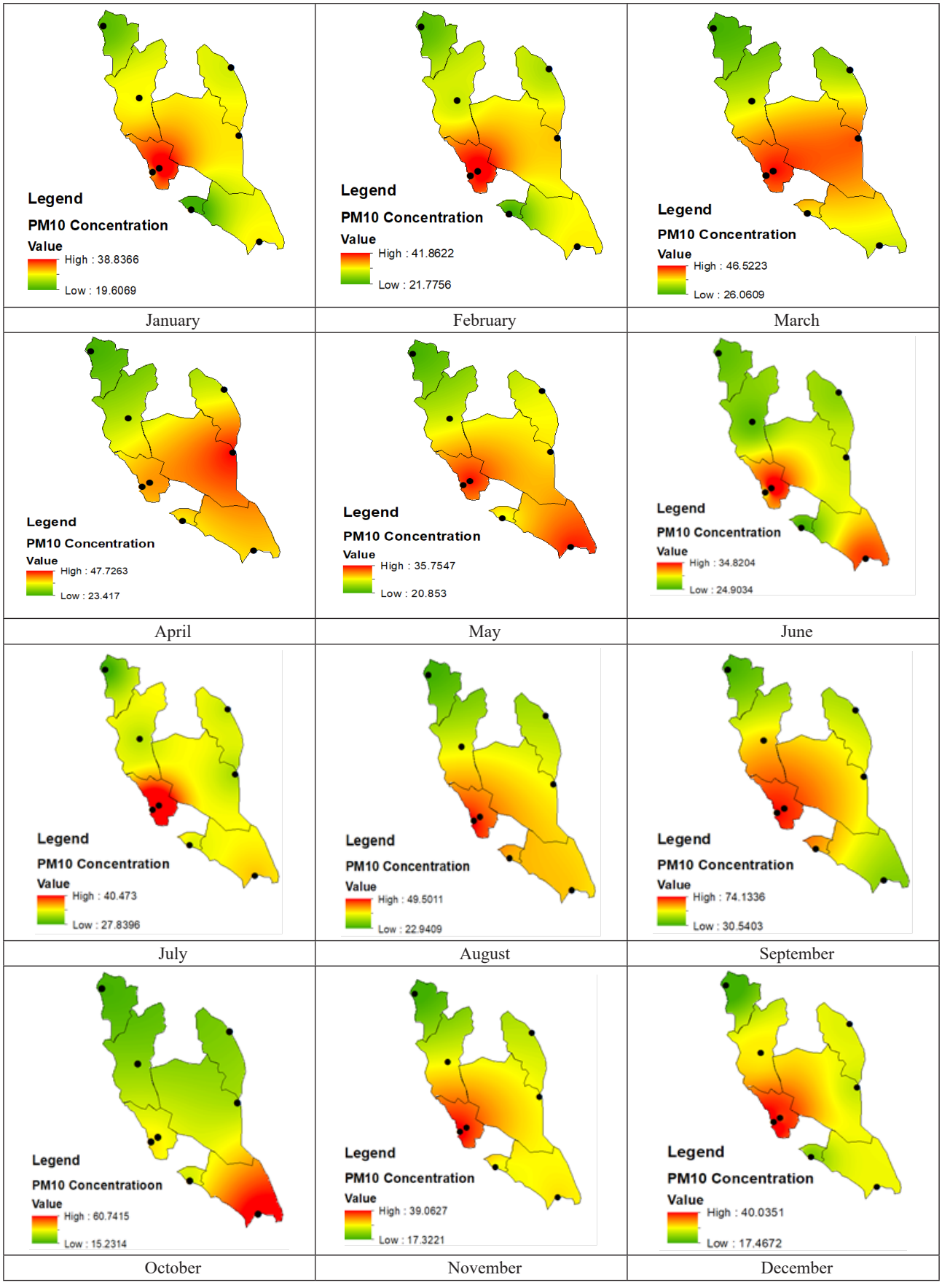

Figure 4. Mapping of PM10 concentration distribution at study area (January-December).

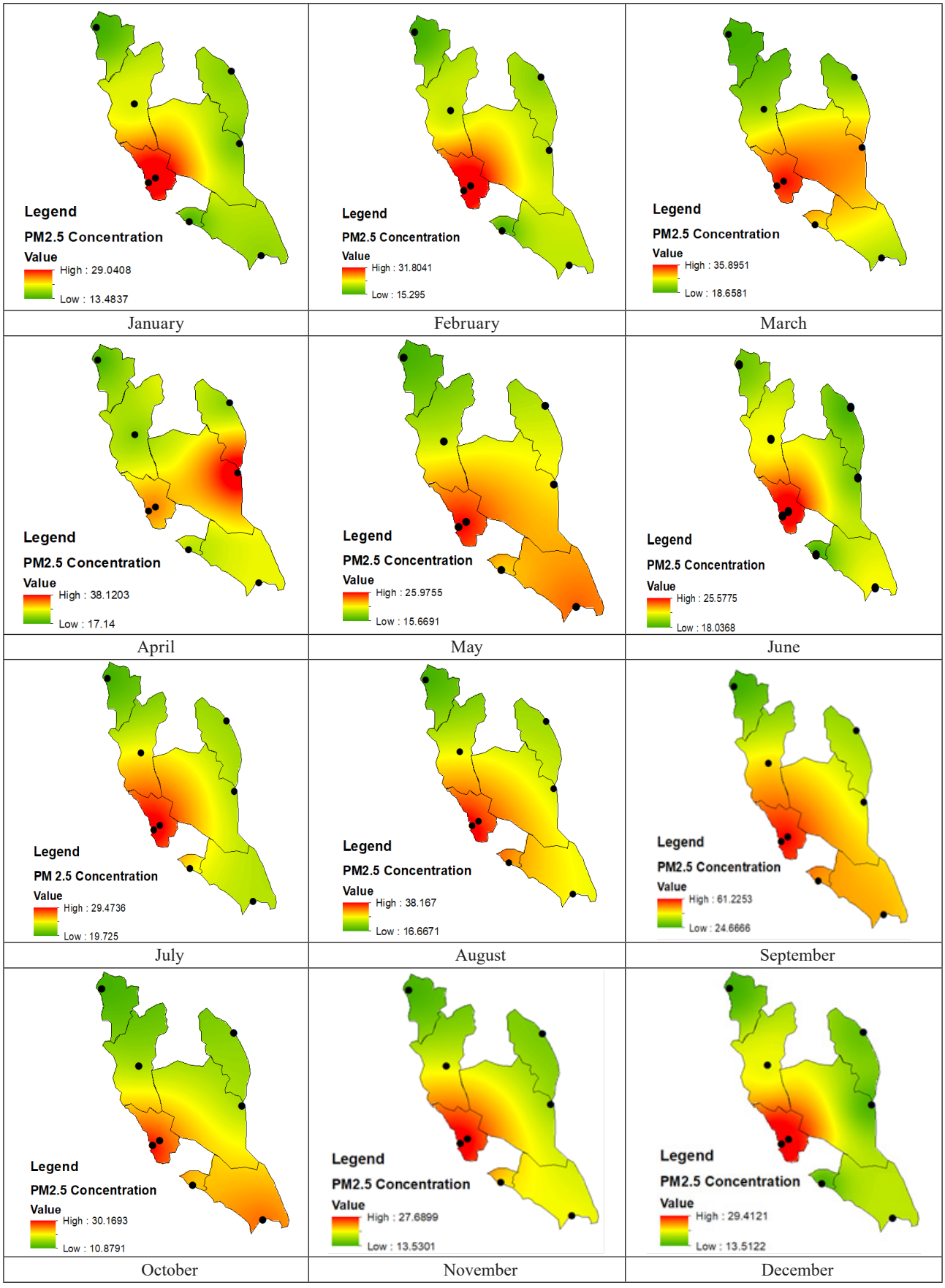

Figure 5. Mapping of PM2.5 concentration distribution at study area (January-December).

Table 3. Data summary of acute respiratory ill diseases.

Year	Healthcare utilization (Respiratory disease)		Statistics	Hospital Shah Alam	Hospital Sungai Buloh	Hospital Tengku Ampuan Rahimah, Klang
2018	Inpatient	AECOPD	N (Valid)	12	12	12
			Mean	30.750	15.420	185.170
			Median	27.000	15.000	173.500
			Std Dev	14.040	5.125	40.296
			Variance	197.114	26.265	1623.788
			Skewness	0.612	0.727	0.990
			Minimum	9	9	144
			Maximum	56	26	260
		AEBA	N (Valid)	12	12	12
			Mean	88.420	46.500	260.500
			Median	88.500	49.500	244.500
			Std Dev	26.559	11.844	54.959
			Variance	705.356	140.273	3020.455
			Skewness	0.775	–0.084	1.642
			Minimum	44	30	203
			Maximum	150	64	400
	Outpatient	AECOPD	N (Valid)	12	12	12
			Mean	0.670	0.580	14.000
			Median	0.000	0.000	8.500
			Std Dev	1.155	1.730	12.799
			Variance	1.333	2.992	163.818
			Skewness	1.638	3.309	1.763
			Minimum	0	0	2
			Maximum	3	6	47
		AEBA	N (Valid)	12	12	12
			Mean	16.420	19.580	41.670
			Median	17.000	14.500	38.500
			Std Dev	7.192	13.521	17.385
			Variance	51.720	182.811	302.242
			Skewness	–0.079	2.393	1.173
			Minimum	5	9	21
			Maximum	29	58	82

Table 3 continued

Year	Healthcare utilization (respiratory disease)		Statistics	Hospital Shah Alam	Hospital Sungai Buloh	Hospital Tengku Ampuan Rahimah, Klang
2019	Inpatient	AECOPD	N (Valid)	12	12	12
			Mean	20.580	14.330	157.080
			Median	18.000	15.000	145.500
			Std Dev	9.199	5.805	33.530
			Variance	84.629	33.697	1124.265
			Skewness	0.465	–0.081	0.789
			Minimum	9	3	107
			Maximum	36	24	229
		AEBA	N (Valid)	12	12	12
			Mean	88.500	43.250	203.670
			Median	82.000	42.500	194.500
			Std Dev	30.527	7.300	45.777
			Variance	931.909	53.295	2095.515
			Skewness	1.008	–0.151	0.752
			Minimum	54	32	152
			Maximum	154	54	297
	Outpatient	AECOPD	N (Valid)	12	12	12
			Mean	5.830	1.420	9.830
			Median	1.500	0.000	10.500
			Std Dev	7.756	2.275	7.802
			Variance	60.152	5.174	60.879
			Skewness	1.429	1.603	0.052
			Minimum	0	0	0
			Maximum	22	6	23
		AEBA	N (Valid)	12	12	12
			Mean	14.250	14.670	39.330
			Median	8.500	11.000	38.500
			Std Dev	14.372	8.195	11.523
			Variance	206.568	67.152	132.788
			Skewness	1.779	0.750	0.652
			Minimum	4	6	23
			Maximum	50	29	63

peat fires caused by agricultural land clearing in Indonesia. It is important to consider that certain health conditions, such as respiratory infections or seasonal allergies, may exhibit seasonal patterns. Factors like haze, increased pollen levels, or climate changes during specific times of the year can worsen respiratory conditions and lead to higher hospital admissions during those periods.

3.4 Trends of healthcare utilization

Figure 6 illustrates the bar diagram for the monthly average of healthcare utilization for 2018 and 2019. The trend in healthcare utilization can be seen in those hospitals. The findings of this study indicate that there was a higher utilization of healthcare services for respiratory illnesses from June until September which coincided with the south-westerly monsoon season. The analysis considered both acute exacerbation of bronchial asthma (AEBA) and acute exacerbation of chronic obstructive pulmonary disease (AECOPD), examining the total and average number of hospital admissions and outpatient visits.

Hospital Tengku Ampuan Rahimah, Klang showed the highest number in healthcare utilization among all study areas. Klang located in the western area experienced higher PM10 and PM2.5 concentration distribution as compared to the eastern and northern parts of Klang Valley. It can be evident from previous analysis in the time series plot (**Figures 2 and 3**), that Klang depicts the highest PM concentration among all study areas.

During these periods, the highest recorded levels of haze were observed due to biomass burning resulting from agricultural land clearing in Indonesia. This situation was exacerbated by the south-west monsoon season, which typically occurs from May

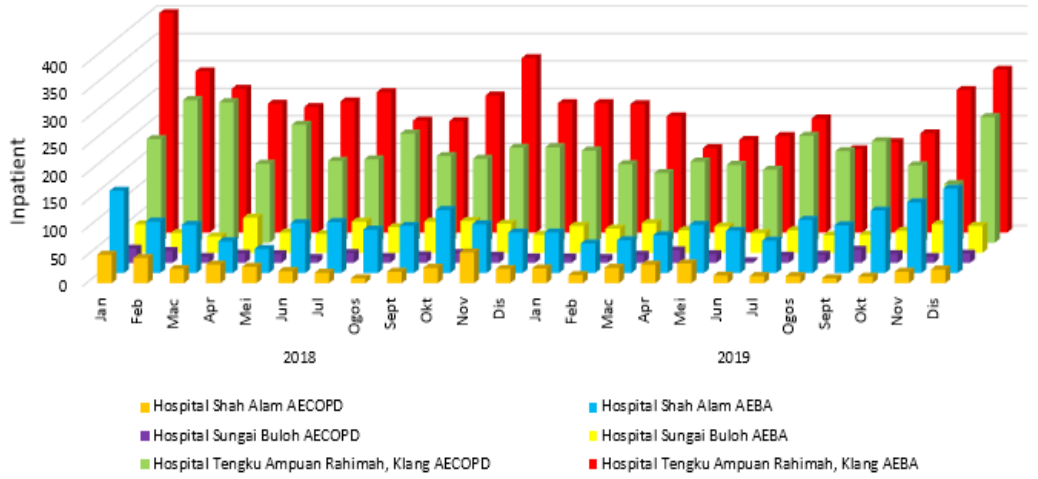

(a)

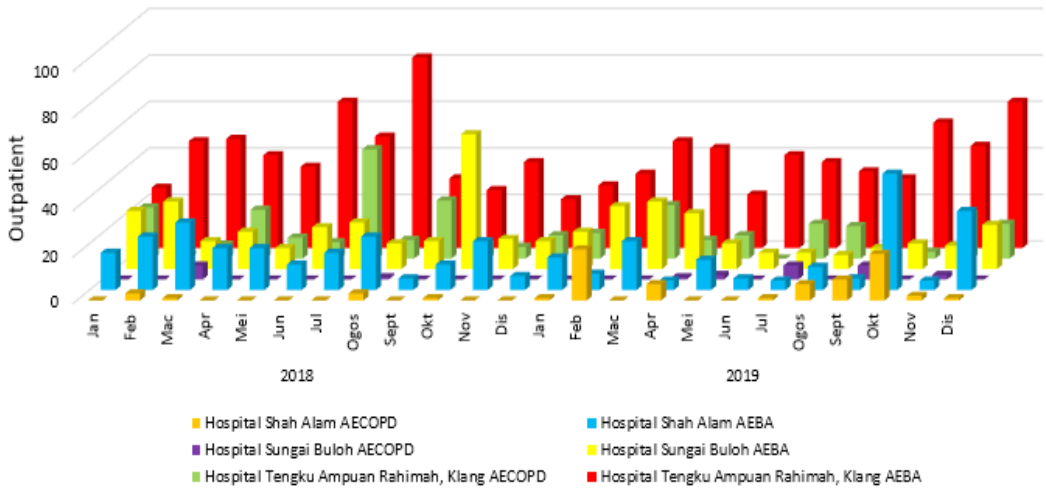

(b)

Figure 6. Monthly histogram plot healthcare utilization (a) inpatient and (b) outpatient.

to September. The prevailing winds from Sumatra, which followed the south west monsoon pattern, took approximately 48 hours to reach all Continuous Air Quality Monitoring (CAQM) stations in Selangor, Malaysia. As the wind carried the particulate matter and gaseous pollutants from the affected region, particularly Selangor's western part, it contributed to the elevated levels of haze in the area [33].

3.5 Association between healthcare utilization and particulate matter concentrations

The Mann-Whitney U test was used to compare the healthcare utilization (AEBA inpatient and outpatient) between two independent groups mainly particulate matter PM10 and PM2.5. Based on **Table 4**, the overall mean AEBA inpatient with particulate matter (PM10 and PM2.5) was higher than the mean AEBA outpatient with particulate matter (PM10 and PM2.5) which indicates that hospital admission in Selangor was higher compared to outpatient. Overall, the p-values for both healthcare utilization variables are less than 0.001 (except for AEBA outpatient in Klang), indicating a strongly statistically significant relationship between healthcare utilization and particulate matter levels in this area. Hence, there was sufficient evidence to reject that there was no difference between the mean of PM10 and PM2.5 with acute respiratory diseases.

In order to observe seasonal association, **Table 5** shows the mean values and p-values for healthcare utilization (AEBA inpatient and outpatient) during the South West Monsoon (SWM) and North East Monsoon (NEM) seasons, along with the particulate matter concentrations (PM10 and PM2.5). Overall, both particulate matter concentrations (PM10 and PM2.5) were statistically significant with healthcare utilization, as indicated by the p-values of < 0.001 (except for AEBA outpatient during the North east monsoon season). The results indicate that higher concentrations of PM10 and PM2.5 are associated with increased healthcare utilization for both AEBA inpatient and outpatient cases during both the SWM and NEM seasons. However, it is important to note that the association with PM2.5 becomes non-significant for AEBA outpatient cases during the NEM season. During haze episodes, particulate matter was the most dominant air pollutant. Previous studies showed that particulate matter triggered inflammatory reactions, mainly affecting the respiratory system, and resulted in AEBA [34]. As a result of exposure to higher concentrations levels of particulate matter during haze episodes, the number of AEBA cases was also expected to rise and subsequently lead to an increase in healthcare utilization during haze episodes, as seen in this study.

Table 4. Association between healthcare utilization and particulate matter concentrations.

Location	Healthcare utilization		PM10	PM2.5
Shah Alam	AEBA inpatient	Mean	63.360	58.573
		P-value	< 0.001	< 0.001
	AEBA outpatient	Mean	26.798	22.011
		P-value	< 0.001	< 0.001
Sungai Buloh	AEBA inpatient	Mean	41.569	36.781
		P-value	0.013	< 0.001
	AEBA outpatient	Mean	27.694	22.906
		P-value	< 0.001	< 0.001
Klang	AEBA inpatient	Mean	136.620	131.251
		P-value	< 0.001	< 0.001
	AEBA outpatient	Mean	40.828	35.460
		P-value	0.536	0.006

Table 5. Association between healthcare utilization and particulate matter concentrations during monsoon season.

Healthcare utilization	Monsoon seasons		PM10	PM2.5
AEBA inpatient	SWM	Mean	74.994	69.785
		P-value	< 0.001	< 0.001
	NEM	Mean	88.162	83.235
		P-value	< 0.001	< 0.001
AEBA outpatient	SWM	Mean	31.944	26.735
		P-value	< 0.001	< 0.001
	NEM	Mean	31.312	26.385
		P-value	< 0.001	0.128

3.6 Association between healthcare utilization and meteorological parameter

Table 6 shows the coefficients, p-values, and VIF (Variance Inflation Factor) values for healthcare utilization (AEBA inpatient and outpatient) meteorological parameters, wind speed (WS), relative humidity (RH), and temperature (T) in different locations (Shah Alam, Sungai Buloh, and Klang). Overall, VIF values recorded were less than 10 which indicates that no multicollinearity issues were involved. In Shah Alam, the p-values for WS, RH, and T were 0.860, 0.431, and 0.019, indicating that only the temperature (T) variable has a statistically significant relationship with AEBA inpatient healthcare utilization.

For AEBA outpatient cases in Shah Alam, none of the coefficients for WS, RH, and T were statistically significant based on their p-values. In Sungai Buloh, none of the coefficients for WS, RH, and T were statistically significant for both AEBA inpatient and outpatient cases. In Klang, for AEBA inpatient cases, the p-values for WS, RH, and T were 0.034, 0.006, and 0.001, indicating that wind speed (WS), relative humidity (RH), and temperature (T) have statistically significant relationships with AEBA inpatient healthcare utilization.

For AEBA outpatient cases in Klang, none of the coefficients for WS, RH, and T were statistically significant based on their p-values. Overall, the results suggest that the weather parameters have varying levels of association with healthcare utilization for AEBA in different locations. Specifically, in Shah Alam, only temperature (T) is significantly associated with AEBA inpatient cases. In Klang, wind speed (WS), relative humidity (RH), and temperature (T)

Table 6. Association between healthcare utilization and meteorological parameters.

Location	Healthcare utilization		WS	RH	T
Shah Alam	AEBA inpatient	Coefficient	9.560	–2.902	–47.620
		P-value	0.860	0.431	0.019
		VIF	1.077	3.060	3.154
	AEBA outpatient	Coefficient	–37.627	0.446	–3.398
		P-value	0.142	0.790	0.695
		VIF	1.077	3.060	3.154
Sungai Buloh	AEBA inpatient	Coefficient	–13.978	–0.152	–0.317
		P-value	0.558	0.924	0.969
		VIF	1.077	3.060	3.154
	AEBA outpatient	Coefficient	17.508	–2.266	–13.031
		P-value	0.505	0.207	0.161
		VIF	1.077	3.060	3.154
Klang	AEBA inpatient	Coefficient	–187.103	–15.230	–92.417
		P-value	0.034	0.006	0.001
		VIF	1.828	1.974	2.149
	AEBA outpatient	Coefficient	–13.242	–2.015	0.206
		P-value	0.687	0.314	0.983
		VIF	1.828	1.974	2.149

show significant associations with AEBA inpatient cases. However, for AEBA outpatient cases, there are no significant associations observed with the weather parameters.

In addition, to provide a clearer understanding, **Table 7** shows the coefficients, p-values, and VIF (Variance Inflation Factor) values for healthcare utilization (AEBA inpatient and outpatient) during the South West Monsoon (SWM) and North East Monsoon (NEM) seasons, along with the weather parameters wind speed (WS), relative humidity (RH), and temperature (T). Overall, VIF values recorded were less than 10 which indicates that no multicollinearity issues were involved. For AEBA inpatient cases during the SWM season, the p-value of WS and AEBA inpatient is 0.002 suggesting that this relationship was statistically significant. However, RH and T do not show significant associations.

During the NEM season for AEBA inpatient cases, the p-value for WS was 0.035, which was also statistically significant. For AEBA outpatient cases during the SWM season, the coefficient for WS was 49.040, indicating a positive relationship with healthcare utilization and it was statistically significant with a p-value of 0.006. However, RH and T do not show significant associations.

During the NEM season for AEBA outpatient cases, none of the coefficients for WS, RH, and T were statistically significant. In summary, the results suggest that wind speed (WS) has a significant positive association with healthcare utilization for AEBA inpatient cases during both SWM and NEM seasons. However, the associations with relative humidity (RH) and temperature (T) are generally not significant. For AEBA outpatient cases, the associations with the meteorological parameters were not statistically significant during both seasons.

In summary, the findings indicate that during the south west monsoon season, there is a significant impact of wind speed on both AEBA inpatient and outpatient cases, with p-values of 0.002 and 0.006, respectively. However, during the north east monsoon season, only AEBA inpatient cases show a significant impact on wind speed, with a p-value of 0.035. Additionally, AEBA inpatient cases during the north east monsoon season also exhibit a significant impact on temperature, with a p-value of 0.051.

Table 7. Association between healthcare utilization and meteorological parameters during monsoon season.

Healthcare utilization	Monsoon seasons		WS	RH	T
AEBA inpatient	SWM	Coefficient	182.850	–0.210	5.337
		P-value	0.002	0.966	0.872
		VIF	4.855	2.158	5.934
	NEM	Coefficient	157.343	9.607	89.800
		P-value	0.035	0.155	0.051
		VIF	4.855	2.158	5.934
AEBA outpatient	SWM	Coefficient	49.040	–2.140	–4.357
		P-value	0.006	0.169	0.670
		VIF	4.855	2.158	5.934
	NEM	Coefficient	12.391	0.690	12.118
		P-value	0.365	0.586	0.159
		VIF	4.855	2.158	5.934

The causal relationship between AEBA inpatient and outpatient with meteorological parameters is given in **Table 8**. The table reveals both positive and negative correlations between AEBA inpatient and outpatient with meteorological parameters. A strong negative correlation was found between AEBA inpatient and temperature in Shah Alam with an r-value of –0.60 while a moderate positive correlation between inpatient and relative humidity with an r-value of 0.40. This result denoted that temperature contributes much influence on inpatients compared to relative humidity. A study by Anderson et al. [35] stated that a larger increase in daily temperature would result in more excess hospitalizations and a lower increase in fewer hospitalizations.

Furthermore, a strong negative correlation was found between meteorological parameters such as relative humidity and temperature ranging from –0.81 to –0.67 which indicated that an increase in temperature causes a decrease in relative humidity and vice versa. Besides, in Klang a strong negative correlation was observed between wind speed and relative humidity with an r-value of –0.59. Meanwhile, a strong positive correlation between wind

speed and temperature with an r-value of 0.63. Overall, in Sungai Buloh, the correlation recorded between AEBA inpatients and meteorological parameters were negatively correlated which indicated that meteorological parameters did not influence the number of AEBA Inpatients during the haze event.

Table 8. Correlation coefficient matrix of AEBA inpatient and outpatient with meteorological parameters.

Shah Alam					
	Inpatient	Outpatient	WS	RH	T
Inpatient	1				
Outpatient	0.32	1.00			
WS	–0.10	–0.35	1.00		
RH	0.40	0.22	–0.02	1.00	
T	–0.60	–0.28	0.17	–0.81	1.00
Sungai Buloh					
	Inpatient	Outpatient	WS	RH	T
Inpatient	1				
Outpatient	0.39	1.00			
WS	–0.14	0.06	1.00		
RH	–0.02	–0.04	–0.02	1.00	
T	–0.01	–0.13	0.17	–0.81	1.00
Klang					
	Inpatient	Outpatient	WS	RH	T
Inpatient	1.00				
Outpatient	1.00	1.00			
WS	0.07	0.07	1.00		
RH	–0.25	–0.25	–0.59	1.00	
T	0.14	0.14	0.63	–0.67	1.00

4. Conclusions

The objective of this project was to analyze the spatial and temporal variations of particulate matter (PM10 and PM2.5) in urban and industrial areas of Malaysia, specifically in Alor Setar, Tasek, Shah Alam, Klang, Melaka, Larkin, Balok Baru, and Kuala Terengganu. Additionally, the study aimed to investigate the relationship between particulate matter and acute respiratory illnesses in the Selangor region, focusing on Klang, Shah Alam, and Sungai Buloh. During the haze events in 2019, the levels of PM10 and PM2.5 exceeded the permissible limits set by the Malaysian Ambient Air Quality Standard (MAAQS). Bandaraya Melaka and Klang had the highest concentrations of PM10, while Bandaraya Melaka and Shah Alam had the highest concentrations of PM2.5 during the same year. The time series analysis revealed that Bandaraya Melaka had the highest peak in haze event in 2019 which happened in September, during the south west monsoon season.

Data analysis of respiratory illnesses diseases revealed that Klang had the highest mean number of inpatient and outpatient cases for AEBA and AECOPD. Besides, the highest healthcare utilization for both AEBA and AECOPD cases occurs mainly from June to September or during the south west monsoon season. The Mann-Whitney U test revealed a statistically significant association between particulate matter and hospital utilization, with p-values below 0.05, indicating sufficient evidence to reject that there was no difference between the mean of PM10 and PM2.5 with acute respiratory ill diseases. Multiple linear regression analysis identified significant associations between healthcare utilization and meteorological parameters. Specifically, for AEBA inpatients in Klang, wind speed, relative humidity, and temperature showed significant associations. Moreover, seasonal variability analysis indicated significant associations between wind speed, temperature, and healthcare utilization during the South West Monsoon (SWM) and North East Monsoon (NEM).

More research is required to determine consistent associations between wildfire smoke exposure and cardiovascular effects, specific causes of mortality, birth outcomes, and mental health outcomes. The current estimations are largely based on common statistical methods, making it difficult to establish a direct causal relationship between haze and certain health conditions due to the complex nature of air pollutants and the lack of accurate epidemiological records. By addressing these research areas, future studies can contribute to a better understanding of the association between particulate matter and respiratory diseases during haze events. This knowledge can inform public health policies, air pollution management strategies, and targeted interventions to protect vulnerable populations and mitigate the health

impacts of haze-related particulate matter exposure.

Author Contributions

Conceptualization, Norazian Mohamed Noor; Methodology, Norazian Mohamed Noor; Software, Afiqah Ma'amor and Izzati Amani Mohd Jafri; Validation, Ahmad Zia Ul Saufie, and Nor Azrita Amin; Formal analysis, Afiqah Ma'amor; Investigation, Afiqah Ma'amor and Nur Alis Addiena; Writing—original draft preparation, Afiqah Ma'amor; Writing—review and editing, Norazian Mohamed Noor; Supervision, Norazian Mohamed Noor; Project administration, Gyorgy Deak and Madalina Boboc.

Conflict of Interest

The authors declare no conflict of interest.

Funding

This research received no external funding.

Acknowledgement

The author would like to thank to Department of Environment Malaysia for the air pollutant dataset and the Ministry of Health (MOH) Malaysia for the health dataset.

References

[1] Wu, S., Deng, F., Wang, X., et al., 2013. Association of lung function in a panel of young healthy adults with various chemical components of ambient fine particulate air pollution in Beijing, China. Atmospheric Environment. 77, 873-884.
DOI: https://doi.org/10.1016/j.atmosenv.2013.06.018

[2] Wang, S., Hao, J., 2012. Air quality management in China: Issues, challenges, and options. Journal of Environmental Sciences. 24(1), 2-13.
DOI: https://doi.org/10.1016/S1001-0742(11)60724-9

[3] Li, Y., Zheng, C., Ma, Z., et al., 2019. Acute and cumulative effects of haze fine particles on mortality and the seasonal characteristics in Beijing, China, 2005-2013: A time-stratified case-crossover study. International Journal of Environmental Research and Public Health. 16(13), 2383.
DOI: https://doi.org/10.3390/ijerph16132383

[4] Latif, M.T., Othman, M., Idris, N., et al., 2018. Impact of regional haze towards air quality in Malaysia: A review. Atmospheric Environment. 177, 28-44.
DOI: https://doi.org/10.1016/j.atmosenv.2018.01.002

[5] Mahmud, M., 2013. Assessment of atmospheric impacts of biomass open burning in Kalimantan, Borneo during 2004. Atmospheric Environment. 78, 242-249.
DOI: https://doi.org/10.1016/j.atmosenv.2012.03.019

[6] Dotse, S.Q., Dagar, L., Petra, M.I., et al., 2016. Influence of Southeast Asian Haze episodes on high PM10 concentrations across Brunei Darussalam. Environmental Pollution. 219, 337-352.
DOI: https://doi.org/10.1016/j.envpol.2016.10.059

[7] Wen, Y.S., bin Mohd Nor, A.F., 2016. Transboundary air pollution in Malaysia: Impact and perspective on haze. Nova Journal of Engineering and Applied Sciences. 5(1).
DOI: https://doi.org/10.20286/nova-jeas-050103

[8] Indonesia Palm Oil Production by Year (1000 MT) [Internet]. Available from: https://www.indexmundi.com/agriculture/?country=id&commodity=palm-oil&graph=production

[9] Zainal, Z., 2016. Root problem of forest fire and solutions in completion (Study in the Riauprovince). Proceedings International Conference on Social Politics. 1.

[10] Forsyth, T., 2014. Public concerns about transboundary haze: A comparison of Indonesia, Singapore, and Malaysia. Global Environmental Change. 25, 76-86.
DOI: https://doi.org/10.1016/j.gloenvcha.2014.01.013

[11] Jafri, I.A.M., Noor, N.M., Rahim, N.A.A.A., et al., 2023. Spatial and temporal analysis of particulate matter (PM10) in urban-industrial environment during episodic haze events in Malaysia. Environment Asia. 16(1), 111-125.
DOI: https://doi.org/10.14456/ea.2023.10

[12] Pavagadhi, S., Betha, R., Venkatesan, S., et al.,

2013. Physicochemical and toxicological characteristics of urban aerosols during a recent Indonesian biomass burning episode. Environmental Science and Pollution Research. 20, 2569-2578.
DOI: https://doi.org/10.1007/s11356-012-1157-9

[13] Khan, M.F., Latif, M.T., Saw, W.H., et al., 2016. Fine particulate matter in the tropical environment: monsoonal effects, source apportionment, and health risk assessment. Atmospheric Chemistry and Physics. 16(2), 597-617.
DOI: https://doi.org/10.5194/acp-16-597-2016

[14] Abba, E.J., Unnikrishnan, S., Kumar, R., et al., 2012. Fine aerosol and PAH carcinogenicity estimation in outdoor environment of Mumbai City, India. International Journal of Environmental Health Research. 22(2), 134-149.
DOI: https://doi.org/10.1080/09603123.2011.613112

[15] Department of Environment., 2010. Air quality: Continuous Air Quality Monitoring (CAQM) [Internet]. Available from: https://www.doe.gov.my/wp-content/uploads/2021/10/Air-Qulaity.pdf

[16] Mohammed, S.A., Yusof, M.M., 2013. Towards an evaluation framework for information quality management (IQM) practices for health information systems—evaluation criteria for effective IQM practices. Journal of Evaluation in Clinical Practice. 19(2), 379-387.
DOI: https://doi.org/10.1111/j.1365-2753.2012.01839.x

[17] Latif, M.T., Dominick, D., Ahamad, F., et al., 2014. Long term assessment of air quality from a background station on the Malaysian Peninsula. Science of the Total Environment. 482, 336-348.
DOI: https://doi.org/10.1016/j.scitotenv.2014.02.132

[18] Hussain, H., 2019. Jerebu bakal pulih, ribut petir pula menyusul [Haze will recover, thunderstorms will follow] [Internet]. Available from: https://www.sinarharian.com.my/article/48783/BERITA /Nasional/Jerebu-bakal-pulih-ribut-petir-pula-menyusul

[19] Official Portal of Department of Environment. Environmental Quality Report 2019 [Internet]; DOE: Putrajaya, Malaysia, 2019. Available from: https://enviro2.doe.gov.my/ekmc/wp-content/uploads/2020/09/EQR-20191.pdf

[20] Kumar, A., Gupta, I., Brandt, J., et al., 2016. Air quality mapping using GIS and economic evaluation of health impact for Mumbai City, India. Journal of the Air & Waste Management Association. 66(5), 470-481.
DOI: https://doi.org/10.1080/10962247.2016.1143887

[21] Jumaah, H.J., Ameen, M.H., Kalantar, B., et al., 2019. Air quality index prediction using IDW geostatistical technique and OLS-based GIS technique in Kuala Lumpur, Malaysia. Geomatics, Natural Hazards and Risk. 10(1), 2185-2199.
DOI: https://doi.org/10.1080/19475705.2019.1683084

[22] Rahman, S.R.A., Ismail, S.N.S., Raml, M.F., et al., 2015. The assessment of ambient air pollution trend in Klang Valley, Malaysia. World Environment. 5(1), 1-11.
DOI: https://doi.org/10.5923/j.env.20150501.01

[23] De Iaco, S., Palma, M., Posa, D., 2005. Modeling and prediction of multivariate space-time random fields. Computational Statistics & Data Analysis. 48(3), 525-547.
DOI: https://doi.org/10.1016/j.csda.2004.02.011

[24] Fan, H., Zhao, C., Yang, Y., 2020. A comprehensive analysis of the spatio-temporal variation of urban air pollution in China during 2014-2018. Atmospheric Environment. 220, 117066.
DOI: https://doi.org/10.1016/j.atmosenv.2019.117066

[25] Amil, N., Latif, M.T., Khan, M.F., et al., 2016. Seasonal variability of PM 2.5 composition and sources in the Klang Valley urban-industrial environment. Atmospheric Chemistry and Physics. 16(8), 5357-5381.
DOI: https://doi.org/10.5194/acp-16-5357-2016

[26] Jaafar, H., Azzeri, A., Isahak, M., et al., 2021. The impact of haze on healthcare utilizations for acute respiratory diseases: Evidence from Malaysia. Frontiers in Ecology and Evolution. 9, 764300.

DOI: https://doi.org/10.3389/fevo.2021.764300

[27] Khan, M.F., Hamid, A.H., Ab Rahim, H., et al., 2020. El Niño driven haze over the southern Malaysian peninsula and Borneo. Science of the Total Environment. 730, 139091.
DOI: https://doi.org/10.1016/j.scitotenv.2020.139091

[28] Tella, A., Balogun, A.L., 2021. Prediction of ambient PM10 concentration in Malaysian cities using geostatistical analyses. Journal of Advanced Geospatial Science & Technology. 1(1), 115-127.

[29] Wang, W., Ying, Y., Wu, Q., et al., 2015. A GIS-based spatial correlation analysis for ambient air pollution and AECOPD hospitalizations in Jinan, China. Respiratory Medicine. 109(3), 372-378.
DOI: https://doi.org/10.1016/j.rmed.2015.01.006

[30] Marmaya, E.A., Mahbub, R., 2018. A comparative study on the environmental impact assessment of industrial projects in Malaysia. IOP Conference Series: Earth and Environmental Science. 117(1), 012020.
DOI: https://doi.org/10.1088/1755-1315/117/1/012020

[31] Daoud, J.I., 2017. Multicollinearity and regression analysis. Journal of Physics: Conference Series. 949(1), 012009.
DOI: https://doi.org/10.1088/1742-6596/949/1/012009

[32] Azmi, S.Z., Latif, M.T., Ismail, A.S., et al., 2010. Trend and status of air quality at three different monitoring stations in the Klang Valley, Malaysia. Air Quality, Atmosphere & Health. 3, 53-64.
DOI: https://doi.org/10.1007/s11869-009-0051-1

[33] Wang, Y., Wild, O., Chen, H., et al., 2020. Acute and chronic health impacts of PM2.5 in China and the influence of interannual meteorological variability. Atmospheric Environment. 229, 117397.
DOI: https://doi.org/10.1016/j.atmosenv.2020.117397

[34] Sansuddin, N., Ramli, N.A., Yahaya, A.S., et al., 2011. Statistical analysis of PM 10 concentrations at different locations in Malaysia. Environmental Monitoring and Assessment. 180, 573-588.
DOI: https://doi.org/10.1007/s10661-010-1806-8

[35] Anderson, G.B., Dominici, F., Wang, Y., et al., 2013. Heat-related emergency hospitalizations for respiratory diseases in the Medicare population. American Journal of Respiratory and Critical Care Medicine. 187(10), 1098-1103.
DOI: https://doi.org/10.1164/rccm.201211-1969OC

BILINGUAL PUBLISHING GROUP

Journal of Atmospheric Science Research

https://journals.bilpubgroup.com/index.php/jasr

ARTICLE

Assessing the Impact of Gas Flaring and Carbon Dioxide Emissions on Precipitation Patterns in the Niger Delta Region of Nigeria Using Geospatial Analysis

***Otutu Anslem Onyebuchi*[1*], *Eteh Desmond Rowland*[2], *Iluma Vieme Phoebe*[3]**

[1] *Department of Physics, Niger Delta University, Wilberforce Island, Bayelsa State, 560001, Nigeria*

[2] *Department of Geology, Niger Delta University, Wilberforce Island, Bayelsa State, 560001, Nigeria*

[3] *Department of Biology, Niger Delta University, Wilberforce Island, Bayelsa State, 560001, Nigeria*

ABSTRACT

This research utilizes geospatial methodologies to investigate the influence of gas flaring and carbon dioxide emissions on precipitation patterns within the Niger Delta region of Nigeria. The study relies on average mean precipitation data sourced from CHRS at the University of Arizona and carbon dioxide emissions data from NASA's AIRS in Giovanni, spanning from July 2002 to November 2011. To carry out the analysis, ArcGIS 5.0 and SPSS 25, employing Inverse Distance Weighting (IDW), were employed to assess CO_2 emissions and rainfall for both November and July during the period from 2002 to 2011. Over the course of this study, it was observed that CO_2 emission exhibited an upward trend, increasing from 327.5226 parts per million (ppm) in July 2002 to 390.0077 ppm in November 2011. Simultaneously, the rainfall demonstrated an increase, rising from 56.66 millimeters to 390.78 millimeters for both July and November from 2002 to 2011. Noteworthy findings emerged from the correlation analysis conducted. Specifically, from July 2000 to 2011, there was a weak positive correlation (0.3858) observed between CO_2 emissions and minimum rainfall, while a strong negative correlation (–0.7998) was identified for maximum rainfall values. In November, both minimum and maximum CO_2 emissions displayed strong negative correlations with rainfall, with coefficients of –0.8255 and –0.7415, respectively. These findings hold significant implications for comprehending the environmental dynamics within the Niger Delta. Policymakers and stakeholders can leverage this knowledge to formulate targeted strategies aimed at mitigating CO_2 emissions and addressing potential climate change-induced alterations in rainfall patterns.

Keywords: Remote sensing; CO_2 emissions; Rainfall; Atmospheric infrared sounder (AIRS); Climate change; Impact; Gas flaring

*CORRESPONDING AUTHOR:

Otutu Anslem Onyebuchi, Department of Physics, Niger Delta University, Wilberforce Island, Bayelsa State, 560001, Nigeria; Email: otutu-anslem@gmail.com

ARTICLE INFO

Received: 11 September 2023 | Revised: 7 October 2023 | Accepted: 17 October 2023 | Published Online: 23 October 2023

DOI: https://doi.org/10.30564/jasr.v6i4.5954

CITATION

Onyebuchi, O.A., Rowland, E.D., Phoebe, I.V., 2023. Assessing the Impact of Gas Flaring and Carbon Dioxide Emissions on Precipitation Patterns in the Niger Delta Region of Nigeria Using Geospatial Analysis. Journal of Atmospheric Science Research. 6(4): 48-63. DOI: https://doi.org/10.30564/jasr.v6i4.5954

1. Introduction

The Niger Delta region in Nigeria, often known as the "Heart of Nigeria", is famous not only for its abundant biodiversity and oil reserves but also for grappling with significant environmental challenges. Among these challenges, increasing attention has been focused on the detrimental effects of gas flaring and carbon dioxide emissions on both the local ecosystem and the global climate [1]. In response, the application of remote sensing technologies has emerged as a powerful tool for monitoring and examining the impacts of these environmental stressors on the delicate balance of rainfall patterns in the area. Remote sensing technologies provide a means to observe and assess the consequences of these environmental stressors on rainfall patterns. This approach enables data collection from a distance, allowing for the monitoring of changes in land cover, vegetation, and atmospheric composition. Such data are crucial in assessing the influence of gas flaring and CO_2 emissions on rainfall patterns. Ismail and Umukoro [2] present compelling evidence that gas flaring exerts a substantial influence on the climate, both at local and global scales. On a local level, gas flaring emits a spectrum of pollutants, encompassing greenhouse gases, particulate matter, and volatile organic compounds, thereby contributing to air pollution. These emissions can give rise to a range of adverse health outcomes, such as respiratory ailments, cardiovascular issues, and cancer. Furthermore, gas flaring can induce alterations in local climate dynamics, where the release of greenhouse gases can trap heat in the atmosphere, elevating temperatures. Although particulate matter can attenuate sunlight and cool the atmosphere, this effect is typically eclipsed by the warming potential of greenhouse gases. On a global scale, methane, a prominent gas emitted during gas flaring, is identified as a greenhouse gas with over 80 times the heat-trapping capability of carbon dioxide over a two-decade span. This underscores the substantial impact even small quantities of methane can have on global warming. Additionally, gas flaring releases black carbon, a pollutant that absorbs sunlight and contributes to atmospheric warming. Black carbon particles can traverse long distances in the atmosphere, influencing climate patterns in distant regions. The research by Ismail and Umukoro [2] also implies that gas flaring can lead to modifications in precipitation patterns. This phenomenon is attributable to the emissions of greenhouse gases and pollutants altering cloud formation and precipitation processes. For instance, greenhouse gases, by trapping heat in the atmosphere, foster increased evaporation and higher water vapor levels in the air, promoting heightened cloud formation and subsequently, increased precipitation. Conversely, particulate matter's capacity to block sunlight and cool the atmosphere can have the opposite effect, resulting in reduced cloud formation and diminished precipitation. Okpobiri et al. [1] utilized geospatial technology to monitor and quantify carbon dioxide emissions and their impact on marine ecosystems in the Niger Delta as indicators of climate change. The authors employed various methods, including satellite imagery, remote sensing, and GIS, to gather and analyze data on these factors. Their findings indicated that the Niger Delta is a significant source of carbon dioxide emissions, and sea surface temperatures are rising in the region. These changes are negatively affecting marine ecosystems, including coral reefs and mangrove forests. The authors concluded that geospatial technology can be a valuable tool for monitoring and assessing the impacts of climate change in the Niger Delta and other coastal regions. Word Bank [3] report, the Global Gas Flaring Reduction Partnership (GGFR) approximates that in the year 2022, gas flaring resulted in the emission of 357 million metric tons of carbon dioxide equivalent (CO_2e). Out of this total, approximately 315 million metric tons were in the form of carbon dioxide (CO_2), while the remaining 42 million metric tons were in the form of methane (CH_4). Additionally, a study by Nduka, et al. [4] revealed that the practice of gas flaring in the Niger Delta region could potentially lead to the development of acid rain, which in turn poses dangers to agricultural crops, woodlands, infrastructure, and the well-being of individuals. Anejionu et al. [5] and Earsel et al. [6] utilized remote sensing for

detecting and mapping gas flares. MODIS is a multispectral instrument that collects data in a variety of wavelengths, including the thermal infrared band. The thermal infrared band is sensitive to the heat emitted by gas flares, so it can be used to detect and map flares. The primary aim of this study is to utilize remote sensing techniques to investigate the interplay between gas flaring, CO_2 emissions, and rainfall patterns and correlation between CO_2 and rainfall in the Niger Delta region of Nigeria. Advanced satellite-based tools will be employed to monitor changes in land cover, vegetation, and atmospheric composition. The results of this research endeavor will enhance our understanding of the environmental challenges facing the Niger Delta and emphasize the importance of adopting sustainable practices in the oil and gas extraction industry.

2. Location of study

The Niger Delta region is located in the South-South geopolitical zone of Nigeria. It is bounded by longitudes 5° 05'E and 7° 35'E and latitudes 4° 15'N and 6° 01'N. The region consists of 9 oil-producing states (Abia, Akwa Ibom, Bayelsa, Cross River, Delta, Edo, Ondo, Imo, and Rivers) and 185 local government areas [7]. It is home to over 800 oil-producing communities and has an extensive network of over 900 producing oil wells and petroleum production-related facilities [8]. According to Sakib [9], the ecological zones in the Niger Delta can be broadly divided into two: the tropical rainforest in the northern part of the delta and the mangrove forest in the warm coastlines of Nigeria. Mangrove forests and swamps, which are characterized by regular saltwater inundation, lie at the centre of a complex and sensitive ecosystem that is vital to the local economy and accommodates important flora and fauna. The Niger Delta is the largest mangrove forest in Africa and the third largest in the world. It is also the richest part of Nigeria in terms of petroleum resources and diverse natural ecosystems supportive of numerous species of terrestrial and aquatic fauna [10]. The Niger Delta is the catchment of the Niger River as it enters the Atlantic Ocean in the Gulf of Guinea in a delta form. Other rivers such as the Cross River, Qua Iboe River, and Imo River to the east and the Forcados and Ethiope Rivers to the west, which also empty into the Gulf of Guinea close to the Niger River, join to constitute the catchments.

2.1 Limitation

The major challenge of this research work is that data acquisition from 2018 to the present has been extremely difficult due to inadequate funding as the materials required for the research are very expensive.

2.2 Literature review

The impact of carbon dioxide (CO_2) on various environmental systems, including groundwater, lakes, ice caps, and oceans, is a critical concern in today's world. This literature review explores the relationship between CO_2 emissions, greenhouse gases, and their effects on the environment, particularly focusing on the Niger Delta region in Nigeria.

Rising CO_2 emissions

The alarming projection made in the World Energy Outlook [13], which foresaw a rise in CO_2 emissions from 26 billion tonnes in 2004 to 40 billion tonnes by 2030, has unfortunately become a reality. According to the Global Carbon Budget 2023, global CO_2 emissions reached 41 billion tonnes in 2022, marking a 1.4% increase from 2021 and representing the highest recorded level of emissions. This increase in CO_2 emissions can be attributed to various factors, including the growing energy demand in developing countries, the persistent reliance on fossil fuels for electricity and transportation, and the expansion of industrial activities. Consequently, this surge in CO_2 emissions is wreaking havoc on our planet, contributing to climate change, which in turn results in more frequent extreme weather events, rising sea levels, and the accelerated melting of glaciers. Evidently, there is an urgent need for action to curtail CO_2 emissions. This entails a shift away from fossil fuels in favour of cleaner energy sources like

solar and wind power, as well as adjustments in our personal lifestyles such as reducing driving and minimizing energy consumption at home. Governments, businesses, and individuals all have a role to play in reducing CO_2 emissions. Governments can invest in renewable energy and energy efficiency initiatives, while businesses can transition to cleaner energy sources and adopt measures to decrease their carbon footprint. Individuals can also make changes to their daily routines, such as driving less, conserving energy at home, and adopting more sustainable dietary choices. While reducing CO_2 emissions presents a complex challenge, it is one that must be addressed to safeguard our planet for future generations.

Greenhouse gases and global warming

Raúl et al. [14] discuss the impact of greenhouse gases (GHGs) on plant oxidative stress. GHGs, such as CO_2, contribute to global warming by trapping heat in the Earth's atmosphere. This can lead to extreme climate events, such as floods, droughts, and heat waves, which can all stress plants and induce oxidative stress. Oxidative stress is a condition in which the production of reactive oxygen species (ROS) exceeds the capacity of the antioxidant system to detoxify them. ROS are highly reactive molecules that can damage cellular components, including DNA, proteins, and lipids. CO_2 can have both positive and negative effects on plant oxidative stress. On the one hand, CO_2 is a substrate for photosynthesis, and increased CO_2 concentrations can lead to increased photosynthetic rates and biomass production. This can help plants to cope with some abiotic stresses, such as drought. On the other hand, high CO_2 concentrations can also lead to increased ROS production. This is because high CO_2 concentrations can increase the activity of Rubisco, an enzyme that is involved in photosynthesis. Rubisco can also catalyze a reaction that produces ROS. Another GHG, nitric oxide (NO), can also have both positive and negative effects on plant oxidative stress. NO is a signaling molecule that can have a variety of effects on plant growth and development. At low concentrations, NO can act as an antioxidant and help to protect plants from oxidative stress. However, at high concentrations, NO can also become a ROS and contribute to oxidative damage. The overall effect of GHGs on plant oxidative stress is complex and depends on a number of factors, including the species of plant, the concentration of GHGs, and the presence of other environmental stressors.

The study conducted by Chiroma et al. [15], revealed that OPEC's carbon dioxide (CO_2) emissions stemming from petroleum consumption have been on the rise, significantly contributing to the issue of global warming. The research employed a combination of a hybrid cuckoo search algorithm and an artificial neural network to forecast OPEC's CO_2 emissions for various time frames: 3, 6, 9, 12, and 16 years into the future. The outcomes demonstrated that this novel model exhibited enhanced precision and efficiency when compared to contemporary methodologies. Furthermore, the investigation underscored that OPEC nations were responsible for 7% of the world's CO_2 emissions in 2010, a substantial proportion considering their 40% share of global oil production. This study's ultimate implication was that precise forecasting of OPEC's CO_2 emissions holds paramount importance for policymakers and stakeholders in crafting effective strategies to combat global warming. This cited passage highlights the profound impact of greenhouse gases like CO_2, which possess a significant global warming potential due to their ability to trap heat in the atmosphere and contribute to climate change. While the greenhouse effect is a natural phenomenon vital for maintaining Earth's temperature, human activities have escalated greenhouse gas levels, leading to detrimental global warming consequences. Global warming poses a grave threat to both the planet and its inhabitants, manifesting in extreme weather events, rising sea levels, and the rapid melting of glaciers. OPEC countries bear a significant responsibility in curtailing their CO_2 emissions to combat global warming effectively.

Gas flaring and pollution

Gas flaring in the Niger Delta constitutes a severe environmental predicament, discharging detrimental pollutants into the atmosphere, thereby exacerbating

air pollution, fostering acid rain, and contributing to noise pollution. According to a study by Nwaichi and Uzazobona [16], the annual emissions of over 100 million tons of CO_2 due to gas flaring in the Niger Delta correspond to the emissions of more than 20 coal-fired power plants. The repercussions of gas flaring on both the environment and human well-being are substantial. The air pollution stemming from gas flaring can lead to respiratory ailments, cardiovascular diseases, and even cancer. Acid rain poses a threat to crops and forests, while noise pollution can result in hearing impairment and various health issues. Furthermore, gas flaring represents a squandering of a valuable resource. Natural gas, a clean-burning fuel, has myriad applications, including electricity generation, heating for homes and businesses, and fertilizer production. By dissipating this gas through flaring, Nigeria is forfeiting a significant source of revenue and opportunities for economic advancement. Several strategies can be employed to curtail gas flaring in the Niger Delta. Firstly, enhancing oil production technologies can facilitate the capture and utilization of more gas. Secondly, establishing gas processing facilities can transform flared gas into marketable commodities. Finally, the government can enforce stricter regulations concerning gas flaring and extend financial incentives to companies that reduce or eliminate their flaring emissions. Mitigating gas flaring in the Niger Delta stands to yield numerous advantages. It would ameliorate air quality, diminish the impact of acid rain, and safeguard human health. Additionally, it would preserve a valuable natural resource and invigorate the Nigerian economy. Legislation and penalties have been introduced to mitigate gas flaring, but challenges remain as seen in **Figure 1**.

Figure 1. Gas flaring site [12].

Rainfall and climate change

The study by Ideki and Weli [17] offers a valuable examination of rainfall fluctuations in North Central Nigeria, employing advanced techniques such as remote sensing and geographic information systems (GIS). Their research reveals a noteworthy decrease in rainfall in this region over recent decades, with an average annual rainfall fluctuation of 896.1 mm during their study period from 2000 to 2017. This decline is particularly pronounced in the early rainy season, displaying a significant negative trend. The study also identifies spatial disparities in rainfall variability, with certain areas witnessing more substantial declines than others. For instance, it notes that high-rainfall regions in the southern part of the area have experienced milder declines compared to low-rainfall zones in the north. These findings align with earlier research documenting rainfall variability in Nigeria and the Sahel region as a whole. Researchers attribute this decline to factors including climate change, shifts in land usage, and the El Niño Southern Oscillation (ENSO). The dwindling rainfall in North Central Nigeria carries a range of adverse consequences for the region, including diminished agricultural output, water scarcity, and heightened susceptibility to droughts and floods. This underscores the urgency of addressing rainfall variability and bolstering climate resilience in the area.

The study highlights the importance of monitoring both CO_2 levels and rainfall. Therefore, the research emphasizes the use of remote sensing to monitor CO_2 levels in the atmosphere and hydrosphere during wet and dry seasons in the Niger Delta region. This approach can provide valuable insights into the relationship between CO_2 and rainfall patterns. In conclusion, the literature review highlights the critical importance of addressing rising CO_2 emissions, understanding their impact on various environmental systems, and monitoring their effects on rainfall patterns, particularly in regions like the Niger Delta. Mitigating CO_2 emissions and managing

their consequences on climate and ecosystems are essential steps in addressing the challenges posed by climate change.

3. Materials and method

3.1 Materials

The subsequent remote sensing data utilized comprise the average mean rainfall data, sourced from the Center for Hydrometeorology and Remote Sensing (CHRS) at the University of Arizona, spanning the period from July 2002 to November 2008. Additionally, the mean Carbon dioxide emissions data were acquired from the Atmospheric Infrared Sounder (AIRS) through NASA's Giovanni platform (accessible at: https://giovanni.gsfc.nasa.gov/giovanni/) for the time frame extending from July 2002 to November 2011. These emissions data were derived from the PERSIANN-CCS system, which enables the categorization of cloud-patch characteristics based on parameters such as cloud altitude, spatial coverage, and texture variability as inferred from satellite imagery. Notably, this system provides real-time, high-resolution (0.04° × 0.04° or 4 km × 4 km) global satellite precipitation data. Additionally, the Niger Delta area map, Mapping Gas Flares in the Niger Delta, and Code of Africa (Impact Africa) by Schick [11] delineates the locations of gas flaring sites and oil and gas fields within the area (**Figure 2**).

3.2 Methodology

Remote sensing data from 44 stations in the Niger Delta from July 2002 to November 2011 was processed using ArcGIS software and the Inverse Distance Weighting (IDW) spatial interpolation method [18]. This allowed us to monitor the trend of carbon dioxide in the region, check the influence of rainfall on carbon dioxide levels, and understand the effect of global warming due to gas flaring. The ArcGIS software was launched and the data was prepared in Microsoft Excel sheets and saved in CSV format. The necessary settings were made in the software, the study area (Niger Delta) was imported, and the CSV file was imported. Then, the Arc toolbox was opened, the spatial analyst tools were selected, and the interpolation option was chosen. The IDW method was selected and the various years were specified. The process extent was selected, the study area was selected, and the spatial analysis option was clicked. Finally, the mask option was selected and the study area was again selected.

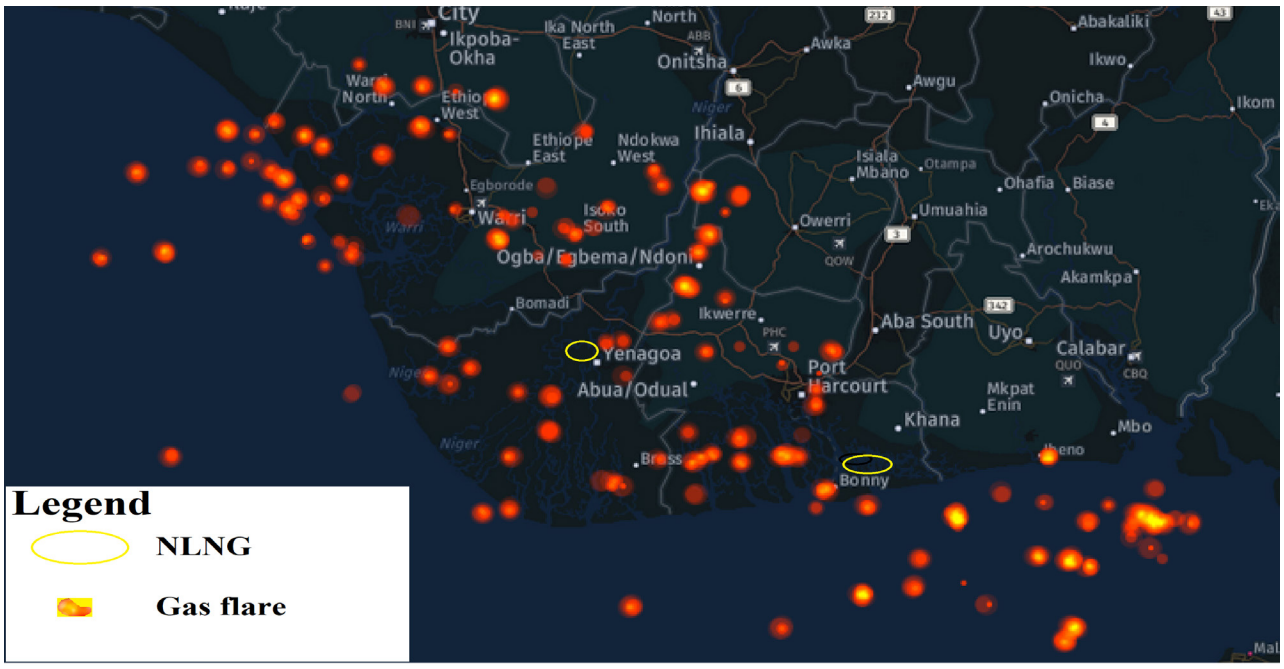

Figure 2. Location map of the Niger Delta region of Nigeria showing gas flaring fields (adapted from Schick [11]).

4. Results and discussions

The Niger Delta region in Nigeria is renowned for its abundant biodiversity and natural resources but confronts various environmental challenges, notably climate change [19]. Carbon dioxide (CO_2) emissions, primarily stemming from fossil fuel combustion, are a prominent driver of global climate change [20]. This study's objective is to assess CO_2 emission levels within the Niger Delta, with a specific focus on the years 2002, 2005, 2008, and 2011. **Table 1** provides data on the minimum and maximum CO_2 emissions for November and July during the years from 2002 to 2011. Numerous factors, including industrial activities, transportation, deforestation, and land-use changes, influence CO_2 emissions in the Niger Delta [20]. Analysing these emissions yields insights into the region's climate change impact, aiding policymakers and stakeholders in crafting effective mitigation and adaptation strategies [19]. July and November hold special significance for carbon dioxide levels and rainfall patterns in the Niger Delta from 2002 to 2011, due to its distinctive climate and environmental dynamics. July marks the height of the rainy season, when warm, moisture-laden air from the Atlantic Ocean migrates inland, resulting in substantial rainfall. This abundant rainfall plays a pivotal role in carbon dioxide regulation. The increased moisture fosters plant growth, enabling photosynthesis that absorbs CO_2 from the atmosphere while releasing oxygen. This process, combined with augmented cloud cover, helps stabilize CO_2 concentrations. Conversely, November signals the transition from the rainy to the dry season. As rainfall diminishes, vegetation loses its lushness, and photosynthesis rates decline. Consequently, CO_2 levels gradually rise as vegetation absorbs less CO_2. Additionally, this transition often ushers in unstable weather patterns and reduced rainfall, potentially impacting the region's water resources and agriculture. Monitoring these two critical months over the 2002-2011 decade is imperative for comprehending long-term climate trends and their consequences on the delicate balance between CO_2 levels and rainfall in the Niger Delta. Changes in these patterns could profoundly affect the region's ecosystems, agriculture, and overall environmental well-being. Thus, continuous monitoring and study of these fluctuations are essential for guiding sustainable practices and adapting to potential shifts in climate and carbon dynamics.

Table 1. Carbon dioxide emission for minimum and maximum.

Year	2002	2005	2008	2011
Min (November)	367.5351	378.1126	383.6403	390.0077
Max (November)	373.4932	380.1209	385.7512	391.608
Min (July)	327.5226	376.8556	382.3989	388.5471
Max (July)	372.7715	379.5303	384.1261	390.7832

Carbon dioxide emissions in July

Gas flaring has been a long-standing environmental problem in the Niger Delta region of Nigeria, resulting in the substantial release of carbon dioxide (CO_2) into the atmosphere. The effect of this practice on the region's CO_2 emissions can be evaluated by examining the data presented in **Table 1** and **Figure 3b**. **Table 1** provides data on the minimum and maximum CO_2 levels in parts per million for the years 2002, 2005, 2008, and 2011. These figures reveal a consistent increase in CO_2 emissions over the course of the decade. The minimum values rose from 327.52 ppm in 2002 to 388.55 ppm in 2011, while the maximum values increased from 372.77 ppm in 2002 to 390.78 ppm in 2011. This upward trend indicates that CO_2 emissions in the Niger Delta have steadily risen during this period. **Figure 3a** visually represents tropospheric CO_2 emissions from July 2002 to 2011. The graph likely exhibits a similar upward trend as observed in the table, confirming that gas flaring has had a significant impact on CO_2 emissions in the region.

These findings have concerning implications. Increasing CO_2 emissions contribute to global climate change, resulting in higher temperatures, rising sea levels, and extreme weather events. Additionally, the Niger Delta region itself faces adverse effects, including air pollution that can harm both human health and ecosystems. Addressing this issue requires a multifaceted approach, including the reduction of gas flaring through improved technology and regulations, as well as a transition to cleaner energy sources. Furthermore,

international cooperation is essential to mitigate the global consequences of such emissions. The spatial distribution map in **Figure 4a** illustrates that in July 2002, areas such as Ondo, Edo, and parts of Delta State had elevated CO_2 levels. In 2005, sections of Edo, Delta, and Bayelsa states exhibited high CO_2 levels in July, as depicted in **Figure 4b**. By July 2008, as shown in **Figure 4c**, only portions of Cross River State displayed elevated CO_2 levels, and in July 2011 (**Figure 4d**), parts of Delta, Bayelsa, and Cross River State experienced increased CO_2 levels. The surge in July's CO_2 emissions can be attributed to various factors, including increased energy consumption for cooling due to rising temperatures, expanded agricultural activities, and potential changes in land-use patterns. Additionally, seasonal fluctuations in economic activities and energy demand may contribute to the observed variations.

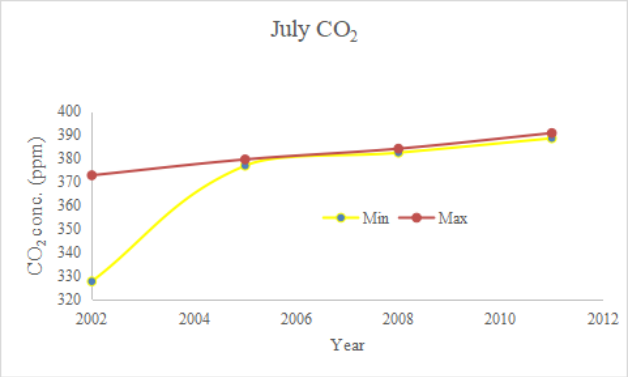

(a)

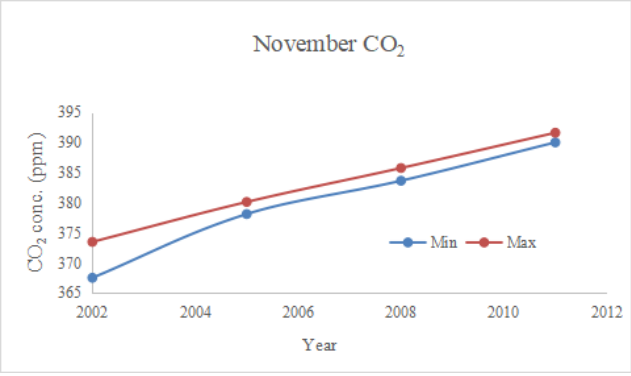

(b)

Figure 3. Tropospheric carbon dioxide emission from July, 2002-2011 (a) and November, 2002-2011 (b) in Niger Delta, Nigeria.

Carbon dioxide emissions in November

To evaluate the impact of gas flaring on CO_2 emissions in the Niger Delta region, we can analyse the data presented in **Table 1** and **Figure 3a**, which depicts the levels of tropospheric CO_2 emissions between November 2002 and 2011. **Table 1** provides information on the yearly minimum and maximum CO_2 emission values. It's evident that both the minimum and maximum emissions have gradually increased from 2002 to 2011. The minimum emissions range from 367.54 to 390.01 ppm, while the maximum emissions range from 373.49 to 391.61 ppm. This upward trajectory clearly indicates a consistent rise in CO_2 emissions during this period. **Figure 3b** visually illustrates this trend, showing a continuous increase in CO_2 emissions over the years. This trend aligns with the growing concerns regarding the impact of gas flaring in the Niger Delta. Gas flaring is a common practice in the region's oil extraction industry, where excess natural gas is burned off into the atmosphere, releasing CO_2 and other harmful pollutants. The increasing trend in CO_2 emissions has several adverse consequences. Firstly, it contributes to global warming and climate change since CO_2 is a greenhouse gas that traps heat in the atmosphere. This can lead to more severe weather events, rising sea levels, and disruptions to ecosystems. Moreover, higher CO_2 emissions can negatively affect human health by contributing to air pollution and respiratory diseases. It can also have detrimental effects on local ecosystems, including marine life and vegetation. The spatial distribution map presented in **Figure 5a** shows that in November 2002, regions encompassing Ondo, parts of Edo, and Delta State displayed elevated CO_2 levels. In **Figure 5b** for 2005, areas including Rivers, Bayelsa, parts of Delta, and Akwa Ibom States exhibited heightened CO_2 levels during November. Moving forward to November 2008 in **Figure 4c**, we observed that Rivers, Bayelsa, parts of Delta, and Akwa Ibom States continued to demonstrate elevated CO_2 levels. In **Figure 4d** for November 2011, parts of Delta, Bayelsa, Rivers, a small section of Akwa Ibom, and Cross River State experienced increased CO_2 levels. These findings collectively point to an overall escalation in CO_2 emissions within the Niger Delta region during the

specified years. This rise in emissions can be attributed to a variety of factors, including population growth, economic development, and the expansion of the industrial sector. Rapid industrialization and urbanization typically lead to a greater demand for energy, resulting in increased burning of fossil fuels and subsequent CO_2 emissions. Identifying the specific sectors responsible for these emissions is crucial in order to develop targeted strategies for mitigation.

Rainfall

The Niger Delta, located in southern Nigeria, is a region characterized by a unique geological and environmental setting, making it susceptible to the impacts of climate change. Rainfall patterns are crucial in this area, as they directly influence vegetation growth, river systems, soil erosion, and overall ecosystem stability. Monitoring and interpreting rainfall trends are essential to understanding how climate change might be affecting this region and, consequently, its geological features.

Rainfall in July

To gain insights into the potential repercussions of gas flaring on precipitation, we can examine **Table 2**, which provides information on rainfall patterns in the Niger Delta during the month of July. **Table 2** illustrates the range of rainfall values for July over a specific timeframe, with values spanning from a minimum of 112.5 mm to a maximum of 463.38 mm. These fluctuations in rainfall are critical for assessing the impact of gas flaring since any increase or decrease in rainfall can significantly influence the region's ecosystems, agriculture, and water resources. For a deeper understanding, it is advisable to scrutinize **Figure 6a**, which depicts the July rainfall data from 2002 to 2011 in the Niger Delta. This dataset offers a temporal perspective on precipitation patterns, allowing us to identify trends and potential associations with gas flaring activities during this pe-

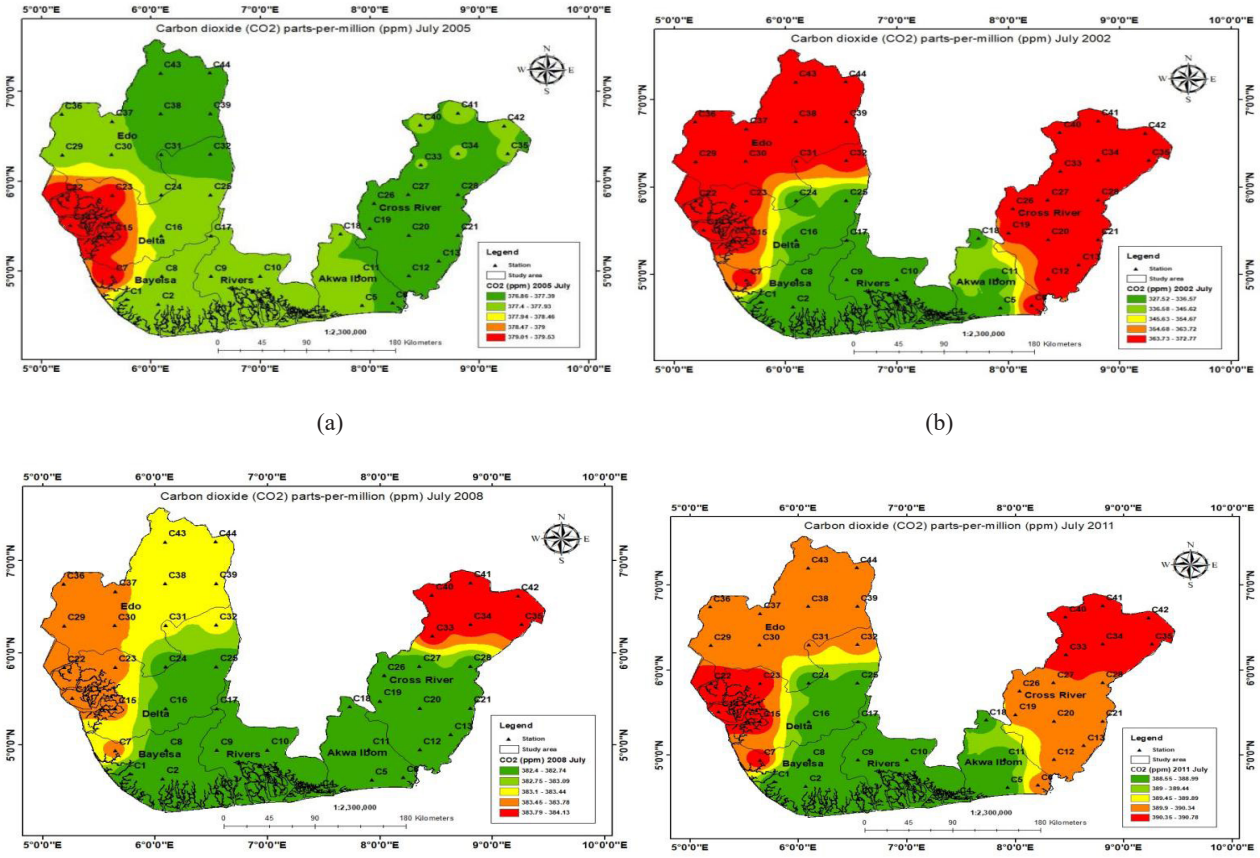

(a) (b)

(c) (d)

Figure 4. Tropospheric carbon dioxide emission in Niger Delta, Nigeria. July (a) 2002, (b) 2004, (c) 2008 and (d) 2011.

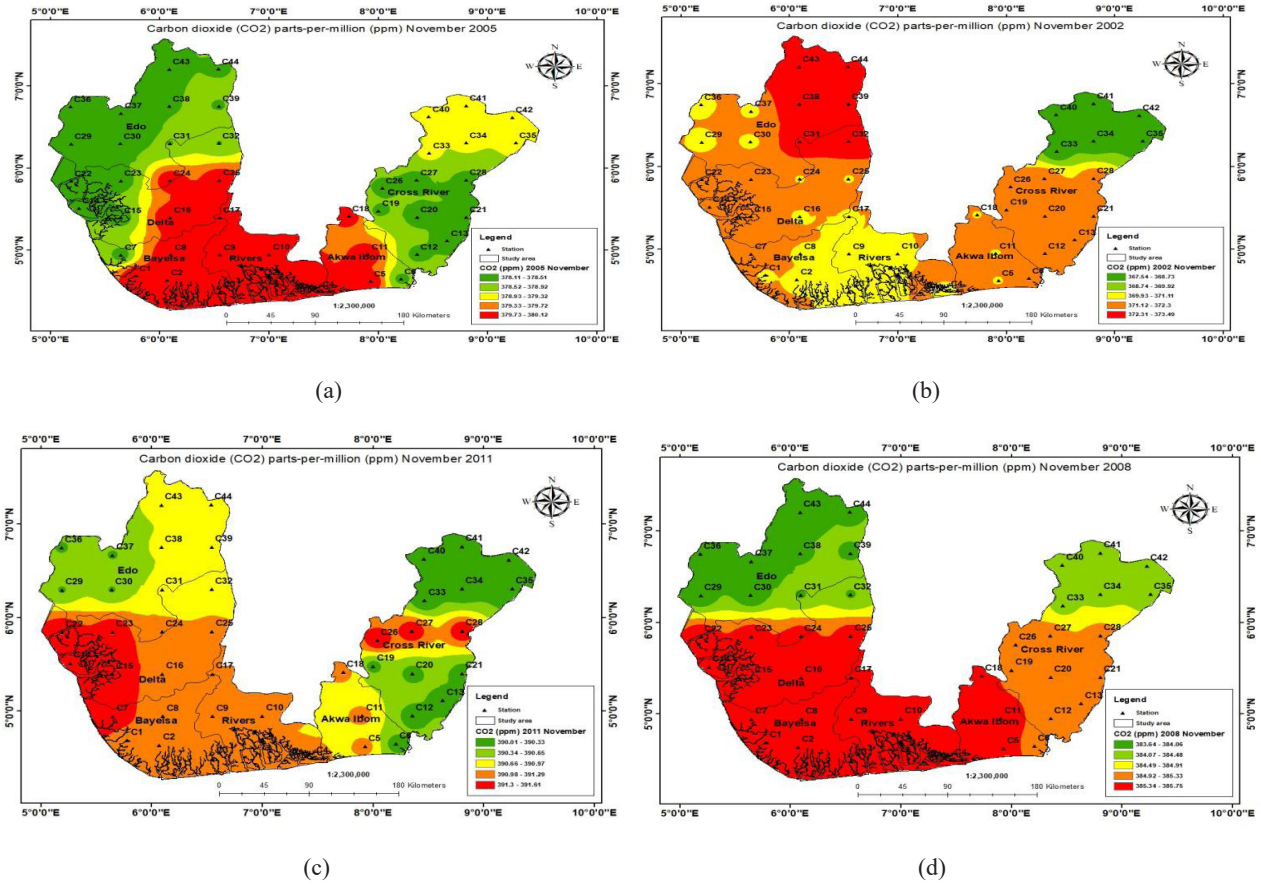

Figure 5. Tropospheric carbon dioxide emission in Niger Delta, Nigeria. November (a) 2002, (b) 2004, (c) 2008 and (d) 2011.

riod. Upon analyzing **Figure 6a**, we can potentially detect shifts or anomalies in rainfall patterns over the years. If there is a consistent trend of increasing or decreasing rainfall that corresponds to the intensity of gas flaring, it could indicate a causative link between the two. Nevertheless, it is crucial to consider other factors such as climate variability and changes in land use that may also impact precipitation. A spatial distribution map reveals that specific areas within Bayelsa, Delta, Akwa Ibom, and Cross Rivers States experienced elevated levels of rainfall in July 2002 (**Figure 7a**). In July 2005 (**Figure 7b**), high rainfall levels were observed in parts of Akwa Ibom and Cross River States. Similarly, in July 2008 (**Figure 7c**), regions within Rivers, Akwa Ibom, and Cross Rivers States displayed increased rainfall levels. In 2011 (**Figure 7d**), portions of Rivers, Edo, Delta, Bayelsa, and Akwa Ibom States witnessed higher levels of rainfall. It is important to note that the July rainfall data does not exhibit a clear and consistent trend. These fluctuations in rainfall can be attributed to various climate drivers and natural variability, underscoring the complexity of the factors influencing precipitation in this region.

Table 2. Rainfall for minimum and maximum.

Year	2002	2005	2008	2011
Min (November)	56.66	54.82	8.18	15.21
Max (November)	338.23	300.19	332.25	253.94
Min (July)	228.9	112.5	382.4	388.55
Max (July)	463.38	393.38	384.13	390.78

Rainfall in November

To comprehend this phenomenon, we can examine **Table 2**, which displays data regarding November's precipitation from 2002 to 2011, as well as **Figure 6b**, which illustrates rainfall trends over the same timeframe. **Table 2** uncovers significant fluctuations in rainfall patterns. In 2002 and 2005, the lowest monthly recorded rainfall stood at 56.66 mm and 54.82 mm, respectively. However, in 2008

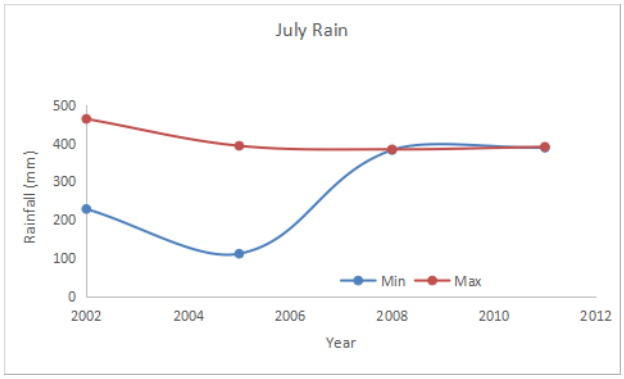

(a)

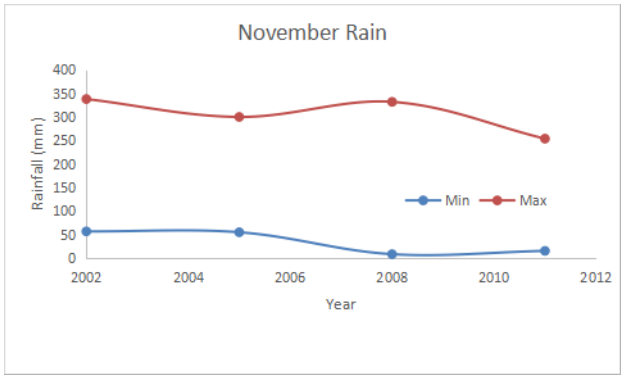

(b)

Figure 6. Rain for July 2002-2011 (a) and November 2002-2011 (b) in Niger Delta, Nigeria.

and 2011, this minimum dropped notably to 8.18 mm and 15.21 mm. This decline in minimum rainfall suggests the possibility of changes in the local water cycle, which could have detrimental impacts on agriculture and water resources. Furthermore, an examination of **Figure 6b** offers a more comprehensive view. Although the data spans from July 2002 to 2011, we can observe variations in rainfall trends. These fluctuations might be influenced by gas flaring activities, as the release of greenhouse gases such as methane can affect atmospheric conditions and modify precipitation patterns. Gas flaring emits pollutants like sulfur dioxide and nitrogen oxides, which can contribute to the formation of acid rain. This could explain the reduced minimum rainfall observed in specific years, notably 2008 and 2011. Acid rain can harm ecosystems, corrode infrastructure, and further disrupt regional climate patterns. When we look at the spatial distribution maps depicted in **Figures 8a-8d**, it becomes evident that particular areas within parts of Akwa Ibom, Cross Rivers, Bayelsa, and Delta States experienced increased levels of rainfall during the period from November 2002 to 2011.

Therefore, the variations observed in the rainfall patterns of the Niger Delta over the ten-year period may have several implications for the region's geological dynamics and environmental health. Changes in precipitation patterns can influence river systems, leading to alterations in sediment transport, erosion, and deposition processes. Additionally, fluctuations in rainfall can impact soil moisture content, potentially influencing groundwater levels and affecting local ecosystems, agriculture, and biodiversity.

Pearson correlation coefficient between CO_2 and rainfall in the Niger Delta

This analysis is based on Pearson correlation coefficients calculated from CO_2 concentration and rainfall data for the Niger Delta region from July and November of 2002 to 2011. The correlation coefficient (r) measures the strength and direction of the linear relationship between the two variables. The values of r range from –1 to +1, with –1 indicating a perfect negative correlation, 0 indicating no correlation, and +1 indicating a perfect positive correlation.

Table 3 presents the Pearson correlation coefficients for CO_2 and rainfall in the Niger Delta for the period of July 2000 to 2011. The minimum correlation coefficient recorded is 0.3858, indicating a weak positive correlation between CO_2 concentration and rainfall. The maximum correlation coefficient is -0.7998, revealing a strong negative correlation between the two variables. In **Table 4**, which covers the period of November 2000 to 2011, the minimum correlation coefficient is –0.8255, indicating a strong negative correlation between CO_2 and rainfall. The maximum correlation coefficient for this period is –0.7415, also indicating a strong negative correlation. Weak Positive Correlation (r = 0.3858): The weak positive correlation between CO_2 concentration and rainfall in the Niger Delta suggests that, to some extent, an increase in CO_2 levels might be associated with a slight increase in rainfall. However, it is important to note that this correlation is weak, meaning other factors likely play a more significant role in in-

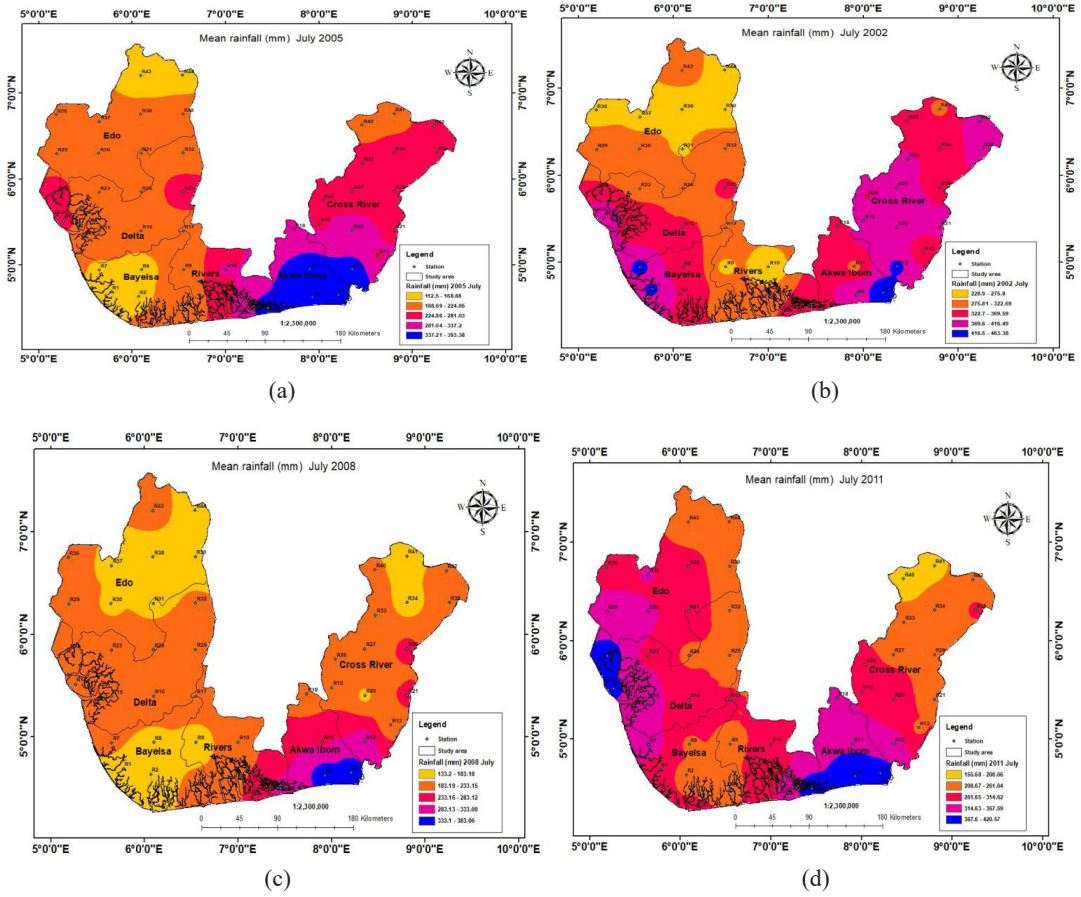

Figure 7. Rainfall in Niger Delta, Nigeria. July (a) 2002, (b) 2004, (c) 2008 and (d) 2011.

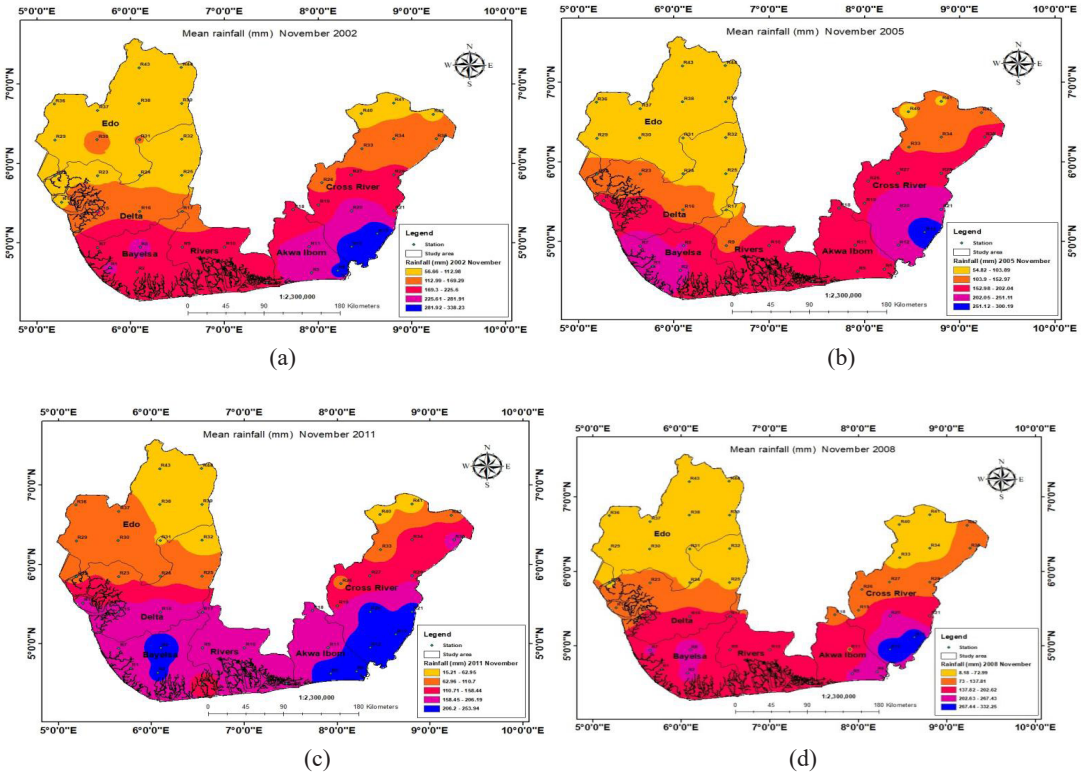

Figure 8. Rainfall in Niger Delta, Nigeria. November (a) 2002, (b) 2004, (c) 2008 and (d) 2011.

fluencing rainfall patterns in the region. Strong Negative Correlation (r = –0.7998 and r = –0.8255): The strong negative correlation observed in both July and November data indicates that as CO_2 concentration increases, there is a decrease in rainfall in the Niger Delta. This finding is particularly concerning, as it suggests that higher CO_2 levels might be associated with drier conditions in the region. Reduced rainfall can have severe consequences for agriculture, water availability, and ecosystem health. Therefore, the observed strong negative correlations between CO_2 concentration and rainfall in the Niger Delta have important implications for climate change in the region. While a weak positive correlation between CO_2 and rainfall might initially appear beneficial, it is essential to recognize that other factors likely have a more substantial impact on rainfall patterns.

Table 3. Pearson correlation coefficient between CO_2 and rainfall from July 2002 to 2011 in the Niger Delta.

2000-2011 (July)	r	Strength	Direction
Minimum	0.3858	Weak	Positive
Maximum	–0.7998	Strong	Negative

Table 4. Pearson correlation coefficient between CO_2 and Rainfall from November 2002 to 2011 in the Niger Delta.

2000-2011 (November)	r	Strength	Direction
Minimum	–0.8255	Strong	Negative
Maximum	–0.7415	Strong	Negative

The negative correlation raises concerns about potential feedback loops. As CO_2 concentrations rise due to human activities like burning fossil fuels and deforestation, it leads to higher temperatures and altered weather patterns. Reduced rainfall can result in decreased vegetation cover and changes in the hydrological cycle, further exacerbating climate change.

Factors such as sea surface temperatures, atmospheric circulation patterns, and local land use changes can influence rainfall in the Niger Delta. Additionally, the relatively short timescale of the data (2002 to 2011) might not fully capture long-term climate trends and variability.

Implications

The analysis of carbon dioxide emissions in the Niger Delta region provides valuable insights into the region's contribution to climate change. The upward trend in CO_2 emissions observed in both November and July indicates a potential increase in greenhouse gas concentrations, which can exacerbate global warming and its associated impacts. Understanding the factors driving CO_2 emissions is crucial for designing effective mitigation and adaptation strategies. Policymakers and stakeholders should focus on implementing sustainable practices and promoting renewable energy sources to reduce dependency on fossil fuels. Efforts should also be directed towards promoting afforestation, sustainable land-use practices, and enhancing public awareness about the consequences of carbon dioxide emissions. Additionally, international collaborations and financial support are necessary to assist countries, like Nigeria, in implementing climate change mitigation and adaptation measures. The findings of this study can serve as a baseline for future monitoring and assessment of carbon dioxide emissions in the Niger Delta region. The rainfall data analysis for the Niger Delta from 2002 to 2011 provides valuable insights into potential climate change impacts on the region. While the data reveals fluctuations in both minimum and maximum rainfall values, caution must be exercised in attributing these variations solely to climate change. Natural climate drivers and geological factors play significant roles in shaping rainfall patterns in the Niger Delta.

5. Conclusions and recommendations

5.1 Conclusions

The analysis of carbon dioxide emissions in the Niger Delta region during the years 2002-2011 reveals a notable increase in emissions. This finding highlights the urgency of taking immediate action to mitigate the adverse effects of climate change.

Encouraging sustainable practices that promote a low-carbon future is essential for fostering a more resilient and sustainable future for the Niger Delta and beyond. By addressing the factors contributing to carbon dioxide emissions, we can pave the way for a more environmentally conscious approach to development in the region. Examining the rainfall data for the Niger Delta from 2002 to 2011 provides valuable insights into potential climate change impacts on the region's hydrology. While the data shows fluctuations in both minimum and maximum rainfall values, it is crucial to exercise caution when attributing these variations solely to climate change. Natural climate drivers and geological factors play significant roles in shaping rainfall patterns in the Niger Delta, underscoring the complexity of the region's climate system. The observed strong negative correlation between CO_2 concentration and rainfall in the Niger Delta reinforces the need to consider this relationship in the context of climate change. The results suggest that increasing CO_2 levels may be associated with reduced rainfall, posing significant implications for the region's ecosystems and communities. Addressing the challenges posed by climate change demands comprehensive research that takes multiple variables into account and incorporates long-term data to develop effective strategies for climate adaptation and mitigation. Therefore, a holistic approach to understanding climate change impacts in the Niger Delta is crucial. The region's vulnerability to the changing climate underscores the importance of implementing sustainable practices and policies to ensure a more stable and sustainable future. This necessitates collaborative efforts across disciplines and sectors to develop adaptive and resilient solutions that can safeguard the Niger Delta's unique environment and support its communities.

5.2 Recommendations

Mitigating Carbon Dioxide Emissions: The overall increase in carbon dioxide emissions during the years 2002-2011 calls for urgent action to curb these emissions. Implementing policies and initiatives that reduce reliance on fossil fuels and promote the use of renewable energy sources, such as solar and wind power, can significantly contribute to lowering carbon dioxide emissions in the region. Sustainable Land Use Practices: Deforestation and land-use changes are significant contributors to carbon dioxide emissions. Encouraging sustainable land use practices, such as reforestation and afforestation, can help sequester carbon and mitigate emissions. Additionally, implementing sustainable agricultural practices that prioritize soil health and carbon sequestration can also play a crucial role in reducing emissions. Climate Resilience and Adaptation Strategies: Given the strong negative correlation between CO_2 concentration and rainfall, the Niger Delta must develop and implement climate resilience and adaptation strategies. These may include improved water management systems, the promotion of water conservation practices, and the development of drought-resistant crop varieties to cope with potential changes in rainfall patterns.

Author Contributions

Otutu, A.O. designed the study and contributed to its writing; Eteh, D.R. processed the data and did statistical analysis and writing; and Iluma, V.P. aided with writing and formatting. All writers contributed to the final draft.

Conflict of Interest

Authors have declared that no competing interests exist.

Funding

The authors stated that no funding was provided.

Acknowledgement

I acknowledge the invaluable contributions of my co-authors, Otutu Anslem Onyebuchi, Eteh Desmond Rowland, and Iluma Vieme Phoebe, in researching and assessing the impact of gas flaring and carbon dioxide emissions on precipitation patterns in the Niger Delta Region of Nigeria through geospa-

tial analysis. I'm also grateful for the guidance and advice provided by Miebaka Oriasi and Mene-Ejegi Omabuwa.

References

[1] Okpobiri, O., Rowand, E.D., Egobueze, F.E., et al., 2023. Monitoring and quantification of carbon dioxide emissions and impact of sea surface temperature on marine ecosystems as climate change indicators in the Niger Delta using geospatial technology. Journal of Atmospheric Science Research. 6(1).
DOI: https://doi.org/10.30564/jasr.v6i1.5107

[2] Ismail, O.S., Umukoro, G.E., 2021. Global impact of gas flaring. Energy and Power Engineering. 4(4), 290-302.
DOI: https://doi.org/10.4236/epe.2012.44039

[3] Global Gas Flaring Tracker Report [Internet]. Word Bank; 2023. Available from: https://www.worldbank.org/en/topic/extractiveindustries/publication/2023-global-gas-flaring-tracker-report

[4] Nduka, J.K., Okafor, V.N., Odiba, I.O., 2016. Impact of oil and gas activities on acidity of rain and surface water of Niger Delta, Nigeria: An environmental and public health review. Journal of Environmental Protection. 7(4), 566.
DOI: https://doi.org/10.4236/jep.2016.74051

[5] Anejionu, O.C., Blackburn, G.A., Whyatt, J.D., 2015. Detecting gas flares and estimating flaring volumes at individual flow stations using MODIS data. Remote Sensing of Environment. 158, 81-94.
DOI: https://doi.org/10.1016/j.rse.2014.11.018

[6] Anejionu, O., Blackburn, A., Whyatt, D., 2013. Remote Mapping of Gas Flares in the Niger Delta with MODIS Imagery [Internet]. Available from: http://www.earsel.org/symposia/2013-symposium-Matera/pdf_proceedings/EARSeL-Symposium-2013_2_2_anejionu.pdf

[7] Maduka, O., Tobin-West, C., 2017. Is living in a gas-flaring host community associated with being hypertensive? Evidence from the Niger Delta region of Nigeria. BMJ Global Health. 2(4), e000413.
DOI: https://doi.org/10.1136/bmjgh-2017-000413

[8] Osuji, L.C., Onojake, C.M., 2004. Trace heavy metals associated with crude oil: A case study of Ebocha-8 Oil-spill-polluted site in Niger Delta, Nigeria. Chemistry & Biodiversity. 1(11), 1708-1715.
DOI: https://doi.org/10.1002/cbdv.200490129

[9] Sakib, S.M., 2021. The impact of oil and gas development on the landscape and surface in Nigeria. Asian Pacific Journal of Environment and Cancer. 4(1), 9-17.
DOI: https://doi.org/10.31557/APJEC.2021.4.1.9

[10] Nwankwoala, H.O., Okujagu, D.C., 2014. A review of wetlands and coastal resources of the Niger Delta: Potentials, Challenges and Prospects. Environment & Ecosystem Science. 5, 37-46.
DOI: https://doi.org/10.26480/ees.01.2021.37.46

[11] Schick, L., 2017. Mapping Gas Flares in the Niger Delta [Internet]. Available from: https://medium.com/code-for-africa/mapping-gas-flares-in-the-niger-delta-f8963f327593

[12] Ndigwe, C., 2022. Nigeria Burns $685m Gas as Flare Sites Project Drags on [Internet]. BusinessDay. Available from: https://businessday.ng/energy/oilandgas/article/nigeria-burns-685m-gas-as-flare-sites-project-drags-on/

[13] World Energy Outlook 2006 [Internet]. OECD iLibrary. Available from: https://www.oecd-ilibrary.org/energy/world-energy-outlook-2006_weo-2006-en

[14] Cassia, R., Nocioni, M., Correa-Aragunde, N., et al., 2018. Climate change and the impact of greenhouse gasses: CO_2 and NO, friends and foes of plant oxidative stress. Frontiers in Plant Science. 9, 273.
DOI: https://doi.org/10.3389/fpls.2018.00273

[15] Chiroma, H., Abdul-Kareem, S., Khan, A., et al., 2015. Global warming: Predicting OPEC carbon dioxide emissions from petroleum consumption using neural network and hybrid cuckoo search algorithm. PloS One. 10(8), e0136140.
DOI: https://doi.org/10.1371/journal.pone.0136140

[16] Nwaichi, E.O., Uzazobona, M.A., 2011. Estimation of the CO_2 level due to gas flaring in the Niger Delta. Research Journal of Environmental Sciences. 5(6), 565.
DOI: https://doi.org/10.3923/rjes.2011.565.572

[17] Ite, A.E., Ibok, U.J., 2013. Gas flaring and venting associated with petroleum exploration and production in the Nigeria's Niger Delta. American Journal of Environmental Protection. 1(4), 70-77.
DOI: https://doi.org/10.12691/env-1-4-1

[18] Intergovernmental Panel on Climate Change (IPCC), 2023. Climate change 2021—The physical science basis. Cambridge University Press: Cambridge.
DOI: https://doi.org/10.1017/9781009157896

[19] Ideki, O., Weli, V.E., 2019. Analysis of rainfall variability using remote sensing and GIS in North Central Nigeria. Atmospheric and Climate Sciences. 9(2), 191-201.
DOI: https://doi.org/10.4236/acs.2019.92013

[20] Burrough, P.A., McDonnell, R.A., Lloyd, C.D., 2015. Principles of geographical information systems. Oxford University Press: Oxford.

BILINGUAL PUBLISHING GROUP

Journal of Atmospheric Science Research

https://journals.bilpubgroup.com/index.php/jasr

ARTICLE

Case Study of Coastal Fog Events in Senegal Using LIDAR Ceilometer

***Semou Ndao*[1*], *Cheikh Modou Noreyni Fall*[1], *Luis Durán*[2], *Assie Regina Djiguene Diatta*[1,3], *Abdou lahat Dieng*[1], *Badara Sane*[1,4], *Amadou Thierno Gaye*[1]**

[1] *Laboratory of Physics of the Atmosphere and Ocean-Siméon Fongang (LPAO-SF), Higher Polytechnic School, University Cheikh Anta Diop (UCAD), PO BOX 5085, Dakar, Senegal*

[2] *Department of Earth Physics and Astrophysics, Complutense University of Madrid, Madrid, 28040, Spain*

[3] *Meteorological Operation Service, Representation of the Agency for the Safety of Air Navigation in Africa and Madagascar (ASECNA) in Senegal, PO BOX 3144, Dakar, Senegal*

[4] *Laboratory of Oceanography and Climate, Experiments and Numerical Approaches (LOCEAN), Sorbonne University (SU), Paris, 75006, France*

ABSTRACT

This study aims to examine the atmospheric conditions characterising fog phenomena on the Senegalese coast focusing on two specific instances that occurred on April 3 and April 30, 2023. These events were detected by the LIDAR Ceilometer installed at LPAOSF/ESP/UCAD and confirmed on the METARs of the meteorological stations at Dakar and Diass airports. The LIDAR's backscatter signal showed that the fog of April 3 started around midnight with a vertical extension at 100 m altitude and dissipated around 10 a.m. The April 30 event characterized by a good vertical extension from the surface up to 300 m above sea level, was triggered just after 2 a.m. and lasted around 3 hours. The results showed that a decrease in temperature, accompanied by an increase in humidity and light wind, is favorable for the triggering and persistence of fog. Sea Level Pressure (SLP) anomaly fields show two distinct configurations. The April 3 event was characterized by a zonal dipole of SLP anomalies between the Sahara and the northern Senegalese coast, while the April 30 event was characterized by a meridional dipole between the Sahara and the Gulf of Guinea area as far as the equatorial Atlantic. A weakening of the pressure around the study area was observed in both cases, allowing moisture advection to favor the onset of fog. The hovmoller diagrams of relative humidity and wind show that a good vertical extension of humidity associated with a westerly wind in the lower layers plays an important role in the formation and persistence of fog. The presence of dry air associated with a weak easterly wind in the middle layers could explain the low vertical extension of the fog on April 3. A strong wind in the lower layers would be responsible for the premature dissipation of the April 30 fog.

Keywords: Coastal fog; LIDAR; Ceilometer; Sea level pressure; Relative humidity; Temperature

*CORRESPONDING AUTHOR:

Semou Ndao, Laboratory of Physics of the Atmosphere and Ocean-Siméon Fongang (LPAO-SF), Higher Polytechnic School, University Cheikh Anta Diop (UCAD), PO BOX 5085, Dakar, Senegal; Email: semoundao2@gmail.com; semou1.ndao@ucad.edu.sn

ARTICLE INFO

Received: 2 September 2023 | Revised: 11 October 2023 | Accepted: 18 October 2023 | Published Online: 27 October 2023

DOI: https://doi.org/10.30564/jasr.v6i4.5943

CITATION

Ndao, S., Fall, C.M.N., Durán, L., et al., 2023. Cases Study of Coastal Fog Events in Senegal Using LIDAR Ceilometer. Journal of Atmospheric Science Research. 6(4): 64-76. DOI: https://doi.org/10.30564/jasr.v6i4.5943

1. Introduction

According to the World Meteorological Organization (WMO), fog is defined as a suspension of fine water droplets near the ground, which can reduce horizontal visibility to less than one kilometer [1]. Fog events can have significant impacts on key sectors of the economy such as transport and agriculture [2], which are already highly dependent on climate in Sahelian countries like Senegal [3]. Fog events can buffer the summer dry season through shading effects and direct water inputs for economically important crops. For the transport sector, these impacts may be harmful. When fog is thick, it creates a sensation of an empty field due to a lack of visual cues, leading to a misjudgment of speeds and distances [4]; it is the inadequacy of these two parameters that causes almost all accidents in foggy weather. In the air transport sector, fog is one of the most dangerous phenomena for aviation, particularly during the take-off and landing phases. The deadliest air accident in the history of civil aviation, with 583 victims, took place on March 27, 1977, due to thick fog at Tenerife airport in the Canary Islands. In France, the Meuse Valley fog of December 1930, still known as Deadly fog of Meuse's valley, claimed dozens of lives [5].

Its hazardous nature for aviation has prompted developed countries to equip themselves not only with suitable observation and monitoring equipment to better understand the "life cycle" of fogs, from their formation to their dissipation, but also for forecasting purposes. Unfortunately, developing countries such as Senegal find it difficult to understand, monitor and predict these phenomena, due to their poor climatic observation infrastructure. However, researchers in the South are increasingly beginning to focus on this phenomenon in order to better characterize it. With this in mind, the Laboratory of Physics of the Atmosphere and Ocean at UCAD's Higher Polytechnic school with the help of Universidad Complutense of Madrid installed a VAISALA LIDAR CL31 in April 2012 to monitor the atmospheric conditions that cause fog. This sensor is nowadays part of UCadMet observatory which is supported and maintained by both institutions. Previous studies have highlighted the need for detailed in situ and remote sensing observations of environmental, microphysical and dynamic processes on multiple spatio-temporal scales to improve fog understanding and predictability [6]. Kim and Yum (2010) mention that fogs, forming over coastal regions, can be classified into two categories: 1) coastal fogs, which form directly over the mainland and their extension is limited to these regions, and 2) marine fogs, which develop in the open ocean and can extend or move towards coastal regions [7]. The sea fogs studied are often of three types: advection, sea smoke and fog resulting from stratus subsidence. Advection fog forms when an atmospheric boundary layer, generally well mixed, is advected onto a colder surface (snow or ice surface, cold water surface) [8]. It is linked to the cooling of the atmosphere on contact with this cold surface, which propagates by turbulence into the neighbouring layers, leading to the condensation of water vapour if the atmosphere is sufficiently humid. Sea-smoke fog generally forms in winter, over a pond or river, when cold air overcomes a warmer water surface [9]. This type of fog is associated with the evaporation of liquid water. Indeed, the difference in vapor pressure between the air and the water surface leads to evaporation, and then the mixing of the water vapor in the cold air leads to super-saturation and consequently to the formation of fog. Concerning coastal fogs, which form directly on the continental part of coastal regions and their extension is limited to these regions [10]. Ryznar (1977) has shown that advection-radiation fog is a coastal phenomenon that results from the radiative cooling of moist air that has been advected onto the continent from the ocean or from a large body of water during the afternoon [11-13]. The dynamic and thermodynamic processes underlying various mechanisms differ, and environmental and microphysical conditions determine which type of fog may appear. Fernando et al. (2020) and Bardoel et al. (2021) identified a case where turbulent mixing between nearly saturated air masses of different temperatures (e.g., a colder gravity current under warmer air) is associated with coastal topography producing

fog [14,15]. One of the most frequently studied coastal fog is advection fog. Choi and Speer (2006) analyzed and described the physical mechanisms leading to the formation of advection fog through a case study on the Yellow Sea, near the Korean coast [16]. These authors have shown that the landforms that delimit this coastal region influence the process of fog formation on the coast in combination with the breeze cycle. These studies confirm that the fogs studied in coastal areas are influenced by several factors on different spatio-temporal scales (advective transport, turbulent exchanges, relief, etc.). Geographically, scientific research on coastal fog has focused more on the American, English, Chinese, Korean and Japanese coasts. This research has focused in particular on the north coast of Scotland and the west coast of California [17-21]. Other studies have focused on the analysis of sea fog in the eastern part of Asia near China, in particular the Yellow Sea [22-24]. Heo et al. (2010) studied fogs of interest on the Korean coast [9]. However, the coastal areas of the eastern North Atlantic that experience a high frequency of fog are little studied in detail, such as the northwest coast of Senegal. Hence the interest in conducting this study to better understand the specificity of the factors controlling the development of these phenomena.

In this study, we focus on the fog events that affected the extreme west coast of Senegal on April 3 and 30 in 2023. The aim of this study is to characterize these two fog events, which respectively caused a fatal road accident on the Dakar freeway and aircraft diversions at Diass airport. The analysis of these two events is based on in situ observations, such as LIDAR from LPAOSF and METAR data from Yoff and Diass airports. The synoptic conditions associated with the formation of these phenomena were analyzed using ERA5 reanalyses. Section 2 describes the data used and the methodological approach adopted. Section 3 presents the results, followed by a discussion. Section 4 presents the main conclusions of the study.

2. Data and methodology

2.1 The data

In order to characterize the two fog events observed in Dakar on April 3 and 30, 2023, we used several types of data, namely lidar data, in situ observations and reanalyses. The LIDAR data used in this work come from VAISALA's CL31 Ceilometer (17.46°W, 14.68 °N). This instrument was installed 20 m above ground on the roof of the Laboratory of Physics of the Atmosphere and Ocean (LPAO) of Cheikh Anta Diop University (UCAD) in April 2012 thanks to the collaboration with Complutense University of Madrid (UCM, Spain) and interMET SME. The acquisition of this device was made possible thanks to a collaboration between Howard University and UCAD through LPAO-SF. This LIDAR is now part of a climate observatory: UCadMet (https://ucadmet.net) named after the two supporting institutions: UCAD and UCM. The operation of the Vaisala CL31 ceilometer is based on an InGaAs laser diode, sending pulses along the zenith direction with an energy per pulse of 1.2 μJ ± 20% [25,26]. This laser diode is eye-safe at a wavelength of 905 nm. The ceilometer uses a single-lens system with overlapping transmit and receive optics. This beam overlap occurs at shallower altitudes, providing an almost complete overlap of the transmitter and receiver field of view at altitudes above 30 m [26]. An inclined mirror separates the transmitting and receiving zones, with a hole in the center. The half-angle beam divergence for our ceilometer measures 0.75 milliradians (mrad) and has 0.66 mrad for the half-angle field of view. This LIDAR has a measurement range from 0 to 7500 m asl, with high temporal resolution (16 seconds, 5400 profiles per day) and high vertical resolution (10 m).

All the technical properties of the LIDAR ceilometer used for this study are summarized in **Table 1** [25,26].

This ceilometer combined with the Boundary

Table 1. Technical properties of VAISALA's CL31.

Property	Value
Laser system	Indium Gallium Arsenide pulsed diode laser
wavelength	905 nm
Pulse properties	1.2 μJ ± 20%
half-angle beam divergence	0.75 milliradian (mrad)
half-angle field of view	0.66 mrad
Measurement range	0-7500 m
Vertical resolution	10 m
Temporal resolution	16 seconds, 5400 profiles per day

Layer View (BL-View) software provides a good vertical profile of the attenuated backscatter signal of atmospheric particles. Several variables are measured, mainly cloud base height, mixing layer level, reflectivity, vertical visibility, atmospheric aerosol load and others [27].

The meteorological observation data used here come from the UCadMet meteorological network and METARs. The UCadMet network, set up in 2012, is the result of various measurement efforts carried out in recent years, mainly thanks to LPAO-SF, UCM and interMET (InterMET Sistemas y Redes S.L.U., Spain). The network is based on automatic weather stations located at a number of sites in the Dakar region. This area extends from the ESP (UCAD) to the island of Gorée. A very heterogeneous area of several kilometers is covered, with a mixture of suburban, urban, rural and maritime environments. Data are sampled every second, then 10-minute averages, maximums, minimums and standard deviation are calculated over a 10-minute integration period. Atmospheric data collected include air temperature at 2 meters height (°C), relative humidity at 2 meters height (%), wind speed at 4 meters height (m/s), and mean wind direction at 4 meters height. Data is periodically checked by visual inspection, and performance reports are produced every three months.

The Meteorological Aerodrome Report (METAR) data used in this work are from Yoff airport (14.73 N-17.50 W) and Diass airport (14.67 N-17.07 W). A METAR is a weather bulletin with a frequency of 30 min or less, mainly used by pilots as part of a pre-flight weather briefing, and by meteorologists, who use aggregated METAR information to aid weather forecasting. Raw METAR is the world's most common format for the transmission of meteorological observation data. It is strongly regulated by the International Civil Aviation Organization (ICAO), which means that it is understood in most parts of the world. A typical METAR contains data on temperature, dew point, wind speed and direction, precipitation, cloud cover, precipitation, cloud cover and height, visibility and barometric pressure. A METAR may also contain information on precipitation amounts, lightning and other information of interest to pilots or meteorologists, such as a pilot report or PIREP, color states and runway visual range (RVR).

In addition to observational data, we also used reanalysis data from ERA5. ERA5 is the fifth generation of European Centre for Medium-Range Weather Forecasts (ECMWF) atmospheric global climate reanalyses, produced by assimilating several satellite and radiosonde observational datasets [28]. It also includes various observational data sets obtained from the WMO's Global Telecommunications System (GTS). The spatial resolution of the data is 0.25° × 0.25° (around 28 km), with 27 pressure levels between 100 and 1000 hPa, including around seven levels in the lowest 1.5 km. Hourly relative humidity and wind are used at different levels to characterize the synoptic environment over Dakar during the fog events studied. Sea Level Pressure (SLP) was also used to monitor the land-sea thermal contrast.

2.2 Methodology

In this study, the fog events that occurred on April 3 and 30, 2023 were detected from the LIDAR backscatter signal. A ceilometer sends out short, powerful laser pulses in a vertical or near-vertical direction. The reflection of light caused by haze, fog, precipitation, aerosols and clouds, known as backscatter, is measured in units of 10^{-9} m^{-1} sr^{-1}. The backscatter signal is generally stronger in the planetary boundary layer where particle concentration is higher, but weaker in the free atmosphere where the atmosphere generally contains fewer particles. BL-View detects the backscatter gradient between the planetary boundary layer and the free atmosphere (the mixing height), as well as other atmospheric structures, such as residual boundary layers and high smoke or aerosol plumes, which can produce strong backscatter gradients. BL-view expresses the intensity of the backscatter signal using color codes for the detection of meteorological phenomena. The color red indicates a signal from clouds, precipitation and fog, and if the color is light blue to yellow, it's an aerosol backscatter signal. To reduce sensitivity to noise and transient details of atmospheric structure, BL-view performs vertical and temporal averaging on ceilometer data. Long averaging intervals avoid false gradient minima generated by signal noise. However, this approach reduces the algorithm's ability to respond to short-scale signal fluctuations in space and time. The level of signal noise depends on range and time of day. The gradient method allows the averaging parameters to be varied. To better determine the spatial expansion of fog events, we compared meteorological parameters such as air temperature, dew point temperature and relative humidity at the three sites of UCAD, Diass and Yoff airports. The dew point temperature at the LIDAR site was calculated using Equation (1) from the relative humidity measured by the UCadMet station [29].

$$T_d = \frac{243.04\left(ln\left(\frac{\mathrm{RH}}{100}\right)+\frac{17.625T}{243.04+T}\right)}{17.625-\left(ln\left(\frac{RH}{100}\right)+\frac{17,625T}{243,04+T}\right)} \quad (1)$$

where T_d is the dew point temperature (in degrees Celsius), T is the Temperature in degrees Celsius and RH is the relative humidity of the air (in percent).

As the relative humidity is not provided directly by the METAR, we calculated it from the dew point temperature using Equation (2) [29].

$$RH = \frac{p_w}{p_s} * 100 \quad (2)$$

where P_w is the ambient vapor pressure and p_s is the saturation water vapor pressure. They are given by the following Equations (3) and (4) [29]:

$$Ps = 6.112 * e^{\frac{17.67T}{(T+243,5)}} \quad (3)$$

$$Pw = 6.112 * e^{\frac{17.67T_d}{(T_d+243,5)}} \quad (4)$$

The following criterion was applied to these meteorological parameters to detect fog events. Indeed, if the relative humidity is above 90% for more than six hours and the weather is marked as fog but not rain or snow, the period is selected as a fog episode [30]. After characterizing the two fog events in terms of duration and intensity, the large-scale environment of atmospheric parameters around these two events was analyzed. Dynamic and thermodynamic variables from ERA5 reanalyses were used.

3. Results and discussion

3.1 Characterization of fog events

The two fog events of April 3 and 30, 2023 over Dakar were detected by the LIDAR Ceilometer and confirmed on the METAR at the Yoff and Diass airport weather stations. The backscatter signal recorded by LIDAR during these two fog events is shown in **Figure 1**. The April 3 event was marked by a high density of fog confined between 0 and 100 m asl. This phenomenon began at around midnight and continued throughout the night, maintaining a high intensity until the early hours of the morning before dissipating at around 10 a.m. at the surface. This high concentration at the surface can be explained by the collapse of the nocturnal boundary layer. During the night, a stable layer of air forms, induced by a temperature inversion. The layer generally dissolves by convection with the appearance of the sun, but it can also remain during the day when solar heating

is not sufficient to disperse the nocturnal boundary layer. However, it is important to note the presence of this signal between 100 and 300 m asl during the day corresponding to maximum sunshine. This could be explained by solar radiation destabilizing the situation at the surface, creating thermals of warm air that rise upwards. The thermal currents continue to rise until their temperature has fallen to the same level as that of the surrounding air. From 5 p.m. onwards, total dissipation was observed across the entire atmospheric column. The configuration of the April 30 event differed from that of April 3 in terms of duration and vertical thickness. The phenomenon started just after 02 a.m., with a significant vertical extension from the surface up to 300 m asl. It lasted three hours before losing its vertical extension and dissipating at the surface, confining itself to between 300 and 400 m asl. This result was confirmed by the horizontal visibility shown in **Figure 2**, where very low visibility (less than 100 m) was observed on April 3 and 30 during the hours of the event. This figure also shows the difference between the two events. On April 3, visibility remained low and constant from 01 a.m. to 11 a.m. On April 30, however, there were two peaks. The strongest peak occurred onset between 2 and 3 a.m., and the secondary peak between 7 and 9 a.m. This type of fog appears to be more dangerous for air transport, as it was reported that at least 4 aircraft were diverted at Diass at the time of the event. And caused the diversion of aircraft due to land at Diass airport. The event of April 30 seems to be less clear-cut, due to the irregular evolution of visibility caused by alternating strengthening and attenuation of weather conditions which favor fog. In fog events such as that of April 3, road transport is often the most affected due to the horizontal reduction in visibility (see **Figure 2**). As illustrated by the heavy collision between a truck and a motorcyclist, which resulted in two deaths on the freeway near Colobane (Dakar, Senegal).

To better characterize these two types of fog, we analyzed surface meteorological parameters such as relative humidity and temperature at the three study sites 1 day before and during the events (**Figure**

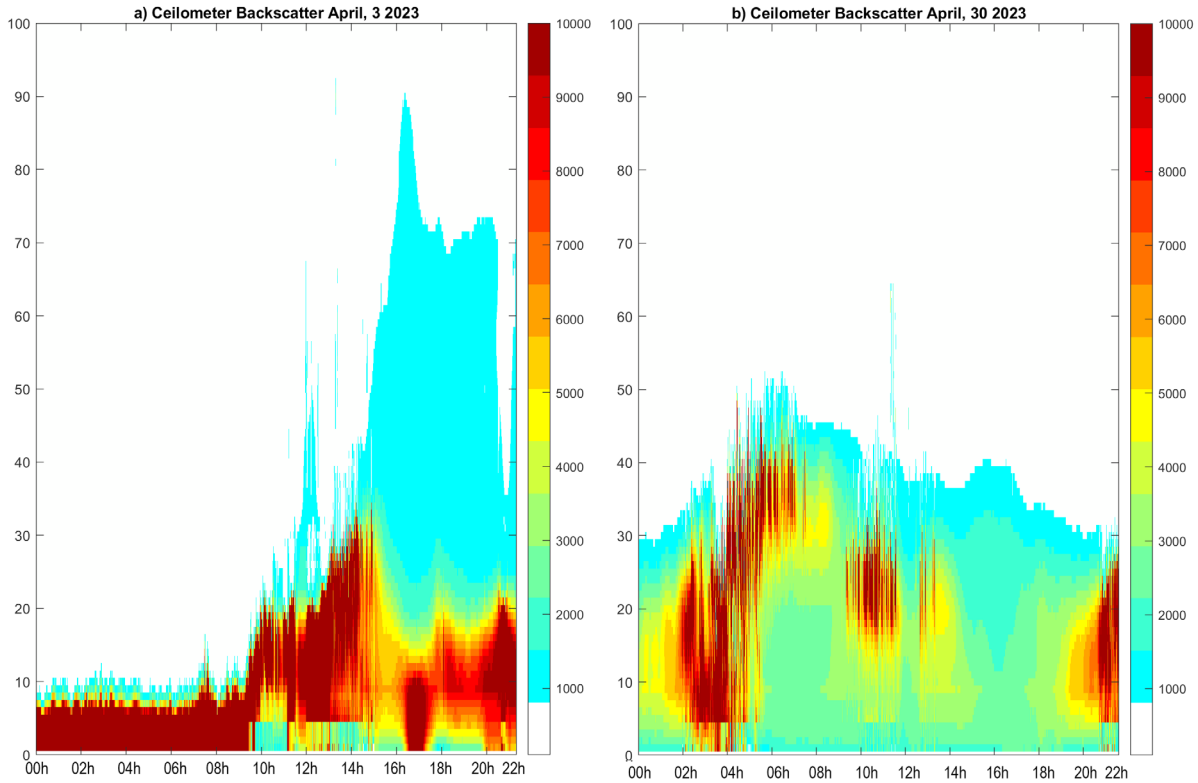

Figure 1. Backscattering of the LIDAR signal for the events of April 3rd and 30th 2023.

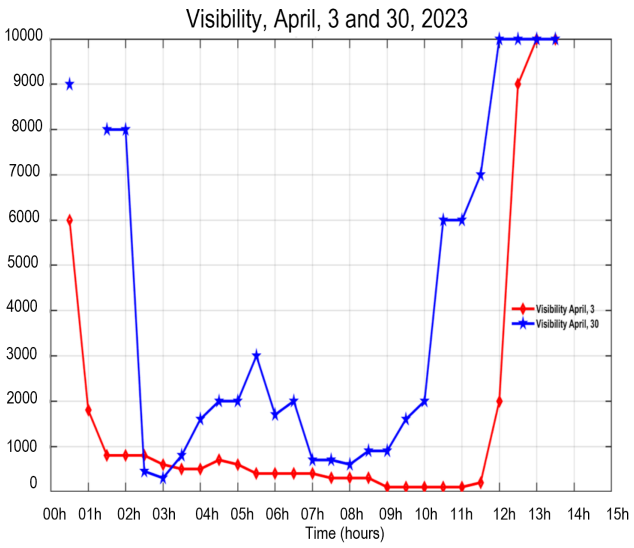

Figure 2. Visibility on April 3 and 30, 2023 in Dakar (METAR AIBD data).

3). This analysis enables us to measure the spatial coherence of these events. The diurnal variation in temperature shows differences between sites the day before the event. The coastal sites of LPAO and Yoff followed a similar pattern, with temperatures reaching 28 and 25 °C respectively at peak sunshine. By contrast, the continental site (Diass airport) showed very marked diurnal temperature variability, with a peak of 35 °C at 12 noon on April 2, the day before the event. This trend was less marked during the April 30 event. However, a slight spatial variation in temperature was observed between these three sites at the time of the fog, with a mean temperature value of around 22 °C. The relative humidity (RH) at the surface measured at all stations exceeded 90% at the time of the events, confirming air mass saturation at all three sites. These results show that a clear drop in temperature, accompanied by an increase in humidity, is conducive to the triggering of fog. However, this condition is not sufficient, given the saturation observed on the night of April 29 without the presence of fog. **Figure 4** shows the wind intensity and direction before and during the events. During the April 3 event, a low-intensity south-westerly wind of around 3 to 10 m/s was observed, bringing moisture to the continent (**Figure 4**). On the other hand, on the eve of the April 30 event, despite saturation combined with a drop in temperature, the high wind intensity inhibited the formation of fog. It took an acceleration of the wind to restore favorable conditions for the April 30th event. Consequently, the impact, location and movement of fog depend on a number of conditions, including wind strength and

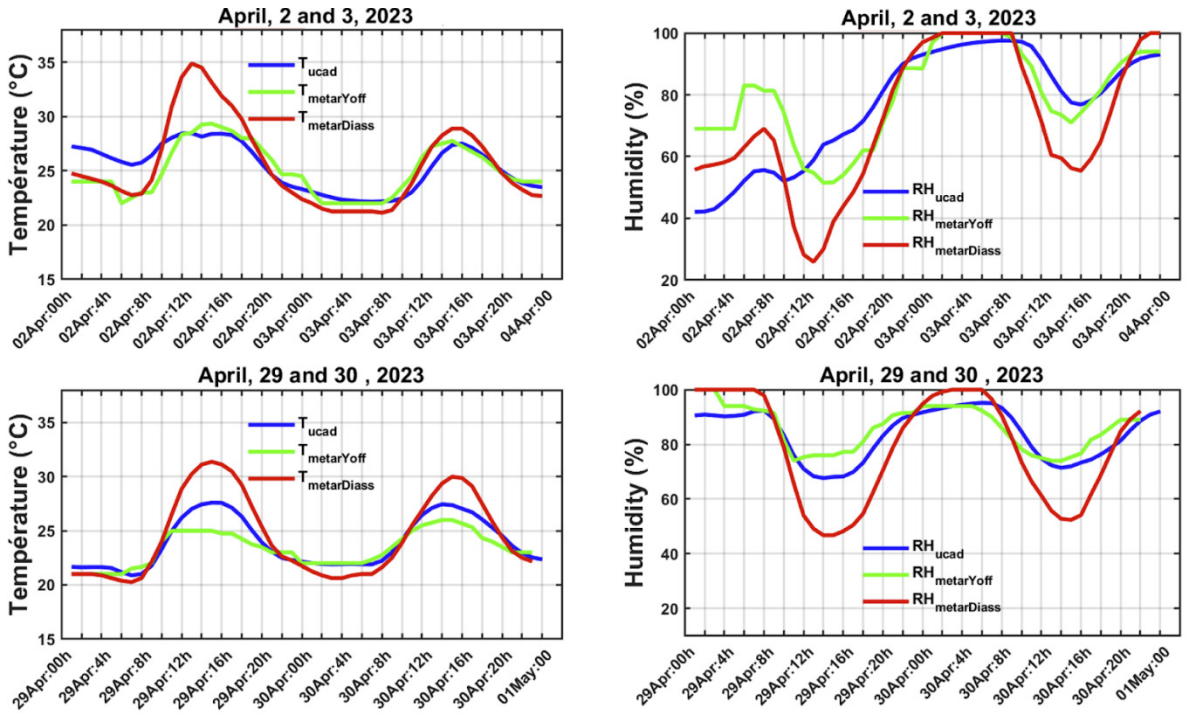

Figure 3. Relative humidity and temperature trends from April 2 to 3 and April 29 to 30, 2023 at Dakar (METAR AIBD data).

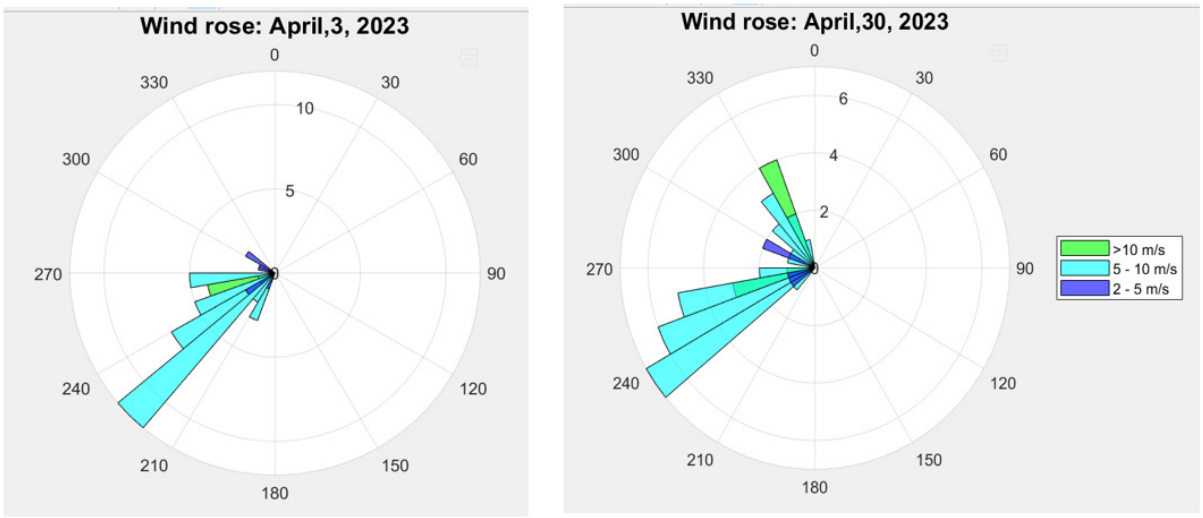

Figure 4. Wind rose from METAR data for Dakar's Blaise Diagne international airport on April 3 and 30, 2023.

direction, ground temperature and humidity. If the wind is strong, fog can dissipate rapidly as the air parcel warms up. On the other hand, if the wind is weak, the fog may persist for longer.

3.2 Analysis of synoptic conditions during fog events

Atmospheric thermodynamic parameters such as minimum sea level pressure (SLP), humidity and winds are factors that influence fog formation, dissipation and frequency of occurrence [31]. SLP can reflect the thermal difference between sea and land, and the spatial distribution of SLP is one of the key factors in fog formation and maintenance. **Figures 5 and 6** show the diurnal variations in SLP anomalies relative to the monthly mean for the month of April 2023 during the April 3 and April 30 fog events. Analysis of these two parameter figures reveals two different patterns. On April 3, a zonal dipole between the continent, more precisely the Sahara (10-25°N; 10°W-10°E), and the northern Senegalese coast was set up during the fog event. The disappearance of this dipole corresponds to the dissipation of the fog at around 11 a.m. to 12 p.m. In addition to this dipole, we observed a decrease in pressure over the Senegalese coast, particularly in our study area, and a strengthening of the Azores anticyclone. This could lead to an influx of moisture from the North Atlantic. This phenomenon, combined with a cooling of the air mass, could explain the persistence of fog until sunrise. For the April 30 event, we observe a dipolar configuration as for April 3, but this time from the south. This meridional dipole is present during the hours of fog, with a strengthening of pressure in the area from the Gulf of Guinea to the equatorial Atlantic, and a decrease in pressure in our study area. Another difference between the two events is the weakening of the Azores anticyclone on April 30, which strengthened during the April 30 event. As a result, moisture transport for the latter event seems to have originated in the equatorial Atlantic, notably in the Gulf of Guinea. Both events could be associated with advection fog. Given the relationship between SLP fields and temperature, this zone of decreasing pressure would correspond to warming. The work of Miller (1958) demonstrated the link between sea surface temperature (SST) and SLP, based on the decrease in surface pressure resulting from warming due to the adiabatic lifting of moist surface air [32]. Saucier's (1955) hypsometric equation illustrates this link, with warm (cold) temperatures resulting in low (high) sea-level pressures [33]. As humidity is a key element in fog formation, advection from a source of moisture is much more favorable than advection from a dry source.

The hovmoller (time-pressure-level) diagrams of relative humidity around our study area (**Figure 7**) show that during the fog event of April 3, the air be-

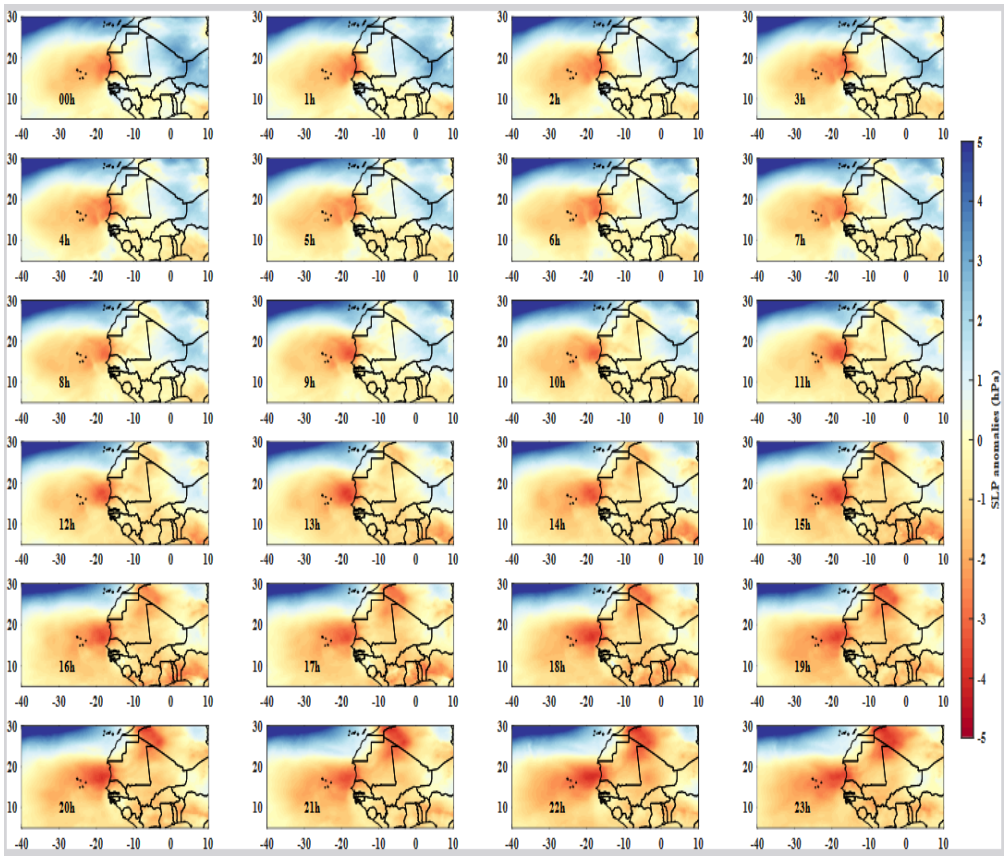

Figure 5. Spatial distribution of SLP anomalies for the event of 3 April 2023 with ERA5 data.

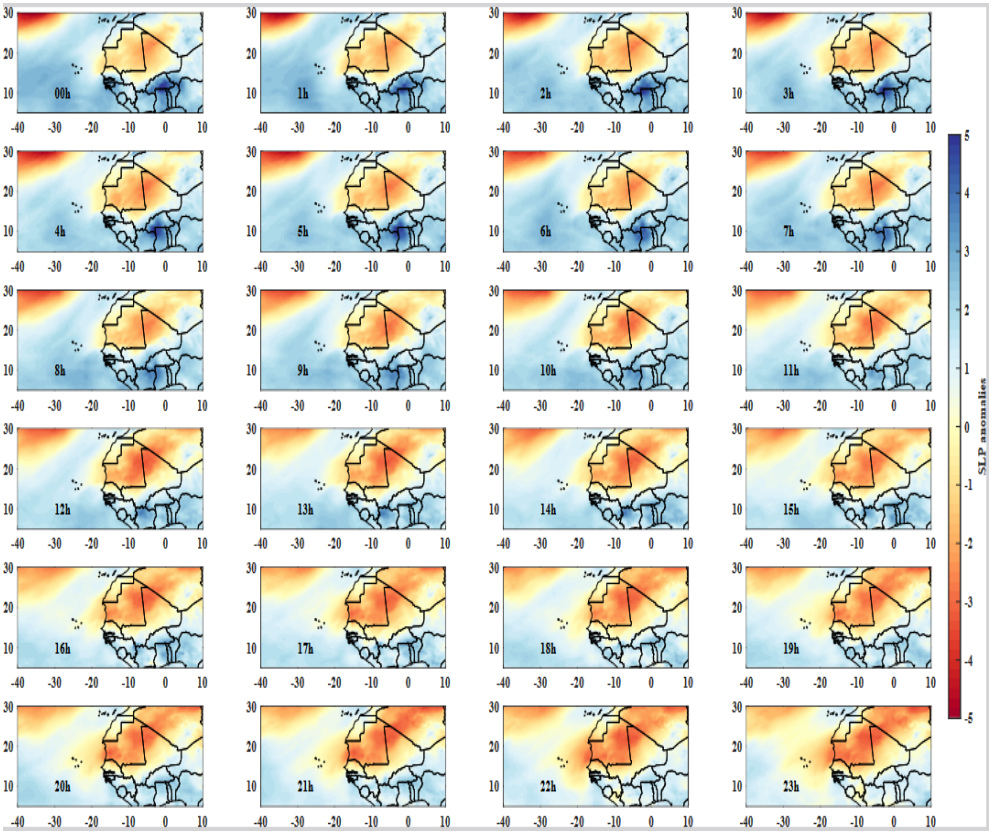

Figure 6. Spatial distribution of SLP anomalies for the event of April 30, 2023 with ERA5 data.

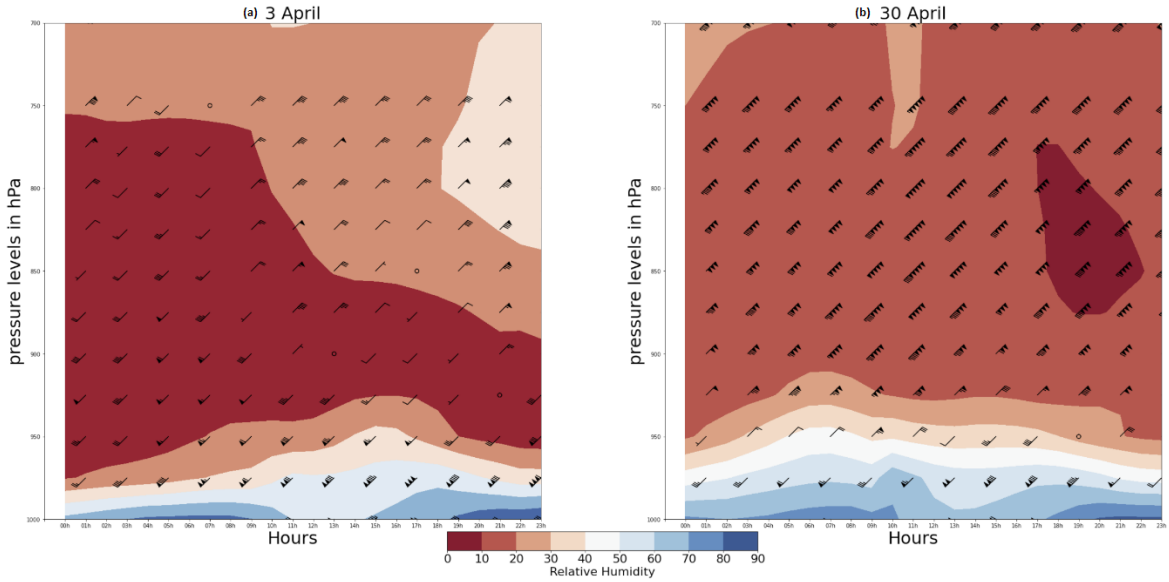

Figure 7. Vertical cross-sections of relative humidity (in color, unit: %), wind field (unit: m/s) for events on April 3 (a) and 30 (b) at different pressure levels.

low 975 hPa (around 300 m) is humid, with humidity levels of between 70% and 80%. This relative humidity increased as the radiation cooled throughout the night and into the morning (between 10 a.m. and 11 a.m.). We also note that relative humidity reached its highest level at the peak of the event (6 a.m. to 11 a.m.), then fell rapidly during the evening (1 p.m. to 5 p.m.). Moreover, during the period of fog formation and persistence, the westerly wind dominated from 1000 to 975 hPa (**Figure 7a**). Moist air from the ocean provided favorable conditions for the formation and persistence of the April 3 fog. Indeed, when relative humidity is high, water begins to condense as temperature drops. This often happens at night, leading to fog formation. Above 975 hPa, the air is dry with a relative humidity of between 10 and 20%. Furthermore, as shown in **Figure 7a**, above 950 hPa, wind speed was low during the global fog process and the prevailing wind direction is from the north-east. The presence of this air tends to confine humidity to the very low layers, favoring the fog's low vertical extension.

For the April 30 event, we observe the same moisture stratification characteristics as for the April 3 fog, but this time the vertical extension is greater (**Figure 7b**). This strong vertical extension of humidity could explain the vertical extension of the April 30 fog. Furthermore, the wind field analysis shows a weak westerly wind in the lower layers and a strong easterly wind in the middle layers (between 950 and 700 hPa) during the hours of the fog event. After the fog event, we note a high wind intensity conducive to fog inhibition. This could explain the short duration of the fog event on April 30.

4. Conclusions

In this work, we studied two fog events observed on April 3 and 30, 2023 over Dakar. Both events were detected by the Ceilometer LIDAR and confirmed on METARs from meteorological stations at Yoff and Diass airports. The backscatter signal recorded by the LIDAR during the April 3 event showed a high density of fog confined between 0 and 100 m asl. This phenomenon began at around midnight and continued throughout the night until the early hours of the morning, before dissipating at around 10 a.m. at the surface. The April 30 event started just after 2 a.m., with a good vertical extension from the surface to 300 m asl and lasted 3 hours.

The characterization of the conditions of formation, persistence and dissipation of the fog events observed on April 3 and 30, 2023 is based on ob-

servations of data from the LPAOSF UCAD-Met network, and the Yoff and Diass METARs. Analysis of surface meteorological parameters such as relative humidity, temperature and wind at 10 m shows that a clear drop in temperature, accompanied by an increase in humidity and a light wind, is conducive to the onset and persistence of fog. In contrast to these conditions, fog dissipation is associated with a strong wind, a decrease in humidity and an increase in temperature due to sunshine. These dissipation conditions are in perfect harmony with the development of the convective boundary layer.

Analysis of the synoptic patterns shows two distinct configurations for the two fog events. Our results highlight a zonal dipole of SLP anomalies between the Sahara and the northern Senegalese coast for the April 3rd event. The April 30 event is characterized by a meridional dipole between the Sahara and the Gulf of Guinea area as far as the equatorial Atlantic. For both events, the fog forms mainly over Dakar under cyclonic or anticyclonic conditions, with a weakening of the pressure around our study area and a strengthening of the pressure over the Sahara. In particular, these conditions are conducive to the formation of advection-radiation fog. Analysis of the hovmoller diagrams of humidity and wind in our study area showed that good vertical extension of humidity combined with a westerly wind in the lower layers play a very important role in the formation and persistence of fog. Furthermore, the presence of dry air and a weak easterly wind above 975 hPa could explain the low vertical extension of the April 3 fog. In addition, the strong wind below 975 hPa could be responsible for the dissipation of the fog, and therefore for the short duration of the April 30 fog event. This analysis can serve as a reference for fog forecasting and early warning. However, given the very limited number of cases, a study over a longer period should enable us to better verify the hypotheses put forward.

Author Contributions

This work was realized in collaboration between all authors. Semou Ndao and Cheikh Modou Noreyni Fall collected and processed data and interpreted the results. They also wrote the first draft of the manuscript. Luis Durán and Abdou lahat Dieng helped to collect Ceilometer's data, contributed ideas and provided valuable comments. Assie Regina Djiguene Diatta collected and processed the METAR data and contributed to interpreting the results and drafting the manuscript. Badara Sane helped to collect Era5 data and provided valuable comments. Amadou Thierno Gaye conceived the idea of the study and supervised the entire work.

Conflict of Interest

The authors declare that there is no conflict of interest.

Acknowledgement

We thank Complutense University of Madrid and interMET for installation and maintenance of Ceilometer's LIDAR CL31. We thank also the European Centre for Medium-Range Weather Forecasts (ECM-WF) for making their Era-5 product available to them and the Agency for the Safety of Air Navigation in Africa and Madagascar (ASECNA) for the METAR data.

References

[1] Fog [Internet]. World Meteorological Organization [cited 2022 Jul 4]. Available from: https://cloudatlas.wmo.int/en/fog.html

[2] Baguskas, S.A., Clemesha, R.E., Loik, M.E., 2018. Coastal low cloudiness and fog enhance crop water use efficiency in a California agricultural system. Agricultural and Forest Meteorology. 252, 109-120.
DOI: https://doi.org/10.1016/j.agrformet.2018.01.015

[3] Fall, C.M.N., Lavaysse, C., Kerdiles, H., et al., 2021. Performance of dry and wet spells combined with remote sensing indicators for crop yield prediction in Senegal. Climate Risk Management. 33, 100331.
DOI: https://doi.org/10.1016/j.crm.2021.100331

[4] Boudala, F.S., Wu, D., Isaac, G.A., et al., 2022. Seasonal and microphysical characteristics of fog at a northern airport in Alberta, Canada. Remote Sensing. 14(19), 4865.
DOI: https://doi.org/10.3390/rs14194865

[5] Zimmer, A., 1930. 'Le brouillard mortel de la vallée de la Meuse': Décembre 1930-Naturalisation de la catastrophe (French) ['Deadly fog of Meuse's valley' (December 1930). Naturalization of the disaster]. Débordements industriels: Environnement, territoire et conflit, edited by Thomas Le Roux and Michel Letté. 115-134.

[6] Gultepe, I., Milbrandt, J.A., Zhou, B., 2017. Marine fog: A review on microphysics and visibility prediction. Marine fog: Challenges and advancements in observations, modeling, and forecasting. Springer: Cham. pp. 345-394.

[7] Kim, C.K., Yum, S.S., 2010. Local meteorological and synoptic characteristics of fogs formed over Incheon international airport in the west coast of Korea. Advances in Atmospheric Sciences. 27, 761-776.

[8] Fu, G., Li, P., Crompton, J.G., et al., 2010. An observational and modeling study of a sea fog event over the Yellow Sea on 1 August 2003. Meteorology and Atmospheric Physics. 107, 149-159.

[9] Heo, K.Y., Ha, K.J., Mahrt, L., et al., 2010. Comparison of advection and steam fogs: From direct observation over the sea. Atmospheric Research. 98(2-4), 426-437.

[10] Wagh, S., Krishnamurthy, R., Wainwright, C., et al., 2021. Study of stratus-lowering marine-fog events observed during C-FOG. Boundary-Layer Meteorology. 181, 317-344.
DOI: https://doi.org/10.1007/s10546-021-00670-w

[11] Ryznar, E., 1977. Advection-radiation fog near Lake Michigan. Atmospheric Environment. 11(5), 427-430.

[12] Fernando, H.J., Gultepe, I., Dorman, C., et al., 2021. C-FOG: Life of coastal fog. Bulletin of the American Meteorological Society. 102(2), E244-E272.
DOI: https://doi.org/10.1175/BAMS-D-19-0070.1

[13] Dione, C., Haeffelin, M., Burnet, F., et al., 2023. Role of thermodynamic and turbulence processes on the fog life cycle during SOFOF3D experiment. Atmospheric Chemistry and Physics Discussions.
DOI: https://doi.org/10.5194/egusphere-2023-1224

[14] Fernando, H.J., Gultepe, I., Dorman, C., et al., 2020. C-FOG: Life of coastal fog. Bulletin of the American Meteorological Society. 1(aop), 1-53.

[15] Bardoel, S.L., Horna Muñoz, D.V., Grachev, A.A., et al., 2021. Fog formation related to gravity currents interacting with coastal topography. Boundary-Layer Meteorology. 181(2-3), 499-521.
DOI: https://doi.org/10.1007/s10546-021-00638-w

[16] Choi, H., Speer, M.S., 2006. The influence of synoptic-mesoscale winds and sea surface temperature distribution on fog formation near the Korean western peninsula. Meteorological Applications: A Journal of Forecasting, Practical Applications, Training Techniques and Modelling. 13(4), 347-360.

[17] Findlater, J., Roach, W.T., McHugh, B.C., 1989. The haar of north-east Scotland. Quarterly Journal of the Royal Meteorological Society. 115(487), 581-608.

[18] Ballard, S.P., Golding, B.W., Smith, R.N.B., 1991. Mesoscale model experimental forecasts of the Haar of northeast Scotland. Monthly Weather Review. 119(9), 2107-2123.

[19] Pilié, R.J., Mack, E.J., Kocmond, W.C., et al., 1975. The life cycle of valley fog. Part I: Micrometeorological characteristics. Journal of Applied Meteorology and Climatology. 14(3), 347-363.

[20] Leipper, D.F., 1994. Fog on the US west coast: A review. Bulletin of the American Meteorological Society. 75(2), 229-240.

[21] Lewis, J.M., Koracin, D., Rabin, R., et al., 2003. Sea fog off the California coast: Viewed in the context of transient weather systems. Journal of Geophysical Research: Atmospheres. 108(D15).

[22] Wong, W.K., Lai, E.S., 2010. Numerical simu-

lation of fog using non-hydrostatic NWP model with third-order turbulence closure. Journal of Hydro-environment Research. 4(2), 131-141.

[23] Diao, X., 1996. Main features of sea fog on Qingdao and its neighbouring sea areas. Marine Science Bulletin-Tianjin. 15, 87-91.

[24] Zhou, B., Du, J., 2010. Fog prediction from a multimodel mesoscale ensemble prediction system. Weather and Forecasting. 25(1), 303-322.

[25] Tsaknakis, G., Papayannis, A., Kokkalis, P., et al., 2011. Inter-comparison of lidar and ceilometer retrievals for aerosol and Planetary Boundary Layer profiling over Athens, Greece. Atmospheric Measurement Techniques. 4(6), 1261-1273.
DOI: https://doi.org/10.5194/amt-4-1261-2011

[26] Guerrero-Rascado, J.L., Costa, M.J., Bortoli, D., et al., 2010. Infrared lidar overlap function: An experimental determination. Optics Express. 18(19), 20350-20369.
DOI: https://doi.org/10.1364/OE.18.020350

[27] Senghor, H., Machu, É., Durán, L., et al., 2020. Seasonal behavior of aerosol vertical concentration in Dakar and role played by the sea-breeze. Open Journal of Air Pollution. 7(9), 11-26.
DOI: https://doi.org/10.4236/ojap.2020.91002

[28] Hersbach, H., Dee, D., 2016. ERA5 Reanalysis is in Production [Internet]. ECMWF. Available from: https://www.ecmwf.int/en/newsletter/147/news/era5-reanalysis-production

[29] Lawrence, M.G., 2005. The relationship between relative humidity and the dewpoint temperature in moist air: A simple conversion and applications. Bulletin of the American Meteorological Society. 86(2), 225-234.

[30] Wang, H., Long, L., Kumar, A., et al., 2014. How well do global climate models simulate the variability of Atlantic tropical cyclones associated with ENSO? Journal of Climate. 27(15), 5673-5692.
DOI: https://doi.org/10.1175/JCLI-D-13-00625.1

[31] Gultepe, I., Tardif, R., Michaelides, S.C., et al., 2007. Fog research: A review of past achievements and future perspectives. Pure and Applied Geophysics. 164, 1121-1159.

[32] Miller, B.I., 1958. On the maximum intensity of hurricanes. Journal of Atmospheric Sciences. 15(2), 184-195.

[33] Saucier, W.J., 1955. Principles of meteorological analysis. University of Chicago Press: Chicago.

BILINGUAL PUBLISHING GROUP

Journal of Atmospheric Science Research

https://journals.bilpubgroup.com/index.php/jasr

ARTICLE

Problems and Opportunities for Biometeorological Assessment of Conditions in Cold Season

***Elena S. Andreeva*[1*], *Sergey S. Andreev*[2]**

[1] *Department of Life Safety and Environmental Protection, Don State Technical University, Rostov-on-Don, 344002, Russia*

[2] *Department of Social and Humanitarian Disciplines of the Rostov Institute for Entrepreneur Protection, Rostov-on-Don, 344029, Russia*

ABSTRACT

The article is devoted to a discussion of the possibilities of biometeorological assessment of the severity of weather conditions during the cold season. The relevance of the study is ensured not only by the fact that residents of a number of states, whose total number is more than 27 million people, live in these extreme climatic conditions, but also by the need to improve biometeorological approaches to assessing the impact of these conditions on the body and health of the population. This study examined biometeorological characteristics that illustrate a measure of cold stress. These include the Siple wind-chill index; Bodman winter severity index; Arnoldi weather hardness coefficient; Mountain wind chill index; weather hardness coefficient according to I.M. Osokin. The results of a comparison of winter severity assessments based on the values of the calculated Siple and Bodman indices made it possible to establish that the Bodman index is more acceptable when assessing mildly severe winters. The most adequate for assessing the "severity" of the cold period against the background of a decrease in air temperature and an increase in wind speed is the Siple index. The need to provide the countries of the world with high-quality hydrometeorological and biometeorological forecast information is justified and relevant. In this regard, these studies are very promising.

Keywords: Biometeorological indices; Severe weather; Cold period of the year; "rigidity" of weather conditions; Cold stress; Biometeorological assessment

*CORRESPONDING AUTHOR:

Elena S. Andreeva, Department of Life Safety and Environmental Protection, Don State Technical University, Rostov-on-Don, 344002, Russia; Email: meteo0717@yandex.ru

ARTICLE INFO

Received: 30 August 2023 | Revised: 7 October 2023 | Accepted: 15 October 2023 | Published Online: 31 October 2023

DOI: https://doi.org/10.30564/jasr.v6i4.5935

CITATION

Andreeva, E.S., Andreev, S.S., 2023. Problems and Opportunities for Biometeorological Assessment of Conditions in Cold Season. Journal of Atmospheric Science Research. 6(4): 77-85. DOI: https://doi.org/10.30564/jasr.v6i4.5935

1. Introduction

As we all know, weather conditions in their totality and duration have a very tangible effect on the human body. In this regard, the main task of biometeorological research is not only a comprehensive study of the above impact, but also the identification of the principles of possible adaptation to it. The idea of the impact of weather conditions on the human body and the development of diseases in it was expressed in the ancient world [1]. It is enough to mention the works of the ancient Greek scientist, doctor, thinker Hippocrates (about 460 B.C. - about 370 B.C.). Subsequently, biometeorological research continued, and their results are available in the works of a number of prominent scientists, such as Avicenna (Ibn Sina) (10-11th century), Paracelsus (Theophrastus von Hohenheim) (15-16th century), A.I. Voeikov (19-20th century) and others [2].

The problems of the impact of weather conditions on the human body are dealt with by the World Meteorological Organization (WMO), one of the areas of activity of which is the development of effective measures to reduce the risk of adverse effects of weather conditions on public health. It is worth mentioning that the issues of developing high-quality forecasts of various hazards associated with weather and extreme weather conditions, including natural disasters or severe weather events, as well as rapid changes in weather conditions, including sudden cold spells or warming of particular relevance. Of course, experts from the World Meteorological Organization understand "severe weather conditions" to mean a slightly wider range of dangerous weather-related phenomena, which include not only low temperatures, but also tropical cyclones, hurricanes, dust storms, etc.

Besides, the first severe weather forecasting project was started in 2006 in southeast Africa with the direct participation of 5 countries: Bostwana, Madagascar, Mozambique, the United Republic of Tanzania, and Zimbabwe. The Regional Specialized Meteorological Center in Pretoria (South Africa) provided these pages with forecast products related to severe weather conditions, and the Regional Specialized Meteorological Center in Reunion (France) provided support in the field of tropical cyclone forecasting, using Eumetsat satellite information. Later, in 2008, the project covered 16 African countries. The obvious success of this project was noted at the Fifteenth World Meteorological Congress (Cg-XV, 2007), during which a joint decision was made to expand the project and its implementation throughout Africa and other countries of the World Meteorological Organization. In subsequent years, the project was extended to other subregions of the world, receiving further development. For this reason, the Eighteenth World Meteorological Congress (Cg-XVIII, 2019) emphasized the role of cascaded severe weather forecasting from global to regional and national levels through the World Meteorological Organization's Global Data and Forecasting System (GDPFS) centres.

Thus, currently, about 80 countries from 9 subregions of the world participate in the WMO Severe Weather Forecasting Program (SWFP), aimed at strengthening the capacity of National Meteorological and Hydrological Services (NMHSs) in developing countries, including least developed and island countries, to provide improved forecasts and severe weather warnings. This SWFP program is based on a global data processing system, including forecasting weather conditions based on a "cascade forecasting process" (from global to national to regional levels). The SERCOM/SC-DRR Advisory Group on Severe Weather Forecasting (AG-SWF) held an extraordinary remote meeting on June 30, 2023.

It is important to emphasize that the implementation of the SWFP Program is largely consistent with the development plan of the World Meteorological Organization, contributing to the achievement of the following strategic goals:

1) Strengthen national early warning systems for weather hazards and increase the coverage of effective responses to weather hazards and associated risks.

2) Increasing the value of meteorological information and introducing innovations in the provision of meteorological information, meteorological services and decision support.

3) Availability of using the results of numerical analysis and forecasting of the Earth's climate sys-

tem in spatiotemporal terms and within the framework of the Global Data Processing and Forecasting System of the World Meteorological Organization.

4) Meeting the needs of developing countries for quality hydrometeorological information as part of providing them with the necessary weather, climate, hydrological and environmental services. Undoubtedly, WMO activities under the SWFP play a very important role in reducing the social and economic impacts of global hazards and threats associated with severe weather and its various phenomena.

There is no doubt that WMO's SWFP activities play a very important role in reducing the social and economic impacts of global hazards associated with severe weather and its various phenomena. Against this background, regional or local problems of severe weather associated with the impact on the human body of various combinations of meteorological elements, including air temperature and wind speed, which together reduce human thermal sensations, deserve special interest.

In addition, by actively working to improve the quality of early warning systems for weather hazards at different levels, including regional and national, the SWFP provides significant support for the United Nations 2030 Agenda for Sustainable Development in accordance with the goals of "sustainable development" and the Sendai Framework for Disaster Risk Reduction for the period 2015-2030. This study aims to investigate the impact of extreme cold conditions caused by winter low temperatures on population health from various severe weather phenomena.

2. Materials and methods

To achieve the goal of the study, reference materials were used in the work, containing long-term (1890-1960; 1960-1990; 2000-2020) numerical characteristics of the climate of a number of territories located at high latitudes (60-80 degrees north latitude). A number of numerical characteristics were considered, illustrating the thermal structure of the environment affecting the human body, known as biometeorological indicators. Thus, more than 30 biometeorological indicators are usually used for scientific research and calculations, divided into 7 main groups [3]. The first group, which includes temperature and humidity indicators, includes the effective temperature of still air, ET; and discomfort index, *DI* (*DY*). The second group, containing temperature-wind indicators or cold stress indices, includes the wind-cold index according to Siple [3-5], *W(K)*; winter severity index according to Bodman (*S*); Arnoldi weather stiffness factor, T; Hill wind chill index, *H*; weather stiffness coefficient according to I.M. Osokin [6-9], S_0. The third group contains temperature-humidity-wind indicators for shady spaces, including equivalent effective temperature, *ET* (taking into account the influence of wind) or *EET*; normal equivalent-effective temperature (taking into account the influence of wind for a dressed person). The fourth group of biometeorological indicators—temperature-humidity-wind—includes radiation equivalent effective temperature, *REET*; biologically active temperature, *BAP*; and reduced temperature index according to V.N. Adamenko and K.Sh. Khairullin, Tpr; heat balance of the human body according to V.I. Rusanov, *Qs*; thermal insulation properties of clothing, *C*. The fifth group of indicators includes the indices of pathogenicity and climate variability: the index of pathogenicity of the meteorological situation according to V.G. Boxsha, *I* [10-12]; weather class of the moment according to V.I. Rusanov, *KPM*; biological index of changing weather conditions according to V.Sh. Belkin, *BISM*; meteorological health index according to O.G. Bogatkin, *MIZ*; indicator of tension of thermoregulation mechanisms according to B.A. Eizenshtat, *G*; heat load index according to K.Ya. Kondratiev, *N*. The sixth group of biometeorological indicators consists of climate continentality indices according to L. Gorchinsky, *Kg* or according to S.P. Khromov, *Khr*. It was proposed to supplement the groups of biometeorological indicators with a group that would contain numerical characteristics of the level of pollution of the surface air layer [1]. So, in the seventh group of biometeorological indicators, it is recommended to include the total index of atmospheric pollution, *API*; atmospheric pollution potential, *PZA*; climatic potential of self-purification of the atmosphere according to T.S. Selegey, *Kmp* or

according to I.L. Linevich, *Km*.

3. Results

As it seems to the authors, when examining the signs of severe weather, that is, the measure of the severity of weather conditions and bearing in mind the regional or local characteristics of territories located in the temperate and arctic latitudes of the Northern Hemisphere, we will consider biometeorological characteristics illustrating the measure of cold stress (the second group of biometeorological indicators), which, reducing a person's heat sensation, thereby limiting his capabilities. The indicators mentioned above include indicators such as wind-cold index according to Siple, *W(K)*; winter severity index according to Bodman (*S*); Arnoldi weather stiffness factor, *T*; Hill wind chill index, *H*; weather stiffness coefficient according to I.M. Osokin, S_0.

Obviously, when assessing human heat sensations, the characteristics of the intensity of the wind flow are essential. In this regard, Paul Siple (1957), an Antarctic researcher, proposed introducing the so-called wind-cold index, *W(K),* to assess the impact of negative air temperature and wind speed on the thermal state of the human body (Equation 1):

$$W(K) = \left(\sqrt{100V} + 10,45V\right)\left(33 - t\right) \quad (1)$$

where *W(K)* wind-cold index, points
V wind speed, m/s
t air temperature, °C

In fact, the Siple wind-cold index allows one to estimate the intensity of heat loss by the human body due to the combined effect of wind speed with various variations in air temperature values. In the scientific literature, there are explanations regarding the extreme values of the Siple index: at $W(K) < 50$, the biometeorological conditions of the cold period correspond to very warm conditions ("hot"); at $W(K) > 1000$, very cold conditions are observed ("very cold"). In this connection, in order to be able to compare the assessments of wind-cold conditions in the winter period based on the calculations of the Siple index with the values of other indices, the authors proposed a detailed scale of gradations for the Siple index values (**Table 1**).

Table 1. Siple index scale, *W(K),* to characterize the conditions of the cold period.

Siple index value, W(K)	Characteristics of the conditions of the cold period of the year
< 50	very warm conditions
50-200	warm conditions
201-350	cool conditions
351-500	slightly cold conditions
501-800	moderately cold conditions
801-1000	cold conditions
1001-2000	very cold conditions
2001-3000	harsh conditions
3001-4000	very harsh conditions
4001-7000	extremely harsh conditions
> 7001	extremely harsh conditions

In addition to the Siple index, one of the most well-known indices, the Bodman index (*S*), is successfully used to assess the severity of winter conditions, which makes it possible to identify the "severity" of winter weather in accordance with the "severity" score scale (**Table 2**).

Table 2. Bodman index scale, (*S*), to assess winter severity conditions.

Bodman index value, (S)	Characteristics of winter conditions
< 1.0	rough, soft
1.1-2.0	little-severe
2.1-3.0	moderately severe
3.1-4.0	severe
4.1-5.0	very harsh
5.1-6.0	hard-severe
> 6.1	extremely severe

When calculating the values of the Bodman index, *(S),* they rely on the assessment of the duration of the cooling process of a vessel with water having an initial temperature of +30 °C and cooled to a temperature of +20 °C (Equation 2):

$$S = \left(1 - 0,004t\right)\left(1 + 0,272V\right) \quad (2)$$

where *S* wind-cold index, points
V wind speed, m/s
t air temperature, °C

Studies by a number of authors have shown [4-6] that assessments of the "severity" of winter weather based on the Bodman index, (*S*), imply a significant variability in the range of air temperature values, that is, with the same score of "severity" of winter weather calculated for a certain value of wind speed, the values of air temperature can vary by 10-15 °C. Due to the fact that these circumstances could not but affect the accuracy of assessments of the biometeorological conditions of winter weather, I.M. Osokin proposed a refinement of Equation (2) by introducing additional coefficients and changing the constants in front of the temperature and wind speed:

$$S = (1 - 0,006t)(1 + 0,20V)(1 + 0,0006H_k)H_b A_c \quad (3)$$

where S wind-cold index, points
V wind speed, m/s
t air temperature, °C
H_k absolute height of the terrain, m
H_b relative humidity factor
A_c coefficient taking into account the role of daily air temperature amplitudes

However, refinements of Equation (2) introduced by I.M. Osokin, did not allow for improving the quality of assessments of biometeorological conditions of the winter period, since the calculations of the "hardness" of winter weather for settlements located in different geographical areas, carried out using the refined Equation (3), showed fairly close results [7,8].

Refinements of Equation (3) introduced by I.M. Osokin, include the altitudinal characteristics of the area, as well as coefficients taking into account relative humidity and daily temperature amplitudes. However, despite the physical validity of their introduction, the above clarifications are apparently not quite mathematically correctly reflected in the final form of the Equation (3). In this connection, Equation (2) is more applicable, the calculation results of which are most consistent with the real conditions of the winter period.

In addition to the indices described above, which describe the severity of winter weather conditions, the weather "severity" coefficient is also known according to I.A. Arnoldi, *T*. [9]. The usefulness of this coefficient is due to the fact that, being an empirical indicator, it allows one to evaluate the "hardness" of winter weather, based on the correspondence of an increase in wind speed by 1 m/s to a conditional decrease in air temperature values by 2 °C (Equation 4):

$$T = t - 2V \quad (4)$$

where T weather "hardness" coefficient according to I.A. Arnoldi, points
V wind speed, m/s
t air temperature, °C

It is important to note that the values of the described I.A. Arnoldi, *T*, correlate with physiological data [10-14], and the degree of functional stress of thermoregulation systems, as studies have shown, depends on air temperature. And, if the actual load on the apparatus of thermoregulation of the human body is determined by the air temperature, then, based on Equation (4), the wind speed has a greater mathematical significance for estimating the numerical values of the coefficient *T*. So, in accordance with observations of the state of the body at various combinations of air temperature and wind speed in the cold period, in the framework of calculating the coefficient *T*, it was found that at air temperature values:

from 0 to –15 °C	the tension of the thermoregulatory apparatus of the human body is weak;
from –16 to –29 °C	average;
from –30 to –45 °C	strong;
from –46 °C or more	excessive.

A positive point is also the fact that this coefficient I.A. Arnoldi, *T*, not only characterizes the measure of the severity of winter conditions, but also makes it possible to justify the needs of a person in clothing that allows him to provide thermal comfort when working outdoors. However, the established discrepancy between the results of observations and the mathematical expression (Equation 4) undoubtedly significantly reduces the accuracy of the I.A. Arnoldi, *T*, results.

The Hill Wind Chill Index is also used to describe the severe biometeorological conditions of the winter period.

There are two mathematical equations for calculating the numerical values of the wind chill index. For the case of dry cooling, Equation (5) is applied:

$$H = \left(0,13 + 0,47V^{0,5}\right)\left(36,6 - T_H\right) \quad (5)$$

where H wind (dry) cooling index, W/m^2
V wind speed, m/s
T_H air temperature, °C

Based on the analysis of the results of calculating the values of the wind (dry) cooling index, H, human heat sensations have the following gradations:

0.35-0.5	hot
0.6-0.9	comfortable
1.0-1.7	cold
1.8-2.3 or more	extremely cold

According to experimental data, possible frostbite of parts of the human body, including limbs, is observed at values of the wind (dry) cooling index, H, equal to or more than 0.7 W/m^2 [15].

The second mathematical equation for calculating the Hill wind chill index takes into account the correction for water vapor pressure and is determined by the Equation (6):

$$H_W = H + \left(0,085 + 0,102V^{0,3}\right)\left(61,1 - e\right)^{0,75} \quad (6)$$

where H_W wind cooling index, W/m^2
H wind (dry) cooling index, W/m^2
V wind speed, m/s
e water vapor pressure, hPa

The wind chill index described above, which takes into account the elasticity of water vapor, characterizes the intensity of heat loss in a moist moving air stream. At the same time, the numerical values of the H_W index, located in the range from 4.5 to 5.5 W/m^2, characterize the uncomfortable weather conditions of the winter period; with a value of the H_W index > 8.0 W/m^2, absolutely uncomfortable winter conditions are established.

Gradations of the values of the Hill wind cooling index, taking into account the elasticity of water vapor, H_W, W/m^2, are presented below:

3.5-4.4	comfortable
4.5-5.5	cold (discomfort)
5.6-7.9	extremely cold
8.0 or more	absolute discomfort

4. Discussion

For a more detailed study and assessment of the applicability of the most adequate biometeorological indicators considered above, a summary table was compiled containing calculated and empirical data (**Table 3**).

Table 3. The results of assessing the applicability of biometeorological indicators of the severity of winter conditions in comparison with empirical data.

Wind speed, m/s	**Air temperature, °C**	**Results of calculations of biometeorological indices**				**The results of observations of human heat sensation, perceived air temperature, °C**
		Siple index, *W(K)*		Bodman index, *S*		
1	0	809	cold conditions	0	mild conditions	–0.8
2	–10	1505	very cold conditions	1.6	little-harsh	–14.1
3	–15	2335	harsh conditions	2.0	little-harsh	–21.5
4	–20	3275	very harsh conditions	2.3	moderately severe	–28.9
5	–25	4330	extremely harsh conditions	2.6	moderately severe	–36.2
8	–30	7050		3.6	severe	–45.4
12	–35	10400	extremely harsh conditions	4.9	very harsh	–54.8
20	–40	17929		7.5	extremely severe	–61.5

Analysis of the obtained results of comparison of estimates of the severity of the winter period based on calculations of such well-known biometeorological indicators as the Siple index *W(K)* and the Bodman index, *S*, with the results of observations of various human heat sensations for some combinations of wind speed (m/s) and air temperature, (°C), presented in **Table 3**, made it possible to establish the following very revealing points:

- with slight frosts in combination with low wind speeds, the Bodman index, *S*, is most accurate for assessing the severity of winter conditions;

- more adequate estimates of the "hardness" of the cold period against the background of lower air temperatures and increased wind speed are given by the Siple index, *W(K*).

5. Conclusions

Thus, as a result of a comparative analysis of a number of biometeorological characteristics illustrating the measure of cold stress and reducing a person's sense of heat, it was found that for milder winter conditions with slight frosts and low wind speeds, the Bodman index is the most acceptable for biometeorological assessment. However, for extremely cold conditions of the winter period against the background of increased surface wind speeds in combination with frosty temperatures, a more adequate assessment of the "severity" of the cold period can be obtained using the Siple index.

In addition, important results of the study include the ranking and comparative assessment of a number of biometeorological indicators used to study the cold period of the year for the weight and reliability of the numerical estimates of the severity of weather conditions in the cold period of the year obtained with their help. The author's scale of gradations of the values of a number of biometeorological indices is also proposed, including the addition of the known gradations of these indices.

The above conclusions and results of the study confirm the need for further study of known biometeorological indicators to identify opportunities for their effective use, as well as to develop new principles and options for assessing the severity of cold period conditions. Since the noted problem [15-19], which consists in providing a sufficiently large number of countries in the world with high-quality hydrometeorological and, in particular, biometeorological forecast information, is relevant at the present time and is unlikely to lose its significance in the near future, the research described above should be continued.

Author Contributions

The authors of this article fully formulated the idea, made calculations, wrote the text, took care of the design of the article.

Conflict of Interest

There is no conflict of interest.

Funding

This research received no external funding.

References

[1] Андреев, С.С., Андреева, Е.С., 2004. Краткая биоклиматическая характеристика Ростовской области (Russian) [Brief bioclimatic characteristics of the Rostov region]. Метеорология и гидрология. 8, 53-60. Available from: https://www.elibrary.ru/item.asp?id=18065411

[2] Головина, Е.Г., Русанов, В.И., 1993. Некоторые вопросы биометеорологии (Russian) [Some issues of biometeorology]. Spb.: Izd. RSHU. TSU. p. 90. Available from: https://www.elibrary.ru/item.asp?edn=yngwab

[3] Extraordinary Meeting of the SERCOM/SC-DRR Advisory Group on Severe Weather Forecasting (AG-SWF) [Internet]. World Meteorological Organization; 2023 [cited 2023 Sept 25]. Available from: https://community.wmo.int/en/meetings/extraordinary-meeting-sercom-sc-drr-advisory-group-severe-weather-forecasting-ag-swf

[4] Tromp, S.W. (editor), 1960. Biometeorology. Proceedings of the Second International Biocli-

matological Congress; 1960 Sep 4-10; London. Paris: International Society of Biometeorology. Available from: https://www.sciencedirect.com/book/9780080096834/biometeorology

[5] Русанов, В.И., 2004. Биоклимат Западно-Сибирской равнины (Russian) [Bioclimate of the West Siberian Plain]. Tomsk. Izd. IOA SO RAN. p. 208. Available from: https://search.rsl.ru/ru/record/01002512762

[6] Essex, C., McKitrick, R., 2004. Taken by storm: The troubled science, policy and politics of global warming. Canadian Public Policy. 30(3). Available from: https://www.researchgate.net/publication/237550498_Taken_by_Storm_The_Troubled_Science_Policy_and_Politics_of_Global_Warming

[7] Дмитриев, В.В., Примак, Е.А., Скрыгина, В.К., 2011. Интегральная оценка устойчивости и экологического благополучия геосистем (Russian) [Integral assessment of the sustainability and environmental well-being of geosystems]. Международный журнал экспериментального образования. 5, 137-138. Available from: https://www.elibrary.ru/item.asp?id=20217597

[8] Резник, Л.Г., Шелякин, А.С., 2001. Интегральные показатели суровости совокупного воздействия климатических факторов (Russian) [Integral indicators of the severity of the cumulative impact of climatic factors]. Межвузовский сборник научных трудов Тюменского индустриального университета. 203-209. Available from: https://www.elibrary.ru/item.asp?id=23260337

[9] Арнольди, И.А., 1962. Акклиматизация человека на Севере и Юге (Russian) [Human acclimatization in the North and South]. M. MedGiz. p. 71. Available from: https://search.rsl.ru/ru/record/01005948756

[10] Андреева, Е.С., 2006. Опасные явления погоды юга России (Russian) [Dangerous weather phenomena in southern Russia]. Spb. Izd. BBM. p. 216. Available from: https://www.elibrary.ru/item.asp?id=21261376

[11] Адаменко, В.Н., Кондратьев, К.Я., 1999. Антропогенное воздействие на природу Севера (Russian) [Anthropogenic impact on the nature of the North]. Apatity. Izd. KNZ RAN. 17-34. Available from: https://www.elibrary.ru/item.asp?id=44251315

[12] Комплексные исследования природной среды Арктики и Антарктики (Russian) [Comprehensive studies of the natural environment of the Arctic and Antarctic]. Сборник тезисов и докладов: Izd. AANII. p. 408. Available from: https://www.elibrary.ru/item.asp?id=43804594

[13] Андонова, А.С., Бабин, А.В., Викулина, М.А., et al., 2013. Влияние изменений климата и опасных природных явлений на природопользование Европейского Севера (Russian) [The impact of climate change and natural hazards on environmental management in the European North]. Spb. Izd. RSHU. p. 124. Available from: https://elibrary.ru/item.asp?id=28437325

[14] Andreev, S.S., Popova, E.S., 2012. Global warming and anthropogenic factor. European Journal of Natural History. 4, 27-28. Available from: https://www.elibrary.ru/item.asp?id=18837071

[15] Денисов, О.В., Губеладзе, О.А., Месхи, Б.Ч., et al., 2016. Комплексная безопасность населения и территорий в чрезвычайных ситуациях. Проблемы и решения (Russian) [Comprehensive security of the population and territories in emergency situations. Problems and solutions]. RnD. Izd DSTU. p. 278. Available from: https://www.elibrary.ru/item.asp?id=28309023

[16] Александров, А.А., Ларионов, В.И., Сущев, С.П., 2019. Анализ и управление техногенными и природными рисками (Russian) [Analysis and management of man-made and natural risks]. Moskow. Izd MGSU. p. 360. Available from: https://www.elibrary.ru/item.asp?id=47352032

[17] Basilaia, M.A., Bogdanova, I.V., Dymnikova, O.V., 2019. Cosmoharmonic principles of environmental safety. Innovative Technologies in Environmental Science and Education. 135,

01079. Available from: https://www.elibrary.ru/item.asp?id=43323252

[18] Плешко, М.С., Насонов, А.А., Дымникова, О.В., et al., 2020. Обеспечение комплексной безопасности работ по восстановлению и реконструкции шахтных стволов (Russian) [Ensuring comprehensive safety of work on the restoration and reconstruction of mine shafts]. Горный информационно-аналитический бюллетень (научно-технический журнал). 7, 104-112. Available from: https://www.elibrary.ru/item.asp?id=43162659

[19] Belushkina, G.V., Bulygin, Yu.I., Deundyak, D.V., 2010. Calculation of the accumulation of harmful substances in a closed volume of a machine running-in room in an emergency situation. Advanced Engineering Research. 10(3), 397-401. Available from: https://www.vestnik-donstu.ru/jour/article/view/993/988?locale=en_US

BILINGUAL PUBLISHING GROUP
Tel:+65 65881289
E-mail: contact@bilpublishing.com
Website:https://journals.bilpubgroup.com

2630-5119
04
9 772630 511232